



**Proceedings of the 11th workshop on
Physical Processes in Natural Waters**

*Warnemünde, Germany,
3 - 6 September, 2007*

Edited by Lars Umlauf, IOW and Georgiy Kirillin, IGB

Berichte des IGB Heft 25/2007

Baltic Sea Research Institute Warnemünde
Leibniz-Institut für Ostseeforschung Warnemünde, IOW

Leibniz-Institute of Freshwater Ecology and Inland Fisheries
*Leibniz-Institut für Gewässerökologie und Binnenfischerei, IGB
im Forschungsverbund Berlin e.V.*

**Proceedings of the 11th workshop on
Physical Processes in Natural Waters**
Warnemünde, Germany, 3 - 6 September, 2007

Herausgeber

Leibniz-Institut für Gewässerökologie und Binnenfischerei (IGB)
im Forschungsverbund Berlin e. V.
Müggelseedamm 310, 12587 Berlin

Direktor (kommissarisch)

Prof. Dr. Gunnar Nützmann

Gestaltung

Götz Greiner (Weimar)

Satz

Christof Engelhardt und Georgiy Kirillin (IGB, Berlin)

Druck

andrea p design, Berlin

Table of Contents

Preface

Organization

1	Internal Waves	1
	The Generation of Internal Waves from Turbulence and Shear <i>SUTHERLAND, B. R., and J. R. Munroe</i>	3
	Generation of internal waves by a supercritical stratified plume <i>Stashchuk, N., and V. Vlasenko</i>	11
	Generation and propagation of inertia-gravity waves in the atmosphere (in analogy to the ocean) <i>Zuelicke, C., and D. Peters</i>	17
	Tidal mixing in the deep basin of Gullmar fjord <i>ARNEBORG, L.</i>	19
	Three-dimensional dynamics of shoaling and breaking oceanic internal waves <i>Vlasenko, V., and N. Stashchuk</i>	23
	The sound of troubled water: Vibrations of and in spherical shells partly filled with water <i>Baeuerle, E.</i>	29
2	Bubbles	31
	The Impact of Hypolimnetic Oxygenation on Oxygen, Iron and Manganese Cycling at the Sediment-Water Interface <i>Bryant, L. D., and J.C. Little</i>	33
	Coupled bubble plume/reservoir model for hypolimnetic oxygenation: Full-scale evaluation <i>Singleton, V. L., D. F. McGinnis, and J. C. Little</i>	39
	Methane transport in the Black Sea: Turbulent fluxes and rising bubbles <i>McGinnis, D. F., A. Lorke, A. Wüest, and CRIMEA Partners</i>	45
3	Internal Mixing	51
	Quantification of erosive processes at the halocline of a meromictic lake <i>Boehrer, B., C. von Rohden, J. Ilmberger, and M. Schultze</i>	53
	Vertical Transport in a Meromictic Mining Lake Studied with a SF ₆ - Tracerexperiment <i>von Rohden, C., and J. Ilmberger</i>	55

Investigation of Ground Water Interconnection and Vertical Transport in a Small Meromictic Mining Lake Using Background SF ₆	61
<i>Illmberger, J., and C. von Rohden</i>	
4 Turbulence	67
A minimal energy- and flux-budget (EFB) turbulence closure model for stably stratified sheared flows	69
<i>ZILITINKEVITCH, S.</i>	
Comparison of dissolved oxygen fluxes in natural waters from simultaneously deployed eddy-correlation devices	71
<i>Lorrai, C., A. Hume, D. F. McGinnis, P. Berg, and A. Wüest</i>	
Estimation of TKE dissipation rate in an inflowing saline bottom plume using a PC-ADP	77
<i>Mohrholz, V., H. U. Lass, and H. Prandke</i>	
Boundary layer effects in topographically constrained bottom gravity currents	79
<i>Umlauf, L., V. Mohrholz, and L. Arneborg</i>	
Turbulent dissipation in the stratified Lake of Geneva forced by wind	81
<i>Bouffard, D., and U. Lemmin</i>	
The impact of surface active films on waves and gas exchange	87
<i>Zuelicke, C.</i>	
Mixing in the lake water body of a deep meromictic lake: role of double-diffusive convection in the dynamics of mixing	89
<i>Bonhomme, C., B. Tassin, Y. Cuypers, and M. Poulin</i>	
5 Numerical Modelling	95
Climate warming and shallow lakes: the role of bottom sediments and water transparency	97
<i>Kirillin, G., S. Golosov, D. Mironov, and C. Engelhardt</i>	
Parameterizations of atmosphere-hydrosphere fluxes: An attempt to quantify uncertainty	99
<i>Stips, A., E. Garcia-Gorriz, and K. Bolding</i>	
Parameterisation of Lakes in Numerical Weather Prediction and Climate Models	101
<i>Mironov, D., E. Heise, E. Kourzeneva, B. Ritter, and N. Schneider</i>	
Impact of along-flow density gradients on sediment transport in estuaries (!), the Wadden Sea (!?) and in lakes (?)	109
<i>Burchard, H., and L. Umlauf</i>	
The transformation of one type of littoral circulation to another in a basin with sloping bottom while passing the temperature of maximum density	111
<i>Demchenko, N. and I. Chubarenko</i>	
Modelling circulation and sediment dynamics in Kondopoga Bay, Lake Onega	117
<i>Podsechin V., N. Filatov, T. Frisk, A. Terzhevik, Ä. Bilaletdin and A. Paananen</i>	

6	Thermo- and Hydrodynamics	121
	Energetics of a River Plume	123
	<i>MacCready, P.</i>	
	Hydrodynamics of Intermittently Closing and Opening Lakes and Lagoons	129
	<i>Gale, E., and C. Pattiaratchi</i>	
	Advective deep-water renewal in Lake Baikal	137
	<i>Schmid, M., N. Budnev, N. Granin, M. Schurter, M. Sturm, and A. Wüest</i>	
	Thermodynamics of water, vapour, ice and seawater	143
	<i>Feistel, R.</i>	
	Some features of the vertical dissolved oxygen structure in shallow ice-covered lakes	147
	<i>Terzhevik, A., S. Golosov, A. Mitrokhov, N. Palshin, M. Potakhin, R. Zdorovenov, and G. Zdorovenova</i>	
	On the effective thermal diffusivity in ice-covered lakes	157
	<i>Golosov, S., I. Zverev, A. Terzhevik, A. Yu, G. Kirillin and C. Engelhardt</i>	
7	Physical-biological Coupling	169
	The role of physics in driving the functional structure of phytoplankton communities: observations from an autonomous profiling platform	171
	<i>Rueda, F. J., A. Hoyer, A. Rigosi, J. Vidal, C. Escot, A. Basanta, E. Moreno-Ostos, I. De-Vicente, V. Amores, and L. Cruz-Pizarro</i>	
	The seasonal evolution of the functional structure of phytoplankton community in a Mediterranean reservoir: influence of external perturbations	173
	<i>Hoyer, A., J. Vidal, C. Escot, A. Basanta, E. Moreno-Ostos and F. J. Rueda</i>	
	Impact of <i>Chironomus plumosus</i> (L.) (Diptera: Chironomidae) on hydrodynamic transport and biogeochemical turnover in lake sediments	179
	<i>Roskosch, A., J. Lewandowski, M. Hupfer, and G. Nützmann</i>	
	A cyanobacterial biomass prediction model for the Gulf of Finland based on a reduced number of input parameters	187
	<i>Lilover, M.-J.</i>	
	Modeling of the influence of intrusions on the biogeochemical structure of the Seas with anoxic layers	193
	<i>Kuznetsov, I. S., E. V. Yakushev, and O.I. Podymov</i>	

Author Index

Preface

The meeting in Warnemünde continues a series of workshops that has started more than a decade ago in Kastanienbaum near Lucerne (Switzerland). The focus of the PPNW workshops is the physics of lakes, covering a broad spectrum of scientific topics including internal wave motion, turbulence and mixing, surface interactions, bio-geochemical interactions, near-sediment processes, and many more. PPNW is an open workshop, actively seeking the contact to neighboring fields like physical oceanography, the atmospheric sciences, and engineering. With 40-50 participants and a small number of invited speakers, the PPNW meetings are characterized by their active workshop atmosphere and a comfortable time frame for presentations and discussion.

The venue of the workshop in 2007 is the Baltic Sea Research Institute (IOW), one of the key institutes of the German oceanographical research infrastructure. IOW is located in Warnemünde, a charming fishermen village at the beautiful shores of the Baltic Sea.

During the first day of the workshop, participants will undertake an excursion to Lake Stechlin north of Berlin, and visit the Institute of Freshwater Ecology and Inland Fisheries (IGB), the co-organizers of this workshop. Both basic and applied research methods are used here to examine complex processes in lake ecosystems. The deep stratified Lake Stechlin is of special importance with respect to long-term ecological research and for comparisons with other lakes.

Lars Umlauf
Baltic Sea Research Institute (IOW)

Georgiy Kirillin
Institute of Freshwater Ecology
and Inland Fisheries (IGB)

Organization

Organizing Committee

Umlauf, Lars , IOW	general organization
Engelhardt, Christof , IGB	organization, excursion, proceedings
Kirillin, Georgiy , IGB	organization, excursion, proceedings
Wrobel, Karin , IOW	secretary
Rüb, Dietmar , IOW	webmaster

International Steering Committee

Bengtsson, Lars	Sweden
Boehrer, Bertram	Germany
Casamitjana, Xavier	Spain
Filatov, Nikolai	Russia
Folkard, Andrew	Great Britain
Kirillin, Georgiy	Germany
Lilover, Madis-Jaak	Estonia
Rueda, Francisco	Spain
Stips, Adolf	Italy
Terzhevik, Arkady	Russia
Umlauf, Lars	Germany
Wuest, Alfred	Switzerland

1 Internal Waves

SUTHERLAND, B. R.¹ & MUNROE, J. R.

The Generation of Internal Waves from Turbulence and Shear

¹Depts. of Physics and of Earth & Atmospheric Sciences, University of Alberta, Edmonton, T6G 2G7, Canada. E-mail: bruce.sutherland@ualberta.ca

Abstract

Internal waves are intimately connected with turbulence, whether through wave-wave interactions and breaking leading to turbulence or whether the turbulence itself excites internal waves. This talk will focus upon the latter process. Laboratory experiments have been performed to examine the generation of internal waves by flow over rough topography and the collapse of mixed patches. These show that internal waves are generated not only by flow over the hills but also by turbulence that is created between and in the lee of the hills. At slow flow rates internal wave frequencies match the excitation frequencies; at fast flow rates internal waves are excited by turbulence and their frequencies are an approximately constant fraction of the buoyancy frequency. In either case the effective amplitude of the hills is reduced and the corresponding wave amplitudes are smaller than predicted as a result of boundary layer separation. The results are extended to examine waves generated in a stratified layer beneath sheared turbulence as would occur, for example, due to a wind driving the surface mixed layer of a lake.

Introduction

The surface mixed region of lakes, the epilimnion, is energetic primarily as a consequence of forcing by winds. On the large scale these can establish basin scale internal wave modes, also known as internal seiches, in a thermally stratified lake. These are manifest as oscillations of the thermocline (the metalimnion), which separates the warmer surface waters from the cooler hypolimnion beneath. Their horizontal wavelength, λ , is on the order of the extent of the

lake itself and their period, T , can be hours or days depending on the size of the lake and the strength of the stratification.

Ignoring the effects of the Earth's rotation, the relationship between the internal wave frequency, $2\pi/T$, and wavenumber, $2\pi/\lambda$, may be estimated by $\omega = ck$, in which c is the shallow water wave speed given by

$$c = \sqrt{g'\bar{H}}, \quad g' = g \frac{\rho_h - \rho_e}{\rho_0}, \quad \bar{H} = \frac{(H - H_e)H_e}{H}. \quad (1)$$

In eq. (1), g' is the reduced gravity, a function of the gravitational acceleration g , the characteristic water density ρ_0 and the difference in the characteristic densities of the hypolimnion and epilimnion, ρ_h and ρ_e , respectively. The quantity \bar{H} measures the effective depth of shallow water waves in a body of water of total depth H , where H_e measures the distance from the surface to mid-depth of the metalimnion.

For example, if the temperature varies from 20°C to 10°C from top to bottom, the reduced gravity is approximately $g' \simeq 0.016 \text{ m/s}^2$, and if $H = 100 \text{ m}$ and $H_e = 20 \text{ m}$, then $\bar{H} = 16 \text{ m}$. Thus eq. (1) gives $c = 0.51 \text{ m/s}$ as the horizontal speed at which long undulations move along the thermocline. A mode-1 wave has horizontal wavelength which is twice the extent of the lake along the distance of propagation. Thus for modes excited by winds blowing along a 5 km long lake, $k = 2\pi/(10 \text{ km}) \simeq 6.3 \times 10^{-4} \text{ m}^{-1}$. In our example, the corresponding frequency is $\omega \simeq 3.2 \times 10^{-4} \text{ s}^{-1}$, which corresponds to a period of about 5 1/2 hours.

In the above example, the metalimnion is assumed to be an infinitesimally thin layer separating the epilimnion and hypolimnion, a reasonably good approximation for internal seiches. But internal waves with smaller spatial and temporal scales can also be excited as a consequence of turbulent eddies in the epilimnion transiently perturbing the thermocline. These do not result in the sloshing motion associated with undulations of the thermocline. Rather the waves propagate vertically downward through the thermocline itself. The wavelength, λ , of the waves is set by the scale of most energetic turbulent eddies. The period is set by the strength of the thermocline's stratification as measured by a quantity called the buoyancy frequency, N . This is given approximately by

$$N = \sqrt{\frac{g}{H_m} \frac{\rho_h - \rho_e}{\rho_0}} = \sqrt{\frac{g'}{H_m}}, \quad (2)$$

in which H_m is the thickness of the metalimnion. With $g' \simeq 0.016 \text{ m/s}^2$ and $H_m = 40 \text{ m}$, $N \simeq 0.02 \text{ s}^{-1}$. This is measured in 'radians

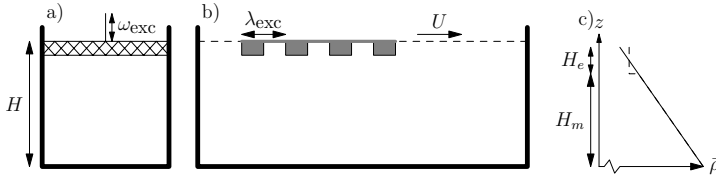


Figure 1: Setup of laboratory experiments of a) grid-generated, stationary turbulence and b) sheared turbulence generated by towed, rough surface. Both experiments initially have uniform stratification with linearly increasing density with depth as indicated by the solid line in c) and then develop a mixed layer of depth H_e , as indicated by the dashed line.

per second'. The corresponding buoyancy period is $T = 2\pi/N \simeq 300$ s, significantly faster than the corresponding internal seiche period.

In experiments, the frequency, ω , of vertically propagating internal waves generated by turbulence is found to be smaller than but close to N . Unlike internal seiches, the frequency is independent of the basin scale. Their phase speed is not fixed, as in (1), but is set by ω and λ .

Neglecting the dynamics of internal seiches, the work presented here focuses upon the circumstance in which internal waves are created by either stationary or sheared turbulence in a mixed region overlying stratified fluid. This is examined by way of laboratory experiments.

Experimental Set-up

Two sets of experiments are discussed here, as illustrated in Figure 1. The first setup is similar to that studied first by Linden (1975). A 49 cm tall tank of width 47.6 cm and breadth 7 cm is filled with uniformly salt-stratified fluid (Fig. 1a). Typically, the density gradient is established so that $N \simeq 1.1 \text{ s}^{-1}$.

A square grid that spans the horizontal cross-section of the tank is positioned near the top of tank and oscillates vertically up and down with a frequency of $\omega_{exc} = 44 \text{ s}^{-1}$ (7 Hz) and peak-to-peak stroke length of 2.6 cm. As a consequence, the fluid is rapidly mixed near the top of the tank. The corresponding density profile before and during an experiment is illustrated in Fig. 1c. The depth of the mixed region is H_e , which increases over time, though ever more slowly as the mixed layer deepens.

Observations show that after 10 s, H_e increases from 15 cm to 17 cm over the next 120 s. It is over this time period that the generation of internal waves below the mixed region are examined. Because the grid oscillates at a frequency much larger than N , it does not directly excite internal waves. Rather they are generated by the impact of turbulent eddies upon the base of the mixed layer.

In the second set of experiments, designed to measure the additional effects of sheared turbulence, a rough surface is towed along the surface of salt-stratified fluid in a 50 cm tall tank of length 197.1 cm and width 17.5 cm (Fig. 1b). Initially the fluid is uniformly stratified, again with $N \simeq 1.1 \text{ s}^{-1}$. Repeating the experiment over and over, surface mixed layer develops so that, once again, the density profile changes as illustrated in Fig. 1c.

The rough surface has four rectangular protrusions with peak-to-peak height 2.60 cm spaced apart equally by $\lambda_{\text{exc}} = 13.7 \text{ cm}$. These are towed at speeds ranging from $U = 0.8$ to 5.2 cm/s , corresponding to forcing frequencies ranging from $\omega_{\text{exc}} \equiv (2\pi/\lambda_{\text{exc}})U = 0.37$ to 2.4 s^{-1} . At the upper range, the forcing frequency exceeds the buoyancy frequency and so internal waves can only be indirectly excited by turbulence.

Experimental Results

A surprising observation in all experiments is that stationary and sheared turbulence generates internal waves in a narrow frequency band, typically with ω lying between $0.5N$ and $0.8N$. This is illustrated in Figure 2, which shows normalized contours of the quasi-steady state internal wave field (Fig. 2a). The criss-cross pattern of waves shows that they propagate at approximately a 45° angle to the vertical, corresponding to waves with $\omega \simeq 0.7N$.

A vertical time series of this experiment (Fig. 2b) shows upward propagating phase lines, which corresponds to waves with downward group velocity, as expected. The vertical phase speed increases from top-to-bottom, indicating that the waves have larger spatial scale lower down in the tank. The smaller scale waves, which have a stronger signal due to larger density perturbations, dissipate more rapidly near their source so that the signal is dominated by large scale waves far from the source.

These qualitative features can be captured by fully nonlinear numerical simulations in two dimensions, where the turbulence is represented by random, fast time-scale perturbations in a mixed region overlying a stratified layer (Figs. 2c and d). Although the structure of the simulated turbulence is quite different from reality, the mechanism for wave generation is effectively the same to the extent that

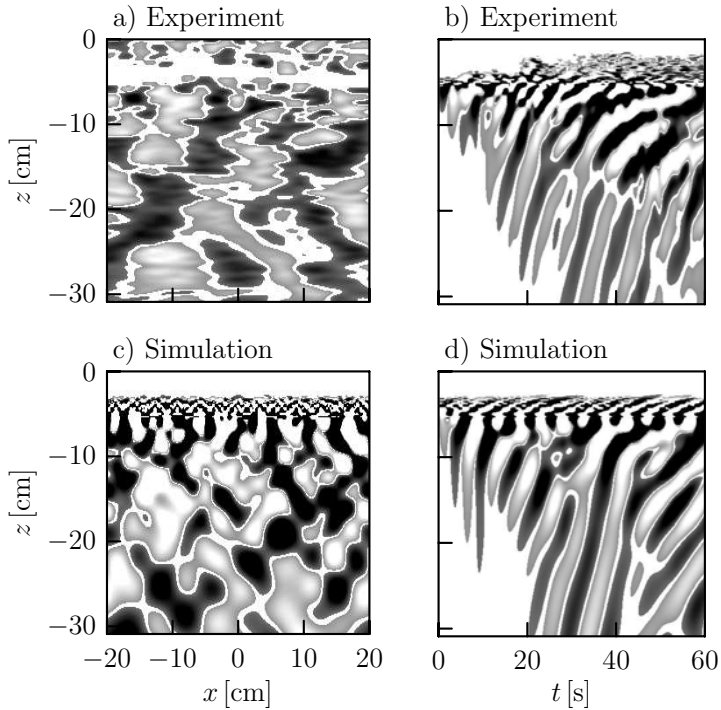


Figure 2: Stationary turbulence experiment showing wave-field well below grid (situated at $z = 0$) at a) a snapshot in time and b) in a vertical timeseries taken midway along the tank. Corresponding images determined from two-dimensional numerical simulations are shown in c) and d), respectively. [Adapted from Dohan and Sutherland (2003) and Dohan (2004)].

the random forcing excites waves most efficiently within a narrow frequency band.

The experimental and simulated wave-fields in Fig. 2 have been normalized by the maximum amplitude at $z = -10$ cm, in order to compare most clearly the wave characteristics. However, the simulated waves have much smaller amplitude than the experimentally generated waves. This implies that the three-dimensional turbulent eddies are more efficient than random two-dimensional perturbations at creating waves. The detailed nature of this wave excitation mechanism are yet to be understood.

When rough topography is towed, waves are again excited within a narrow frequency range. Rather than forming a criss-cross pattern,

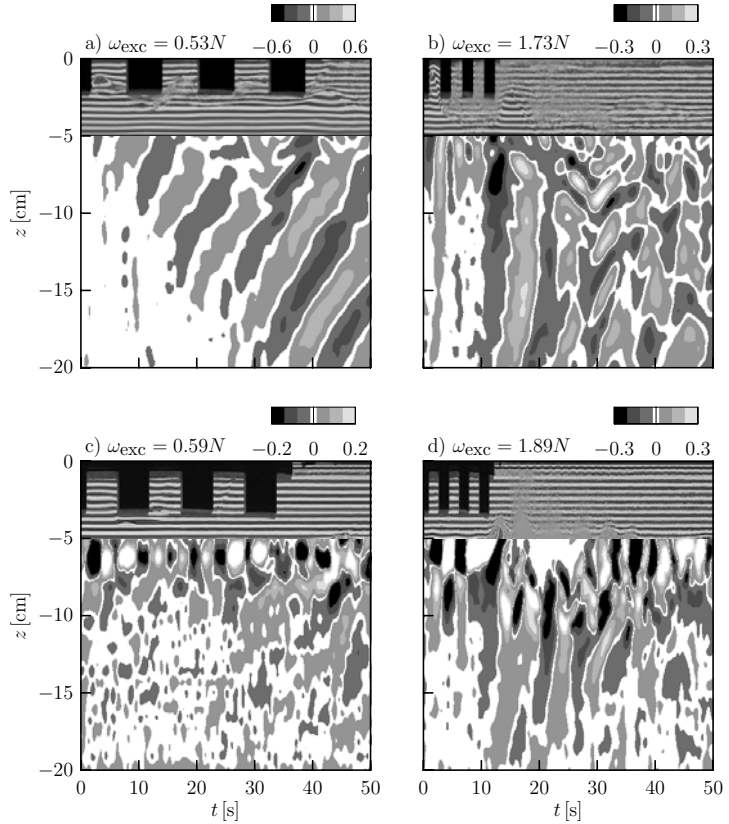


Figure 3: Waves generated from a towed rough surface in uniformly stratified fluid and with tow speed set such that a) $\omega_{\text{exc}} = 0.53N$ and b) $\omega_{\text{exc}} = 1.73N$. Waves generated below a mixed region of depth $H_e = 7$ cm with tow speed set such that c) $\omega_{\text{exc}} = 0.59N$ and d) $\omega_{\text{exc}} = 1.89N$. Gray scale contours correspond to values of N^2_t field measured in s^{-3} . [Plots in a) and b) are adapted from Aguilar and Sutherland (2006)].

however, in this case the waves have phase lines oriented downward and to the right, not to the left. This corresponds to downward propagating waves with positive horizontal phase speed.

Time series taken from four experiments are shown in Figure 3. In the top two plots, the rough surface is towed along the surface of a uniformly stratified fluid. At such slow tow speeds that the effective excitation frequency ω_{exc} is less than the buoyancy frequency, N , the rough features directly excite waves, whose amplitudes become

larger in the lee of the forcing (Fig. 3a). At faster towing rates, with $\omega_{\text{exc}} > N$, the waves directly above the surface are evanescent but the turbulence in the lee is stronger. This excites waves with smaller vertical scales but with frequencies comparable to $0.5N$ (Fig. 3b).

If the surface is towed at a slow speed through a mixed region of depth $H_e \simeq 7$ cm, the amplitude of the waves is substantially smaller, with a barely perceptible signal directly above the surface (Fig. 3c). At faster towing speeds, however, the turbulence in the lee interacts strongly with the stratified fluid below the mixed layer and internal waves are generated with comparable characteristics and amplitudes (Fig. 3d).

The field plotted in all four figures measures the magnitude of the time derivative of the squared buoyancy frequency field, N_t^2 . This is a measure of the rate of change of density gradients due to internal waves, and is measured directly by a non-intrusive optical technique called ‘synthetic schlieren’. From linear theory, N_t^2 is proportional to the vertical displacement amplitude, ξ , through the relation $N_t^2 = N^3 \sin \Theta k_x \xi$, in which $\Theta = \cos^{-1}(\omega/N)$ is a measure of the wave frequency.

Using the observed values of k_x and ω , the turbulently generated waves are found to have vertical displacements as large as 2% of the horizontal wavelength. Such waves are weakly nonlinear in the sense that they are one-fifth the amplitude of breaking waves (Sutherland (2001); Aguilar and Sutherland (2006)).

Conclusions

We have surveyed some recent experimental results examining the generation of internal waves from stationary and sheared turbulence in a surface mixed layer. Although turbulence exhibits a broad frequency spectrum, the waves are generated in a narrow frequency band and with relatively large amplitude. Cumulatively, the energy of these waves may not be so large as interfacial waves associated with internal seiches. However, the fact that the waves can propagate vertically downward and interact nonlinearly implies they may have important long range impact upon localized mixing in the interior of stratified lakes.

References

- AGUILAR, D. A. AND SUTHERLAND, B. R. 2006. Internal wave generation from rough topography. *Phys. Fluids* 18:Art. No. 066603.
- DOHAN, K. 2004. Internal Wave Generation from a Turbulent Mixed Region. PhD thesis, University of Alberta.

- DOHAN, K. AND SUTHERLAND, B. R. 2003. Internal waves generated from a turbulent mixed region. *Phys. Fluids* 15:488–498.
- LINDEN, P. F. 1975. The deepening of a mixed layer in a stratified fluid. *J. Fluid Mech.* 71:385–405.
- SUTHERLAND, B. R. 2001. Finite-amplitude internal wavepacket dispersion and breaking. *J. Fluid Mech.* 429:343–380.

STASHCHUK, N.¹, VLASENKO, V.²

Generation of internal waves by a supercritical stratified plume

¹*University of Plymouth,
Address, PL4 8AA, Ply-
mouth, United Kingdom. E-
mail:nstashchuk@plymouth.ac.uk*

²*University of Plymouth,
Address, PL4 8AA, Ply-
mouth, United Kingdom. E-
mail:vvasenko@plymouth.ac.uk*

Abstract

The generation of internal waves by propagating supercritical river plume is studied using the MITgcm. The fluid stratification, parameters of the propagating waves and bottom topography were taken close to those observed near the Columbia River mouth.

Introduction

High-frequency internal waves (IW) are typically the most energetic vertical motions of the World Ocean. In some places their amplitude reaches 100 m and more (Ostrovsky and Stepanyants, 1989). IWs produce shear currents and turbulence (Garrett, 2003) that mix water and supply nutrients from the abyss to the surface photic layer and enhance bioproductivity (Briscoe, 1984). It is commonly believed that one of the principal sources of IWs is the interaction of tidal currents with oceanic bottom topography (Vlasenko et al., 2005). However, there are many evidence of their non-tidal nature. The synthetic aperture radar (SAR) images shown in Figures 1 and 2 present a real challenge for investigators. They reveal the sea surface signature of IWs radiated from the Columbia River and Dnieper River plumes. Direct in-situ measurements across the Columbia River plume have shown that the plume-attached IWs are of similar amplitude to those generated by tide over topography (Nash and Moum, 2005). It is significant that these IWs may be generated in the absence of any apparent tidal forcing. As a confirmation of

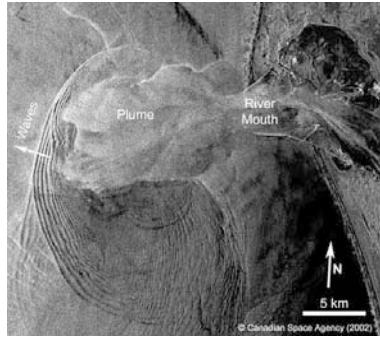


Figure 1: SAR image acquired on 9 08 1999 (Radarsat-1) showing enhanced surface roughness associated with internal waves generated by the Columbia River plume (Nash and Moum, 2005).

this fact, similar packet of IWs propagating from the Dnieper River plume is shown in Figure 2. The Black Sea is a non-tidal basin, so it is clear that the generation mechanism of these IWs has nothing to do with tides.

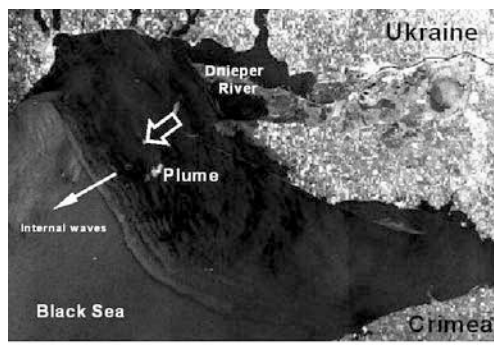


Figure 2: SAR image acquired on 14 June 2005 (Envisat ASAR) indicating internal waves generated by the Dnieper river waters penetrating into the non-tidal Black Sea (Courtesy of Prof. Alpers, ESA).

River water being less saline intrudes into the sea as a surface layer and forms the head of gravity current at the boundary between the plume and the sea. Such a system contains IWs propagating along with the plume. At the beginning of motion the plume propagates faster than these waves. It is hypothesised that IWs are released when the propagation speed of the plume becomes smaller

than the phase speed of IWs. As a result, the head of the gravity current disintegrates into series of radiated waves.

Model results

Formulated as a hypothesis, this mechanism was studied for the case of the Columbia River plume with the help fully-nonlinear fine-resolution non-hydrostatic MIT general circulation model (Marshall et al., 1997).

The motion starts when the lock located in the mouth and separated river and ocean is lifted. To obtain the structure of the plume similar to the observed one (see Figure 1), the motion is initiated using a realistic tidal current. Another initial conditions for the model were organized in such a way to take into account the real river discharge which varies between 2,500 in late summer to 17,000 $\text{m}^3 \text{s}^{-1}$ in spring (Hickey and Banas, 2003) and the daily tidal range is equal to 2.46-2.55 m (Orton and Jay, 2005). Strong tidal currents and buoyancy input sometimes cause these fronts to exhibit large density contrasts ($\Delta S > 20$ ppt over $< 150\text{m}$), sharp convergence ($\Delta U > 0.5 \text{ m s}^{-1}$ over $< 150 \text{ m}$), and rapid propagation (sometimes excess of 1 m s^{-1}).

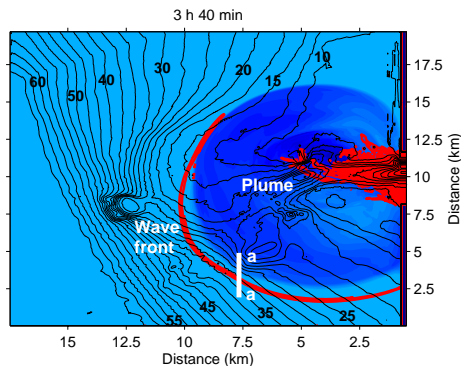


Figure 3: Surface distribution of the plume (salinity) overlaid with bottom topography at $t = 3 \text{ h } 40 \text{ min}$ after the start of the numerical experiment. Lines with large velocity gradients show the location of the wave packet. In this experiment ebb tidal current is included.

Figure 3 represents the distribution on the surface of less saline river waters intruding the Pacific Ocean at 3 h 40 min after the lock was opened. Here the density difference is accompanied by the tidal current. The distribution of surface salinity is overlapped with the bottom topography and distribution of the largest values of the sur-

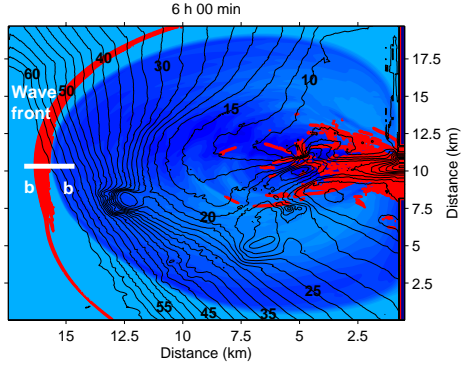


Figure 4: The same as in Figure 3 but at $t = 6$ h 00 min.

face velocity gradient $\partial U / \partial r$. The latter helps to trace the detachment of the generated internal waves from the plume front. The places with large values of $\partial U / \partial r$ show the position of the waves around the plume front. In Figure 3 the wave front is partly separated from the plume due to predominance of the local phase velocity of internal wave (0.4 m s^{-1}) over velocity of plume propagation.

Spatial variability of the plume characteristics along with irregular bottom topography provide unequal conditions for IW generation at different cites of the plume front. In fact, its central part

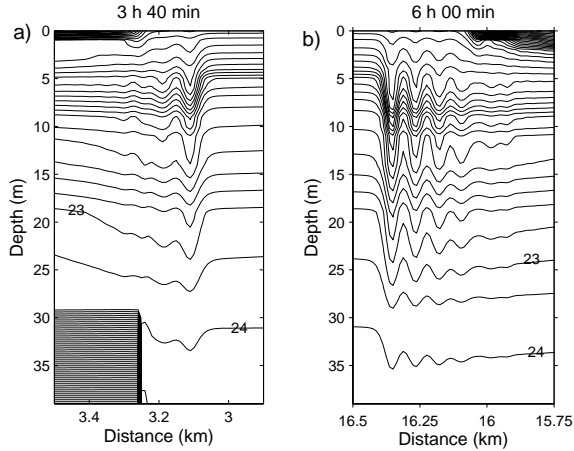


Figure 5: Density sections with wave fission from the plume front: a) along section a-a (Figure 3) and b) along section b-b (Figure 4).

propagates faster than lateral boundaries. This is the reason why subcritical conditions i.e. $Fr < 1$, where Fr is Froude number, come true at the periphery of the front earlier than that in its central

part. From this moment of time the velocity of the wave propagation starts to increase due to the increase of the depth whereas the velocity of the front decreases as a result of water spreading and ebb tide slackening.

Figure 4 represents the latest stage of the plume evolution (at time moment $t = 6$ h). At this moment of time the whole internal wave is detached from the plume.

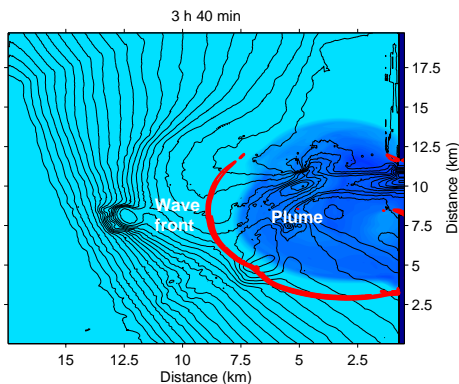


Figure 6: Surface distribution of the plume (salinity) overlaid with bottom topography at $t = 3$ h 40 min. Lines with large values of velocity gradient show the location of the wave packet.

The cross-front snapshots of density in Figure 5 shows the structure of the released internal wave trains propagating from the plume front. The wave train shown in Figure 5a propagates with velocity 0.4 m s^{-1} and its leading wave has amplitude about 5 m. The other wave train (find cross-section b-b in Figure 4) being more energetic, propagates with the velocity 0.7 m s^{-1} and its leading wave has amplitude about 10 m.

It was found that internal waves are also generated by the propagating plume even without tidal forcing but only due to large river discharge ($>10000 \text{ m}^3 \text{ s}^{-1}$). This result is presented in Figure 6. It can be treated as another confirmation of the new mechanism of internal wave generation implying that IWs are released when the propagation speed of the plume becomes smaller than the phase speed of IWs, i.e. when $Fr < 1$. As a result of this fact, the head of the gravity current disintegrates into series of radiated waves. The wave trains are spawned when the speed of frontal propagation drops below the intrinsic propagation speed of internal waves in the coastal ocean outside the plume front.

Acknowledgment

This work was funded by Natural Environmental Research Council grant NE/E01030X/1.

References

- M. Briscoe, 1984, Tides, solitons and nutrients. *Nature*, 312, 1-5.
- C. Garrett, 2003, Internal tides and ocean mixing. *Science*, 301, 1858-1859.
- B.M. Hickey and N.S. Banas, 2003, Oceanography of the U.S. Pacific Northwest coastal ocean and estuaries with application to coastal Ecology. *Estuaries*, 26(48), 1010-1031.
- J. Marshall, C. Hill, L. Perelman and A. Adcroft, 1997, Hydrostatic, quasi-hydrostatic, and non-hydrostatic ocean modeling. *J. Geophys. Res.*, 102(C3), 5733-5752.
- J.D. Nash and J.N. Moum, 2005, River plumes as a source of large-amplitude internal waves in the coastal ocean. *Nature*, 437(15), 400-403.
- P.M. Orton and D.A. Jay, 2005, Observations at the tidal plume front of a high-volume river outflow, *Geophysical Research Letters*, 32, doi:10.1029/2005GL022372.
- L.A. Ostrovsky and Yu. Stepanyants, 1989, Do internal solitons exist in the ocean? *Rev. Geophys.*, 27, 293-310.
- V. Vlasenko, N. Stashchuk, and K. Hutter, 2005, *Baroclinic tides: theoretical modeling and observational evidence*. Cambridge University Press, 372 p.

ZUELICKE¹, C. & D. PETERS

Generation and propagation of
inertia-gravity waves in the
atmosphere (in analogy to the
ocean)

¹ *Baltic Sea Research Institute
Warnemünde, Dept. of Physical
Oceanography and
Instrumentation, Seestraße 15
18119, Rostock, Deutschland. E-
mail: christoph.zuelicke@io-
warnemuende.de*

Abstract

Several phenomena account for the generation of inertia-gravity waves in the atmosphere: orography, convection and jets. While the first two are well-understood, the third process is still not well resolved. We study a shallow water model to justify an empirical formulae. This parameterization is validated with data from ten field campaigns and related mesoscale model simulation. They were run under the influence of a poleward breaking planetary Rossby wave with strong upper level jets. Hence, the new forcing function could be used in ray tracing models which are used in the meteorological and maritime community.

ARNEBORG, L.

Tidal mixing in the deep basin of Gullmar Fjord

Earth Sciences Centre, Göteborg University, Box 460, 40530 Göteborg, Sweden. E-mail: laar@oce.gu.se

Abstract

Microstructure measurements and mooring data inside the sill of Gullmar Fjord show that the main mixing below sill level occurs at the phase of maximum inward velocities in the bottom layer. Most of the mixing takes place in a nearly homogeneous layer above a strong downslope bottom jet. The main hypothesis is that breaking lee waves formed just downstream of the mooring are responsible for the overturning layer. During the present observations the lee waves are caused by the baroclinic tidal bottom layer currents, but there is evidence that the same process is responsible for mixing caused by internal seiches in the fjord.

Introduction

The main energy source for mixing in deep fjord basins is believed to come from internal tides generated at the sill (Stigebrandt and Aure, 1989). This is analogous to the mixing in the deep oceans that seems to be dominated by tidal interaction with steep topography (e.g. Munk and Wunsch, 1998). Gullmar fjord is a 120 m deep fjord on the Swedish west coast, with a sill depth of 43 m. The tidal sea level difference is only about 0.12 m, but still tides have been shown to be important for the deep mixing, even though other processes (wind forced baroclinic and barotropic seiches) are also important (Arneborg and Liljebladh, 2001a,b). The result of an effort to map the mixing in the fjord basin in 2001 was that the deep mixing is concentrated to the sill region (Arneborg et al. 2004). This result led to the most recent experiment in September 2004, which was focused on the sill region.

During three days, microstructure shear measurements were performed at three stations located at 60, 70 and 80 m depth inside the entrance, Fig. 1. During the same time moorings with ADCPs and CT loggers were placed near the entrance, among which one

was placed at the 80 m microstructure station. At each microstructure station 4 profiles were performed in one burst before continuing to the next station. The repeat interval of one station was about 2 hours.

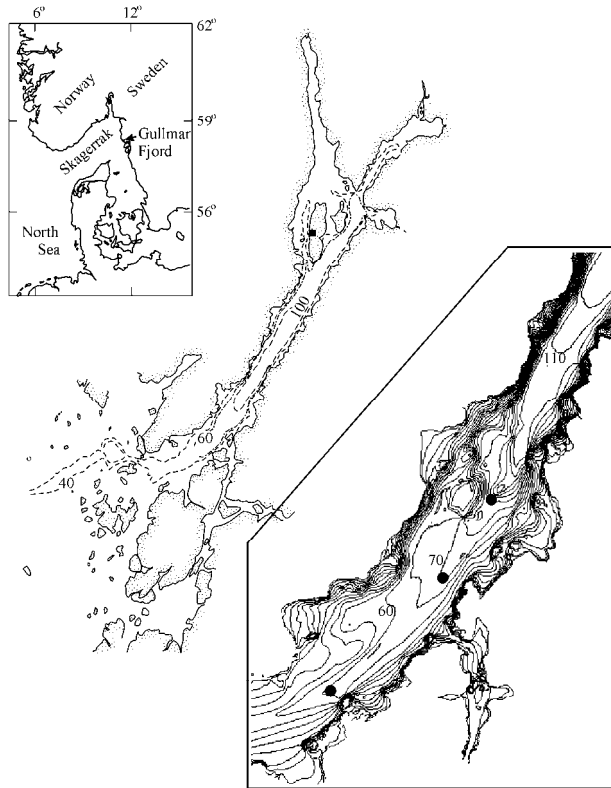


Figure 1 Map of Gullmar Fjord. The upper insert shows the location Gullmar Fjord on the Swedish west coast, while the lower insert shows the detailed topography inside the sill. The depth difference between isobaths is 5 m. The microstructure stations are marked with black dots.

Results

The dissipation rates of turbulent kinetic energy below sill level show a strong semidiurnal tidal signal with a peak associated with a downslope (inward) bottom jet below a less dense, nearly homogeneous, stagnant, layer with large overturns. Two examples

near days 271.9 and 272.5 at the 80 m station are seen in Fig. 2. Most of the dissipation is occurring in overturning motions in the stagnant layer, whereas about 1/3 is happening in the bottom boundary layer of the bottom jet.

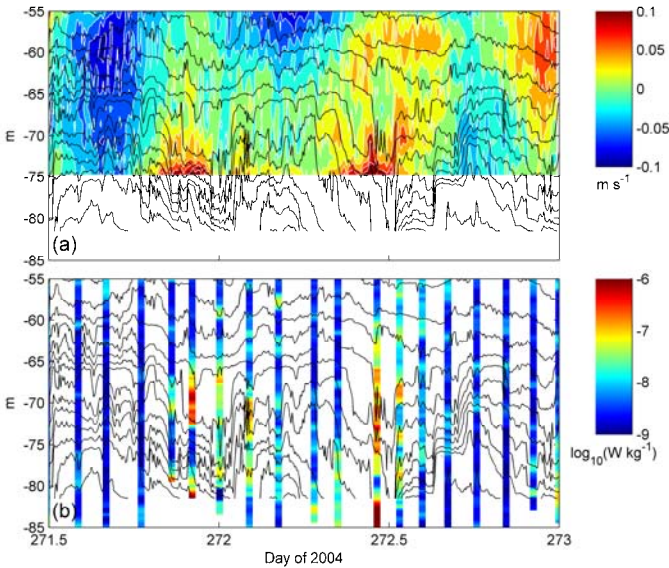


Figure 2 Zoom in on the largest dissipation events at the 80 m station. (a) Velocities in the main fjord direction (positive towards the head) and isotherms from the mooring. (b) Burst averaged dissipation rates of turbulent kinetic energy from the turbulence probe and isotherms from the mooring. Mean isothermal depth difference is 2.5 m.

The overturning layer shows a frontal behaviour with large gradients both in time and space, and with signs of high-frequency fluctuations in the mooring data. The layer is probably generated by internal wave breaking. The 80 m station is located in a narrow channel at the top of a steep slope, Fig. 1. During inward flow in the bottom layer, lee waves may form there, eventually breaking and generating the overturning layer, similarly to what has been observed in the atmosphere (Lilly 1978) and in Knight Inlet (e.g. Klymak and Gregg 2004). The main difference to Knight Inlet is that the present dissipation mechanism is associated with the baroclinic response of the fjord rather than with the barotropic tidal forcing. The same process may be the main dissipation mechanism of the wind generated internal seiches in the fjord, which are important for the basin water mixing, but which was not strong during the present microstructure measurements. Mooring data

from periods with strong internal seiching indicate that this is the case.

Acknowledgements

I thank Bengt Liljebladh, Hartmut Prandke, Selma Pacariz, Torsten Hanson, Hedvig Hernevik, Daniel Hansson, Karin Wesslander, and the captain and crew onboard R/V Skagerak for their help with the measurements. The work was supported by the Swedish Research Council.

References

- ARNEBORG, L., C. JANZEN, B. LILJEBLADH, T. P. RIPPETH, J. H. SIMPSON, A. STIGEBRANDT, 2004. Spatial Variability of Diapycnal Mixing and Turbulent Dissipation Rates in a Stagnant Fjord Basin, *J. Phys. Oceanogr.*, 34: 1679 – 1691.
- ARNEBORG, L., B. LILJEBLADH, 2001a. The internal seiches in Gullmar Fjord. Part I: Dynamics. *J. Phys. Oceanogr.*, 31: 2549-2566.
- , 2001b. The internal seiches in Gullmar Fjord. Part II: Contribution to basin water mixing. *J. Phys. Oceanogr.*, 31: 2567-2574.
- KLYMAK, J.M., M.C. GREGG, 2004. Tidally generated turbulence over the Knight Inlet sill. *J. Phys. Oceanogr.*, 34: 1135-1151.
- LILLY, D.K. 1978. A severe downslope windstorm and aircraft turbulence event induced by a mountain wave. *J. Atmos. Sci.*, 35: 59-77.
- MUNK, W., C. WUNSCH, 1998. Abyssal recipes II: Energetics of tidal and wind mixing. *Deep Sea Res. I*, 45: 1977-2010.
- STIGEBRANDT, A., J. AURE, 1989. Vertical mixing in basin waters of fjords. *J. Phys. Oceanogr.*, 19: 917 - 926.

VLASENKO, V.¹, STASHCHUK, N.²

Three-dimensional dynamics of shoaling and breaking oceanic internal waves

¹*University of Plymouth, PL4 8AA, Plymouth, United Kingdom. E-mail: vvlasenko@plymouth.ac.uk*

²*University of Plymouth, PL4 8AA, Plymouth, United Kingdom. E-mail: nstashchuk@plymouth.ac.uk*

Abstract

The three-dimensional (3D) shoaling of large amplitude internal waves (LAIW) is studied using the MITgcm. The vertical fluid stratification, parameters of the propagating waves and bottom topography were taken close to those observed in the Andaman Sea.

Introduction

A growing number of observations demonstrate that weakly nonlinear theories (even modified and extended) in many cases fail to describe the strongly nonlinear effects occurring during shoaling of LAIW. This basically concerns the shelf-break areas where internal wave amplitude reaches the saturation level and where some other strongly nonlinear effects, such as wave breaking and water mixing take place. A more consistent description of the wave dynamics in such areas can be based on numerical simulation of the fully-nonlinear hydrodynamic equations. Note, however, that 2D numerical models cannot be directly applied to the investigation of the shoaling of LAIW in areas with substantial curvature of shelf bathymetry. An example of such a situation is shown in Figure 1 presenting a packet of tidally generated internal waves approaching the shelf-slope area in the Andaman Sea. The maritime regime of the Andaman Sea contains internal solitary waves of extraordinary amplitude (>60 m). A group of LAIW in the chosen area of the Andaman Sea normally propagates eastward (as presented in Figure

1). In the place of wave shoaling the bottom topography has several

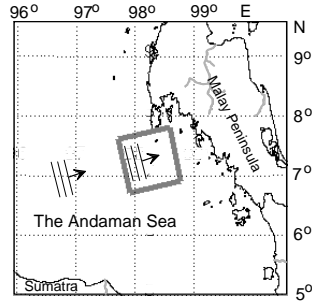


Figure 1: The fragment of the Andaman Sea with the gray rectangle showing the studied area.

headlands and canyons so that some 3D effects of wave-bottom interaction may develop in the swash zone. Far from the shelf break where the packet of LAIW is located at isobaths 300-400 m, the signature of the waves presents parallel lines. This study was motivated by the intention to understand the 3D dynamics of oceanic internal waves at the more critical stage of their evolution, viz. disintegration, breaking and associated turbulent mixing.

Model results

Figure 2 represents a series of the sea surface topography produced by propagating a LAIW of depression with amplitude of 80 m at different stages of its shoaling. This signature is overlapped with the bottom topography. The black color corresponds to the free surface elevations produced by the internal waves of depression, whereas the white color represents the position of the negative free surface displacements generated by the internal waves of elevation. The gray background was chosen as an undisturbed zero level.

The white thin line adjoining the black strip in Fig. 2a indicates that the trailing edge of the propagating LAIW (initially 2D wave) starts to evolve over the local topography obstruction in the area where the water depth is less than 250 m. One hour later (Fig. 2b) the surface signature of the propagating LAIW reveals a remarkable spatial anisotropy which is getting stronger over time. It is clear that the wavelength of the LAIW does not remain constant along the wave front. Note also that a series of secondary dispersive waves starts to evolve at the trailing edge of the LAIW in the shallow water

zone (find alternative white and black strips accompanying the trailing edge of the internal wave). This dispersion is getting stronger over time, and the dispersive wave tail occupies gradually increasingly larger areas (compare Fig. 2b and 2c).

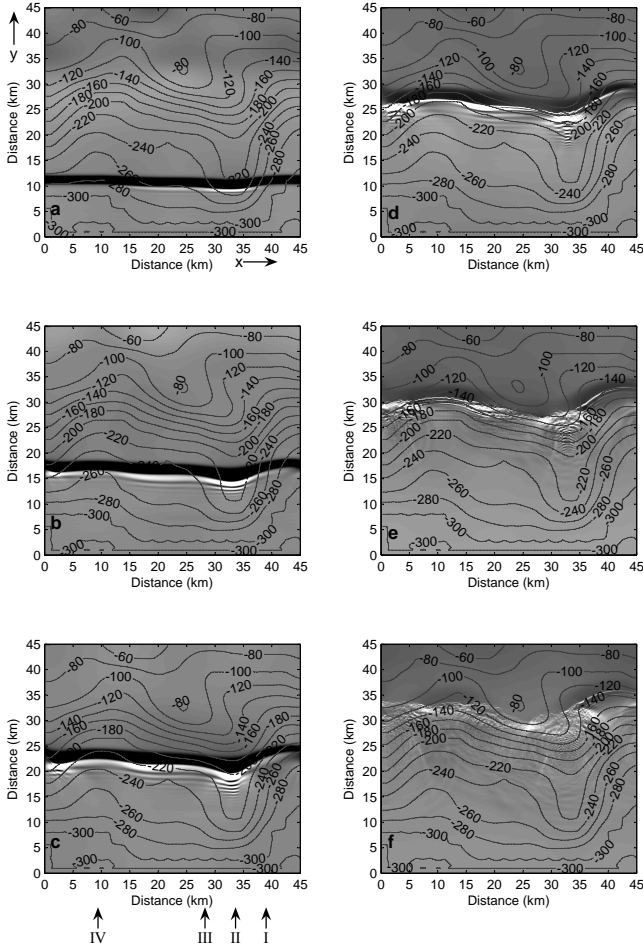


Figure 2: Sea surface topography produced by a LAIW at different stages of shoaling: (a) $t = 1$ h 6 min; (b) $t = 2$ h 13 min; (c) $t = 3$ h 20 min; (d) $t = 4$ h 26 min; (e) $t = 5$ h 33 min; (f) $t = 6$ h 40 min.

In addition to dispersion, the wave refraction is also seen in Fig. 3 because various fragments of the LAIW propagate in different background conditions. As a result, the wave front is distorted, and the curvature of the wave front is dramatically increased over time.

The final stage in the process of wave transformation is the wave breaking. Wave disintegration can be traced in Fig. 2 starting from panel d. The latter shows the initial stage of the LAIW destruction, which is mostly completed one hour later (see Fig. 2 e). Figure 2 f shows that the propagating wave is involved in breaking event except of the area at the right periphery of Figure 2 (between $x=35$ and $x=45$ km) where white strips can be treated as evidence of the changing polarity of incident LAIW.

It is clear that the wave refraction in the 3D case leads to the localized changes in the curvature of the wave fronts. This effect, in turn, may cause the energy focusing in the places of localized bottom obstacles where wave fronts are usually concave and as a result of this fact the energy flux is directed towards the centre of curvature. Such features of the oceanic bottom topography like banks or bottom headlands may work as “optical lenses” focusing the energy. In the opposite case of convex configuration of wave pattern the density of wave energy is normally less than that in the initial plane wave. An answer can be found from the comparison of 2D and 3D cases presented in Figure 3.

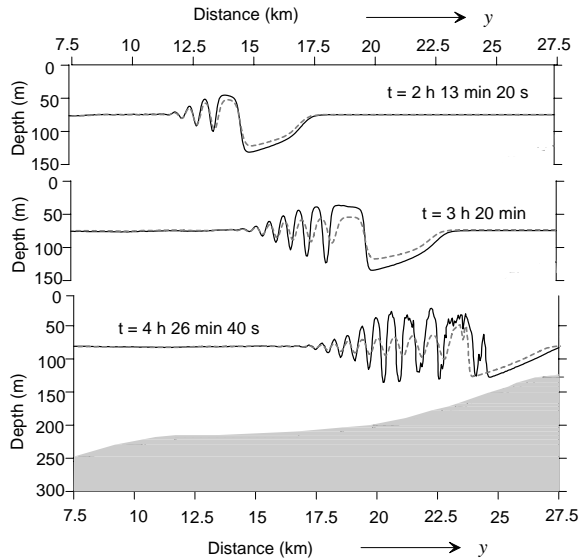


Figure 3: Time series showing the evolution of a LAIW in section II (Fig. 2). Solid and dashed lines represent 3D and 2D model results.

In the 2D modeling the bottom profile was the same as in sections II (see Fig. 2) but without alongshore variations of bottom to-

pography. We restrict our analysis considering only one isopycnal, $\rho(z) - \rho(0) = 4 \text{ kg m}^{-3}$, which makes our conclusion more obvious. The fact that the 3D wave has an excess of energy along cross-section II in comparison with the 2D counterpart is evident in Fig. 3. The discrepancy between 2D and 3D waves becomes apparent from the moment when the wave front starts to distort due to refraction in the area of the bathymetry adjacent the headland. This discrepancy between 2D and 3D wave profiles accumulates over time as long as the wave front is getting more concave. From the comparison of the solid and dashed lines it is seen that the difference in wave amplitude is almost twofold (see wave profiles at $t=4 \text{ h } 26 \text{ min}$). It is expected that the difference in wave energy is fourfold.

Figure 4: (a) Sea surface topography produced by a shoaling LAIW overlaid with bathymetric map. (b) Dependence of the total wave energy integrated over (y, z) on the x -coordinate. The energy is normalized by its initial value at $t=0$.

An opposite process occurs in cross-section III where the shoaling 3D internal wave loses more energy in comparison with 2D wave. The front of the 3D wave in this section is convex due to refraction (see Fig. 2) which leads to the wave scattering and hence to the decrease of energy density (or energy flux) in this section.

Figure 4 shows the distribution of the total wave energy, $E(x, t)$ (kinetic and available potential energy) integrated across the wave front (across the shelf, in fact) in section (x, z) normalized by its initial value, E_0 , calculated at $t = 0$. The upper panel showing the sea surface elevation of the LAIW at $t = 3 \text{ h } 20 \text{ min}$ with overlaid bottom topography is presented here for better illustration of the effect of wave refraction. The initial normalized value of energy is shown by the horizontal dotted line $E/E_0 = 1$.

The analysis of the $E(x, t)/E_0$ profiles taken at different moments of wave shoaling reveals an effect of redistribution of wave energy along the wave front. The peaks marked by letters A, B and C identify the area with an excess of wave energy in comparison with its initial value. As it is clear from Figure 4, the energy accumulates over time in the region of wave focusing. Scrutiny of the $E(x, t)/E_0$ curves and their correlations with the bottom topography indicates that the energy is accumulated in the areas of headlands where the wave front has a concave profile due to refraction. We can expect also that the energy focusing must be more effective at locations with larger bottom curvature (the energy peak over headland C is larger than that in areas A and B).

Conclusions

Many general features of wave shoaling in three dimensions look similar to those occurring in a 2D case. This relates first of all to the qualitative behavior of LAIWs over an inclined bottom. Wave disintegration, steepening and breaking may be described in terms of 2D waves. However, the 3D process of wave shoaling differs from a 2D evolution in many quantitative characteristics which have some important implications. First of all, it was found that the process of wave refraction developing in the areas of local bottom elevations or depressions in a 3D case produces concave or convex fragments of the wave fronts. This, in turn, leads to the transverse redistribution of energy along the wave fronts. Scrutiny of the energy characteristics of the propagating LAIWs has shown that concave wave fragments work as optical lenses focusing the wave energy to the centers of curvature. This effect, being less remarkable for small-amplitude waves, is highly important for LAIWs. Indeed, in a shallow water zone where LAIWs have their amplitude close to the limiting value, the breaking event develops faster if there is an extra source of energy. Wave focusing provides such an extra source. In a general oceanographic context, it should be expected to find spots of higher levels of turbulent kinetic energy (TKE) in the areas of local banks and headlands. The situation with bottom depressions is quite opposite: these areas should be potential places with low level of TKE.

BAEUERLE, E. ¹

The sound of troubled water: Vibrations of and in spherical shells partly filled with water

¹ *Moislinger Wasseransichten
moiwa oHG, Moislingen 4,
21369 Nahrendorf, Deutschland.
E-mail: erich.baeuerle@t-
online.de*

Abstract

Draw a bow across the string of a violin, pluck it or strike it, and the vibrating string will exert forces on the bridge that set the body into vibration, and the body radiates sound. Strike the edge of a shallow spherical shell which is partly filled with water and you will get the impression of a sharp, metallic tone that dies out quickly, followed by the slowly decaying hum tone. That sound is radiated normal to the vibrating surfaces of the shell where it is not covered by water.

The sound of the shell is very much dependent on the size, shape, and hardness of the mallet. In addition, it depends on the size of the puddle made up by the water which is filled into the bowl. That means, that fine tuning can be done by adjusting the water level.

To compute the sound signals of the shell in the case of coupling between the fluid and the shell it is reasonable to solve an eigenvalue equation for the resonance modes of the fluid-shell system which is nonlinear. The resonance frequencies have an imaginary part which describes the damping of each mode. These damping factors are proportional to the radiation of the modes in the fluid (Filippi et al. 2001). If the accelerations normal to the vibrating surface of the shell get larger, capillary waves appear on the free surface. The resulting patterns resemble steep standing two-dimensional Faraday waves (Jiang et al. 1996). Above a certain critical value the water surface may get unstable, what enables droplets to be ejected from the free-surface wave crests some distance into the air. We hear the superposition of the sound of the shell and the splash of the plunging water drops.

As the amplitudes of the vibrations of the shell are comparable to the order of its thickness typical non-linear behaviour can be observed, such as energy exchange between modal configurations and generation of harmonics of the fundamental frequency.

Another mechanism which demonstrates the effects of the water loading on the modal frequencies becomes audible when the water

in the shell is sloshing periodically with one (or several) of its free oscillations (seiches). The sound of the vibrating shell is modulated synchronously with the local falling and rising of the water level. The just mentioned findings will be performed on a 1 m shell in order to stimulate the perception by our senses.

References

- JIANG, L., TING, C.-L., PERLIN, M. & SCHULTZ, W.W.. 1996. Moderate and steep Faraday waves: instabilities, modulation and temporal asymmetries. *J. Fluid Mech.*, 329: 275 - 307.
- FILIPPI, P., HABAULT, D., MATTEI, P.O. & MAURY, C., 2001. The role of the resonance modes of the response of a fluid-loaded structure. *Journal of Sound and Vib.*, 239: 639 - 663.

2 Bubbles

BRYANT, L.¹ & LITTLE, J.¹

The Impact of Hypolimnetic Oxygenation on Oxygen, Iron and Manganese Cycling at the Sediment-Water Interface

¹ *Virginia Tech, Civil and Environmental Engineering, 418 Durham Hall, Blacksburg, Virginia 24061-0246 U.S.A.*
E-mail: lebryan1@vt.edu
jcl@vt.edu

Abstract

Aquatic ecosystems, drinking water quality and hydropower plants are all negatively impacted by depleted levels of dissolved oxygen (DO). Hypolimnetic oxygen depletion may result in the release of iron (Fe) and manganese (Mn) from the sediments, thereby decreasing water quality and increasing drinking water treatment costs. To address these issues, hypolimnetic oxygenation diffuser systems are being used increasingly by drinking water utilities to replenish DO while preserving stratification.

We are examining how the cycling of DO, Fe and Mn at the sediment-water interface is impacted by diffuser-induced variations in turbulence and DO levels in the water column. Experiments were performed using a network of measurements at a drinking-water-supply reservoir equipped with an oxygenation diffuser system in Virginia, USA. In-situ porewater analyzers (“peepers”) were used to obtain soluble (<0.45 micron) Fe and Mn profiles. A profiling lander is currently being used in-situ to track how DO, temperature, pH and redox potential are changing at the sediment-water interface as a function of oxygenation. Fe²⁺ and Mn²⁺ microelectrode and DO microsensor profiles of sediment cores are also being obtained in coordination with peeper deployments and lander measurements. Preliminary data show that sediment-water fluxes of DO, Fe and Mn vary significantly as a result of diffuser operations. Our results indicate that hypolimnetic oxygenation may be successfully used to improve drinking water quality by increasing DO levels and subsequently decreasing Fe and Mn levels within the bulk water column. This research will be used to gain further understanding of how DO and turbulence levels impact mechanisms of oxygen

transport, changes in sediment microbial populations and corresponding sediment-water biogeochemical fluxes.

Introduction

Hypolimnetic oxygenation systems (e.g., bubble-plume diffusers) are being used increasingly by drinking water and hydropower utilities to replenish DO while preserving stratification (McGinnis et al. 2001; Beutel 2003; Singleton and Little 2006; Singleton et al. 2007). One of the primary goals of hypolimnetic oxygenation systems from a drinking-water standpoint is to suppress the flux of Fe and Mn by increasing the oxidized zone within the sediments (Beutel 2003). It is therefore important to understand the mechanisms of oxygen transport between the water column and the sediments. As DO levels in the reservoir water column increase due to hypolimnetic oxygenation, soluble, reduced metals will oxidize and precipitate out. As these oxidized particles approach the sediment surface, where oxygen conditions may be quite variable, potentially significant changes in oxygen consumption rates and corresponding metal fluxes at the sediment-water interface may occur (Zhang et al. 1999). Enhanced fluxes of soluble metals out of the sediment, which have been observed as a result of diffuser activity in preliminary data, may also oxidize upon reaching the oxic zone, further adding to changes in sediment composition and oxygen consumption processes at the sediment-water interface. Little work has been done thus far to quantify the impact of diffuser activity on SOD, oxygen penetration into sediments, soluble chemical fluxes at the sediment-water interface and the corresponding drinking water quality. Understanding how variations in influential parameters such as oxygen concentrations and turbulence levels affect sediment-water fluxes is crucial for accurately quantifying SOD, optimizing water quality and successfully managing lakes and reservoirs (Beutel 2003; Lorke et al. 2003; Higashino et al. 2004).

Experimental Site and Methods

This research focuses on how the cycling of DO, Fe and Mn at the sediment-water interface is impacted by diffuser-induced variations in turbulence and DO levels in the water column. Experiments were performed using a network of measurements at Carvin's Cove (CC), a drinking-water-supply reservoir equipped with an oxygenation diffuser system in Virginia, USA. In-situ porewater analyzers ("peepers") were used to obtain soluble Fe and Mn profiles and to determine how Fe and Mn fluxes vary temporally as a result of diffuser operations (Hesslein 1976). DO microsensor (Unisense A/S OX-100) profiles of sediment cores were obtained in coordination with peeper measurements. Fluxes of DO, soluble Fe

and Mn across the sediment-water interface were then calculated from DO, Fe and Mn profiles using Fick's Law for diffusion within the sediment (Lavery 2001).

Results

Results support the primary research goal of using oxygenation diffuser systems to improve drinking water quality by increasing DO levels and decreasing Fe and Mn levels within the reservoir prior to traditional treatment at the treatment plant. Levels of total Fe and Mn in the water column are found to decrease in conjunction with diffuser activity (Figure 1), thus minimizing treatment required at the plant. In addition to directly impacting the water column, results suggest that concentrations of DO, Fe and Mn at the sediment-water interface and within sediment porewater also vary significantly as a result of diffuser operations. DO microsensor profiles of sediment cores show that the sediment oxic zone increases in response to diffuser-induced increases in turbulence and DO in the water column immediately (within 5 cm) of the sediment surface (Figure 2).

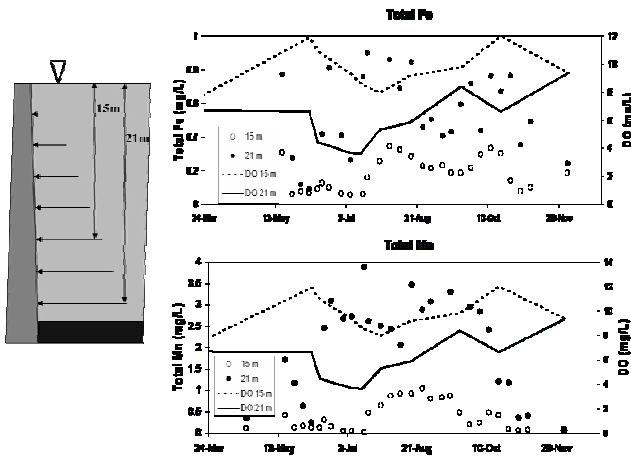


Figure 1 Trends in total Fe and Mn levels in the water column during 2006 diffuser operations at Carvin's Cove. Data from two depths (15 m and 21 m) are shown. The seven depths at the dam at which water can be drawn for treatment are shown by arrows in the figure on the left. Note that an increase in Fe and Mn is seen at both depths when DO is low (during period when diffusers are turned off) and a significant decrease in Fe and Mn is seen when DO is elevated (when diffusers are in operation). Data courtesy of P. Gantzer.

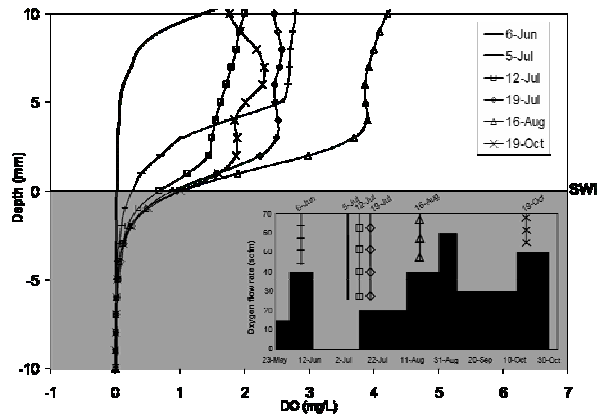


Figure 2 Changes in sediment core DO profiles at the sediment-water interface (SWI) as a function of 2006 diffuser operations and the corresponding oxygen flow rate. The solid-line profile (5-Jul) was the sole profile obtained during the period when both diffusers were turned off, showing anoxic water above the sediment and no DO penetration into the sediment.

Data from peeper profiles suggest that diffuser operations may have a strong impact on suppression of Fe and Mn fluxes out of the sediment via increasing the sediment oxic zone (Figure 3). While only a minor increase in Fe is seen in the water overlying the sediment and within the sediment porewater during the period when the diffusers were turned off, a significant increase in Mn is seen during this period. Mn is more easily reduced than Fe (Scholkovitz 1985), thus Mn may be released more quickly from the sediment (while Fe is more easily retained) when the oxic zone is decreased during low DO conditions (Figure 2).

Future Work

In-situ lander (Unisense MP4) experiments are currently being performed to track how DO, temperature, pH and redox profiles across the sediment-water interface change as a function of oxygenation. Future work will also include obtaining profiles of reduced Fe²⁺ and Mn²⁺ using ion-selective microelectrodes and correlating these profiles with lander and peeper data. Results from an initial trial experiment performed at CC in 2006 with these ion-selective microelectrodes were quite promising. Biochemical studies of changes in the sediment microbial populations as a function of diffuser operations, additional analyses of Fe and Mn fluxes using sediment trap data and the development of a computer model that will enable accurate predictions of spatial and temporal variations in biogeochemical fluxes will also be performed.

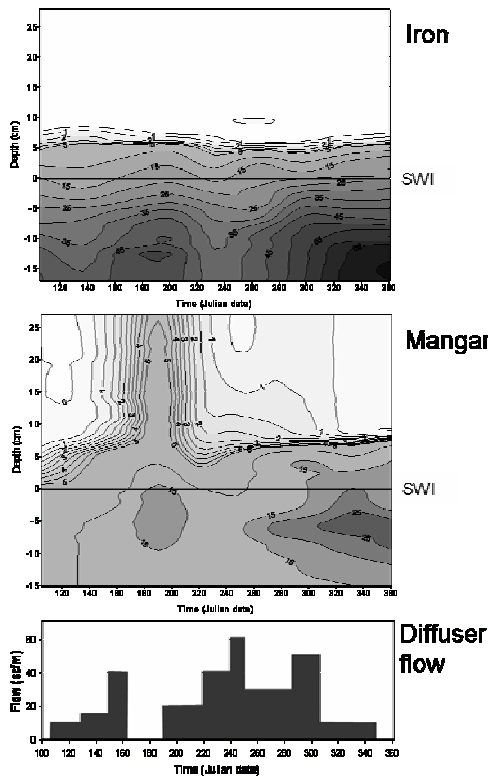


Figure 3 Temporal variations in soluble Fe and Mn at the sediment-water interface (SWI) in correlation with 2006 diffuser operations. Fe and Mn data shown collected in-situ with peepers. Note slight increase in Fe and significant increase in Mn at the SWI and in water immediately over sediment during period when diffusers turned off (Julian dates 166-193 (15-June thru 12-July)), suggesting fluxes of Fe and Mn out of the sediment into the water column increase during the period when diffusers turned off.

Conclusions

Our results indicate that hypolimnetic oxygenation may be successfully used to improve drinking water quality by increasing DO levels and subsequently decreasing Fe and Mn levels within the bulk water column and suppressing fluxes at the sediment-water interface. Results will be used to optimize the operation of hypolimnetic oxygenation systems and to specifically improve the management of and resulting raw water quality in CC. While this research focuses on diffuser-induced changes in DO and turbulence levels, variability in these controlling processes may also be induced naturally (e.g., via reservoir overturn, wind-induced seiching, and hydraulic inputs during storm events); hence, results of this research should also be applicable on a much broader scale.

Acknowledgements

We acknowledge financial support from the National Science Foundation (NSF IGERT Program), the Environmental Protection Agency (EPA STAR Doctoral Fellowship), and the Western Virginia Water Authority.

References

- BEUTEL, M. 2003. Hypolimnetic anoxia and sediment oxygen demand in California drinking water reservoirs. *Lake and Reservoirs Mgmt.* 19(1).
- HESSLEIN, R. 1976. An In-situ sampler for close interval porewater studies. *Limnol. Oceanogr.* 21(6): 912-914.
- HIGASHINO, M, GANTZER, C ET AL. 2004. Unsteady diffusional mass transfer at the sediment/water interface: Theory and significance for SOD measurement. *Wat. Res.* 38(1): 1-12.
- LAVERY, P, OLDHAM, C, GHISALBERTI, M. 2001. "The use of Fick's First Law for predicting porewater nutrient fluxes under diffusive conditions." *Hydrol. Process.* 15: 2435-2451.
- LORKE, A, MULLER, B ET AL. 2003. Breathing sediments: The control of diffusive transport across the sediment-water interface by periodic boundary-layer turbulence. *Limnol. Oceanogr.* 46(6): 2077-2085.
- MCGINNIS, D, LITTLE, J ET AL. 2001. Hypolimnetic oxygenation: coupling bubble-plume and reservoir models. *Asian WATERQUAL, IWA Regional Conf., Japan.*
- SINGLETON, V, GANTZER, P ET AL. 2007. Linear bubble plume model for hypolimnetic oxygenation: full-scale validation and sensitivity analysis. *Water Resour. Res.* 43(W02405).
- SINGLETON, V, LITTLE, J. 2006. Designing hypolimnetic aeration and oxygenation systems: a review. *Environ. Sci. Technol.* 40: 7512-7520.
- SCHOLKOVITZ, E. 1985. Redox-related geochemistry in lakes; alkali metals, alkaline-earth elements, and ¹³⁷Cs. In: STUMM, W (ED). *Chemical Processes in Lakes.* Pp. 119-138, John Wiley & Sons, New York.
- ZHANG, H, DAVISON, W ET AL. 1999. Remobilisation of major ions in freshly deposited lacustrine sediment at overturn. *Aquat. Sci.* 61: 354-361.

**SINGLETON, V.L.¹ & MCGINNIS,
D.F.², & LITTLE, J.C.¹**

**Coupled bubble-
plume/reservoir model for
hypolimnetic oxygenation:
Full-scale evaluation**

¹ *Department of Civil &
Environmental Engineering,
Virginia Tech, Blacksburg, VA,
24061-0246 USA. E-mail:
vickies@vt.edu, jcl@vt.edu*

² *Surface Waters - Research and
Management, Federal Institute
for Environmental Science and
Technology (Eawag),
Kastanienbaum, CH-6047,
Switzerland. E-mail:
dan.mcginnis@eawag.ch*

Abstract

Bubble-plume diffusers are increasingly used to replenish hypolimnetic dissolved oxygen while preserving stratification. While bubble plumes are successful at adding oxygen, the added energy may induce large-scale hypolimnetic mixing. Plume-induced mixing changes the thermal structure of the reservoir, while plume performance depends strongly on the ambient density gradient. Here we account for this complex plume-reservoir interaction by coupling a bubble-plume model with an existing two-dimensional hydrodynamic and water quality reservoir model, CEQUAL-W2 (W2). To evaluate the coupled models, data were used from field-scale testing conducted in 1998 with a linear bubble-plume diffuser in Spring Hollow Reservoir, Virginia, USA. The coupled model slightly under-predicted the extent of hypolimnetic warming. Although sediment oxygen demand was estimated as a zero-order process in the reservoir model, the coupled model simulations agreed very closely with the observed increase of dissolved oxygen in the hypolimnion.

Introduction

Hypolimnetic anoxia negatively affects water quality downstream of hydropower reservoirs, the drinking-water treatment process, and

cold-water fisheries. Bubble plumes are commonly used for hypolimnetic oxygenation, which preserves stratification while adding oxygen to the deepest layer of the water body. The plume is in intimate contact with the ambient water and is strongly influenced by the prevailing thermal, and hence density, gradient. Although considerable research has been conducted on the hydraulics of bubble plumes, the first comprehensive model that included oxygen transfer was developed by Wüest et al. (1992). The incorporation of oxygen transfer is critical when pure oxygen gas is used and for deep plumes because the rapid dissolution rate has a strong influence on plume buoyancy.

While bubble plumes are successful at adding oxygen, the added energy may induce large-scale hypolimnetic mixing. Plume-induced mixing changes the thermal structure of the reservoir, and plume performance depends strongly on the ambient density gradient. The specific plume-induced mixing mechanisms need to be identified and incorporated in a coupled bubble-plume/reservoir model for successful design and operation. The only coupled model currently available (Schladow 1993) uses a one-dimensional reservoir model, focuses on destratification, and does not account for oxygen transfer within the plume. In this work, a linear bubble-plume model, which includes gas transfer, is coupled with a two-dimensional reservoir model, and the results are compared to data collected from a full-scale linear bubble-plume diffuser.

Coupled Model Components

The linear bubble plume model utilizes the discrete-bubble approach (Singleton and Little 2006) and is composed of horizontally-integrated equations based on the conservation of mass, momentum, and heat. Eight flux equations are solved simultaneously to predict water flow rate, plume temperature, oxygen and nitrogen concentration, salinity, and plume rise height. The model accounts for density stratification due to vertical temperature and salinity gradients. Entrainment is assumed to be proportional to the local plume water velocity. Bubble size varies as the bubbles rise due to expansion and dissolution, and bubble slip velocity and gas transfer coefficients are functions of bubble radius (Wüest et al. 1992). The bubble plume model equations were originally developed by Wüest et al. (1992) for a circular geometry, but were modified by McGinnis et al. (2001) for a linear geometry and further refined and validated by Singleton et al. (2007) with full-scale data over a range of gas flow rates.

The linear bubble-plume model was coupled with a reservoir model, CE-QUAL-W2 (W2) Version 3.2. W2 is a laterally-

averaged, two-dimensional hydrodynamic and water quality model that was developed by the U.S. Army Corps of Engineers (Cole and Wells 2003). In addition to hydrodynamics, W2 models basic eutrophication processes such as nutrients, algae, dissolved oxygen, organic matter, and sediment interactions. W2 includes horizontal, but not vertical momentum, and accounts for momentum transfer from inflowing branches. A principal aspect of the model is the ability to calculate the two-dimensional velocity field in stratified reservoirs. Input data required for W2 include bathymetry, initial temperature and constituent profiles, inflow and outflow data, meteorological data, hydraulic and kinetic parameters, and calibration data.

Coupling Procedure

To couple the bubble-plume model with W2, the diffuser is represented as five discrete segments in consecutive columns because its depth varies along the length. The plume model is used to compute the flow rate of ambient water entrained as the plume rises, and the flow rate and discharge depth of the water detrained at the top of the plume. Entrainment removes water of known temperature and oxygen concentration from a range of depths (Figure 1, light gray cells), while detrainment returns the total volume of entrained water at the specified discharge depth after adding the predicted mass of oxygen (Figure 1, dark gray cells). To conserve mass and heat, plume operation is simulated within W2 by using the model's pump algorithm (Cole and Wells 2003). This feature is typically used to transfer water between segments but was applied to lift water within a segment to simulate plume-induced mixing. The pump discharge depth, influent depth range, and flow rate are calculated by the plume model. The mass of dissolved oxygen added by the plume is simulated in W2 by five tributaries, which have assumed nominal flow rates and dissolved oxygen concentrations calculated from the predicted oxygen addition rates for each diffuser segment. The temperatures of the small tributaries (plume detrainment) are also calculated by the plume model.

The bubble-plume/W2 manual coupling procedure was completed as follows. Using the initial reservoir conditions prior to diffuser startup, the plume model was run for each of the five diffuser segments, accounting for varying diffuser elevations. Using the five sets of predicted plume data, the coupled plume/W2 model was then run for six hours. The predicted ambient temperature and dissolved oxygen profiles obtained at the end of this six-hour period were then used as input boundary conditions for the plume model to generate a new set of predicted plume entrainment and detrainment

data for each plume segment. The entire procedure was repeated in six-hour increments until the end of the diffuser operating period.

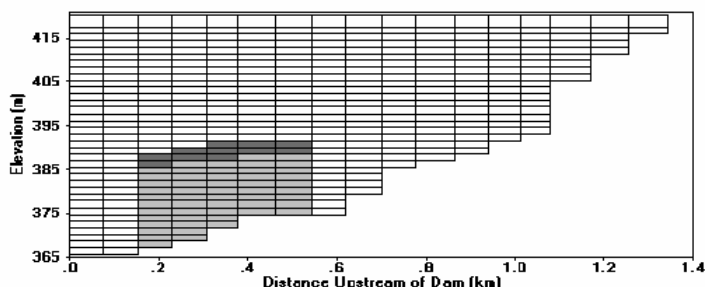


Figure 1. Longitudinal cross-section of grid representation for Spring Hollow Reservoir, Virginia, USA in CE-QUAL-W2. Light and dark gray cells indicate regions of linear bubble-plume entrainment and detrainment, respectively for coupled model.

Site Description and Field Data Collection

Data were collected during operation of a full-scale linear diffuser installed in Spring Hollow Reservoir (SHR), Virginia, USA. SHR is a small side-stream reservoir that is supplied by water pumped from the Roanoke River. The reservoir is a drinking water source and is managed by the Western Virginia Water Authority. Table 1 provides the diffuser operating parameters during testing with compressed air from 28 September–13 October 1998. Temperature and dissolved oxygen profiles were collected adjacent to the dam, approximately 75 m downstream of the end of the diffuser. During testing, no water was pumped from the river into the reservoir, thereby simplifying reservoir hydrodynamics. The primary hydraulic forcing during testing was diffuser operation.

Table 1. Conditions for coupled model application for Spring Hollow Reservoir, Virginia, USA.

Parameter	Value
Diffuser length (m)	360
Gas flow rate (Nm ³ /hr) ^a	43
Average diffuser depth (m)	49
Reservoir maximum depth (m)	55
Reservoir surface area (10 ⁶ m ²)	0.38
Reservoir total volume (10 ⁶ m ³)	7.4

^a1 Nm³ denotes 1 m³ of gas at 1 bar and 0 °C.

Coupled Model Application

The coupled bubble-plume/W2 model accurately simulated the evolution of temperature profiles and warming as a result of plume operation (Figure 2, left). The mixing energy added by the plume is sufficient to erode the thermocline throughout the entire diffuser

operating period. The model also reasonably simulates the decreased mixing and warming below the diffuser elevation for October 2–9. The mixing induced by the plume caused the hypolimnion to become more isothermal and increased the temperature gradient at the top of the hypolimnion. The hypolimnetic temperature was increasingly under-predicted as the run progressed, being slightly less than observed values by October 9. This is likely due to under-prediction of mixing by W2. Because W2’s pump algorithm was used to model the induced plume flow rate within each segment, each outflow/pump influent was treated as a lateral withdrawal. Therefore, the momentum associated with each outflow was not conserved (Cole and Wells 2003).

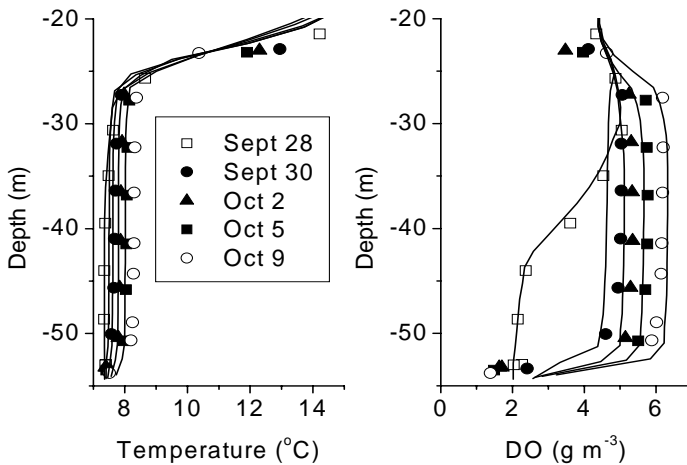


Figure 2. Predicted and observed hypolimnetic temperature and dissolved oxygen profiles during linear diffuser operation during 1998 in Spring Hollow Reservoir, Virginia, USA. Predicted profiles by coupled bubble-plume/CE-QUAL-W2 model.

The coupled model reproduces the progression of dissolved oxygen increase in the hypolimnion well, with especially good agreement at the end of the diffuser operating period on October 9 (Figure 2, right). The bubble-plume model calculated essentially 100 percent oxygen transfer for the entire duration of the diffuser test. Hypolimnetic dissolved oxygen is slightly under-predicted on Day 273, which may be related to the default values in W2 for longitudinal eddy viscosity ($1 \text{ m}^2 \text{ s}^{-1}$) and diffusivity ($1 \text{ m}^2 \text{ s}^{-1}$). As mentioned previously, profiles were measured approximately 75 m longitudinally downstream of the end of the linear diffuser. The coupled model provides reasonable results for the persistent low dissolved oxygen concentrations below the diffuser depth, but the dissolved oxygen immediately above the sediments was over-predicted towards the end of diffuser operation. One possible

explanation for this may be underestimation of the zero-order sediment oxygen demand value used for the simulations. Additionally, vertical mixing could have been overestimated by W2, mixing higher dissolved oxygen water from above into the region below the diffuser depth. This effect is also seen in the coupled model's overestimation of temperature directly above the sediments for the same testing days (Figure 2, left).

Future Work

Preliminary coupling of the linear bubble-plume model with W2 produced encouraging results. Therefore, the coupled model will be more extensively evaluated using additional data collected under various reservoir and diffuser operating conditions. The coupling procedure will be further refined to more accurately represent the interaction between the bubble-plume and the reservoir. Coupling of the plume model with W2 holds promise as an engineering tool for design and evaluation of hypolimnetic oxygenation systems.

Acknowledgements

Financial support was provided by the U.S. National Science Foundation and Western Virginia Water Authority.

References

- COLE T M and WELLS S A. 2003. *CE-QUAL-W2: A Two-Dimensional, Laterally Averaged, Hydrodynamic and Water Quality Model, Version 3.2*. U.S. Army Engineering and Research Development Center, Vicksburg, MS.
- MCGINNIS D F, LITTLE J C and WÜEST A. 2001. *Hypolimnetic oxygenation: Coupling bubble-plume and reservoir models*. Asian Waterqual 2001: First IWA Asia-Pacific Regional Conference, Fukuoka, Japan. 12-15 Sept.
- SCHLADOW S G. 1993. Lake destratification by bubble-plume systems: Design methodology. *J. Hydraul. Eng.* 119: 350-368.
- SINGLETON V L and LITTLE J C. 2006. Designing hypolimnetic aeration and oxygenation systems - A review. *Environ. Sci. Technol.* DOI:10.1021/es060069s.
- SINGLETON V L, GANTZER P and LITTLE J C. 2007. Linear bubble plume model for hypolimnetic oxygenation: Full-scale validation and sensitivity analysis. *Water Resour. Res.* 43:
- WÜEST A, BROOKS N H and IMBODEN D M. 1992. Bubble plume modeling for lake restoration. *Water Resour. Res.* 28: 3235-3250.

MCGINNIS, D.F.¹ & LORKE, A.², &
WÜEST, A.¹ & CRIMEA PARTNERS

Methane transport in the Black Sea: Turbulent fluxes and rising bubbles

¹ *Eawag, Kastanienbaum, CH-6047, Switzerland. E-mail: dan.mcginis@eawag.ch*

² *Limnological Institute, University of Konstanz, Mainaustrasse 252, D-78464 Konstanz, Germany.*

Abstract

The Black Sea's contribution to the global methane flux is a growing concern. Subsurface methane is released into the water column from destabilizing methane hydrates, mud volcanoes and other active seep areas. Vertical methane transport can occur due to bubble transport, methane-enriched plumes and turbulent diffusion. The combination of measurements, data analysis and modeling reveal that the amount of methane transported to the surface from plumes and gas bubbles is very low, and only from bubble release sites which are shallower than 100 m. Furthermore, the low diffusivities and relatively high methane oxidation rates hinder large methane contributions to the atmosphere. Overall, the Black Sea's atmospheric methane flux is thought to be very minor (on the order of hundreds of Mg yr⁻¹) compared to a worldwide release of 500 Tg yr⁻¹.

Introduction

The Black Sea is the largest anoxic water body in the world. Permanent stable stratification has led to anoxia over the past several thousand years, with the aerobic surface waters separated by a permanent chemocline at 100 to 200 m depth. Mixing in the Black Sea is important for upward fluxes of dissolved nutrients (productivity) and methane (atmospheric escape).

Methane has 21 to 25 times the global warming potential as the same mass of carbon dioxide [IPCC, 1996]. Therefore, because of the large pools of methane stored in the water and sediment, the Black Sea's atmospheric methane contribution has become of

interest. The growing concern is mainly due to the suspected dissociation of methane hydrates resulting from global warming. Due to the rapid vertical transport of methane by bubble ebullition or plumes, the fear is that this contribution feeds the global methane budget, creating a feedback loop which further destabilizes the hydrates. The suggestion that methane reaches the surface is supported by the observation by local residents on the Crimean Peninsula of a “burning sea” after an earthquake, thought to be the result of mud volcano methane eruption.

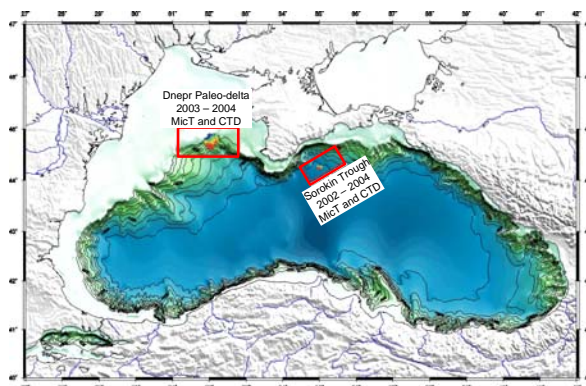


Figure 1 Study sites on the Black Sea.

To resolve the relevant methane transport mechanisms, measurements were collected within the EU-funded CRIMEA project during three cruises aboard the *RV Professor Vodyanitskiy* between May and June 2003 to 2005 (study locations shown on Figure 1). Vertical diffusivities were determined using dissipation estimates and Thorpe scale analysis from temperature microstructure profiles and CTDs obtained on the shelf along the Crimea Peninsula (100 m depth) and at the Dvurechenskiy mud volcano area (DMV; Sorokin Trough; 2000 m depth). These are then compared to a methane bubble transport model to determine relative time scales.

Results

In the following, we present the results of turbulent diffusion estimates from the Black Sea Shelf (Dnepr Paleo-delta), and the deep water (Sorokin Trough). The former is estimated from microstructure profiles while the latter from CTD profiles. We also present evidence of large-scale mixing events in the deep-water.

Mixing on the shallow shelf: Figure 2 shows dissipation estimates from 44 temperature microstructure profiles obtained in 2004. Data were fitted to the theoretical Batchelor spectrum to estimate the

dissipation rate of turbulent kinetic energy, which in turn was used to calculate the turbulent diffusivity. On the shelf, dissipations ranged from $10^{-8} \text{ W kg}^{-1}$ at the boundaries to $10^{-11} \text{ W kg}^{-1}$ in the interior, with the dissipation resembling a somewhat parabolic shape (Figure 1, right). It is interesting to note that the dissipation structure is very similar to profiles obtained in Lake Alpnach (Switzerland; Figure 1, left), with turbulence increasing towards both the surface and bottom boundary layers. Turbulent diffusivity in the Black Sea was calculated to be between $10^{-5} \text{ m}^2 \text{ s}^{-1}$ at the boundaries to near-molecular in the interior.

In context of methane transport, this implies that methane (or other constituents) dissolved below 40 m would only be transported vertically at rates approaching molecular diffusion for heat (pseudo vertical velocity as low as $\sim 0.1 \text{ m yr}^{-1}$ at 40 m). It should be noted, however, that vertical transport would be much faster at the slope (sediment-water interface) boundaries.

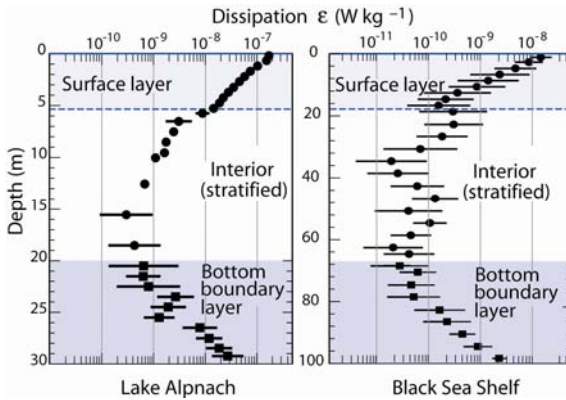


Figure 2 Comparison of dissipation profiles from the freshwater Lake Alpnach [Wüest et al., 2000] and the Black Sea shelf. Note that dissipation is about 1 order of magnitude lower in the Black Sea.

As a rough estimate of basin-wide diffusive methane emissions, if we assume a vertical diffusivity $K_z = 1 \times 10^{-6} \text{ m}^2 \text{ s}^{-1}$. The upward flux of dissolved methane into the surface 40 meters (surface mixed layer) can then be calculated as

$$F_{\text{CH}_4} = A_z K_z \frac{\partial C_{\text{CH}_4}}{\partial z},$$

where A_z is the area of the Black Sea at 40 m, and the right-hand term is the methane concentration gradient. Using a concentration gradient of 0.3 nM m^{-1} yields a basin-wide vertical flux in the surface layer of 70 Mg yr^{-1} ($1.6 \times 10^{-4} \text{ g m}^{-2} \text{ yr}^{-1}$).

Mixing in the deep-water: Thorpe scale analysis [Thorpe, 1977] was performed on CTD data obtained at Sorokin Trough near the DMV in 2002 (profile from O. Schmale, personal communication), 2003 and 2004. The resulting profile can then be used to locate turbulent overturns and associated small- to large-scale temperature inversions (Figure 3). Thorpe displacement analysis of data from the deep site shows substantial (over 100 m depth) overturns at around 1500 m depth in 2003 and up to 50 m at ~1250 m depth in 2004. However, during 2002, much smaller overturns (< 25 m) were observed. These 2002 overturn sizes and distributions are consistent with overturn lengths from off-seep, reference sites (not shown).

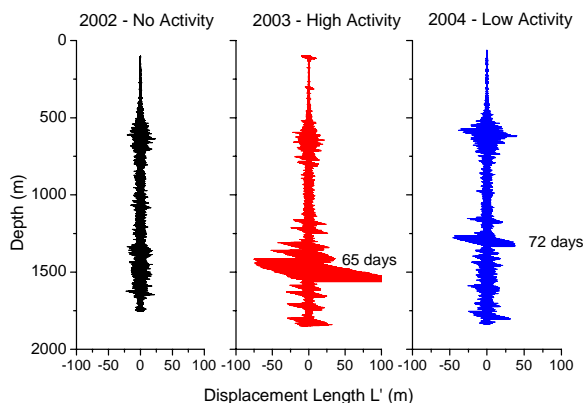


Figure 3 Thorpe analysis from profiles obtained over Dvurechenskiy mud volcano for three different cruises.

Because there are no other sources of energy input at this depth, one likely explanation for these significant overturns is plume-induced mixing, however, from this analysis it is still inconclusive which buoyancy source(s) drives the plume (e.g. heat flux or bubbles). These temperature inversion features correspond well with hydroacoustic flares (thought to be methane bubbles) observed over DMV [McGinnis *et al.*, 2006]. The observed flares, accompanied by the large scale overturns, seem to indicate fluid expulsion from the DMV, or bubble-induced upwelling (plumes).

Diffusivities are estimated by assuming the Thorpe length scale is equal to the Ozmidov length scale. The diffusivities can then be calculated as

$$K_Z = \gamma_{\text{mix}} L_T^2 N$$

with $\gamma_{\text{mix}} = 0.15$ and N^2 , the stability frequency, shown on Figure 4.

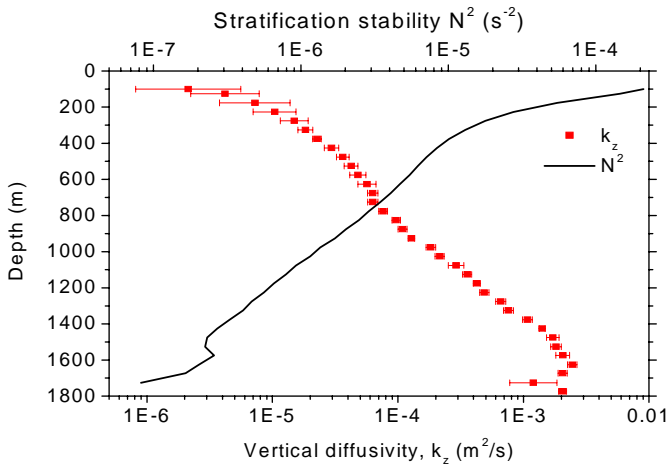


Figure 4 Calculated diffusivity and stability profile for the Black Sea deep water.

The stratification stability N^2 (Figure 4) indicates that the interior is surprisingly well mixed, and very weakly stratified. The bottom ~300 meters (not shown) is well mixed owing to the presence of the convective bottom boundary layer. Due to the weak stratification, plumes with relatively low buoyancy driving forces can rise fairly high in the water column. However, methane plume releases reaching the surface and causing the “burning sea” effect would need to come from “catastrophic eruptions” with high dissolved and/or gaseous methane concentrations (see Outcome).

Outcome

Preliminary conclusions indicate that methane plumes from deep water sources, while perhaps strong (e.g. up to $\sim 0.025 \text{ Tg yr}^{-1}$), still stop well below the surface where the methane is oxidized to CO_2 before reaching the atmosphere (methane residence time due to oxidation is approximately 1 – 2 years; *Schmid et al., 2007*).

For a catastrophic deepwater release to occur, the plume model predictions indicate that a short term eruption of $16,000 \text{ kg s}^{-1} \text{ CH}_4$ (100 m radius source size) would transport 30% of methane (both gaseous and dissolved) to the surface [*Kourtidis et al., 2006*]. Similarly, a strictly thermal fluid outburst (no methane) of the same source size would only need to be $25 \text{ }^\circ\text{C}$ warmer than the local ambient temperature to also reach the surface.

While bubble methane transport (25 cm s^{-1}) is much more efficient than turbulent transport ($\sim 0.1 - 1 \text{ m yr}^{-1}$), methane can reach the surface only at shallow sites ($< \text{about } 100 \text{ m}$), however most is dissolved and oxidized in the water column [McGinnis *et al.*, 2006]. Plume formation, while less likely in shallower regions, will also increase the amount of methane which reaches the surface due to upwelling, and may allow slightly deeper sources to reach the atmosphere.

The high oxidation rates and low diffusivities in the Black Sea lead to surface flux estimates of less than a few hundred Mg yr^{-1} , allowing us to conclude that the Black Sea is not, compared to a worldwide release of 500 Tg yr^{-1} , a significant contributor of methane to the atmosphere.

Acknowledgements

The authors express their deepest gratitude to the captain and crew of the *RV Professor Vodyanitskiy* and the CRIMEA partners (Contribution of high-intensity gas seeps in Black Sea to the methane emission to the atmosphere) project for their support. The project was supported by the EC project EVK-2-CT-2002-00162 (CRIMEA). The first author was also supported by the Swiss National Science Foundation (Grant 200020-103827.1).

References

- IPCC (1996), *Climate Change 1995: The Science of Climate Change*, 572 pp., Cambridge University Press, Cambridge and New York.
- Kourtidis, K., I. Kioutsioukis, D. F. McGinnis, and S. Rapsomanikis (2006), Effects of methane outgassing on the Black Sea atmosphere, *Atmospheric Chemistry and Physics*, 6, 5173-5182.
- McGinnis, D. F., J. Greinert, Y. Artemov, S. E. Beaubien, and A. Wüest (2006), Fate of rising methane bubbles in stratified waters: How much methane reaches the atmosphere?, *Journal of Geophysical Research*, 111(C09007), doi:10.1029/2005JC003183.
- Schmid, M., M. De Batist, N. Granin, V.A. Kapitanov, D.F. McGinnis, I.B. Mizandrontsev, A. I. Obzhirov, and A. Wüest (2007), Sources and sinks of methane in Lake Baikal - a synthesis of measurements and modeling, *Limnol. Oceanogr.*, in Press.
- Thorpe, S.A. (1977), Turbulence and mixing in a Scottish Loch, *Philosophical Transactions of the Royal Society of London Series A*, 286, 125-181.
- Wüest, A., G. Piepke, and D.C. Van Senden (2000), Turbulent kinetic energy balance as a tool for estimating vertical diffusivity in wind-forced stratified waters, *Limnol. Oceanogr.*, 45, 1388-1400.

3 Internal Mixing

**BOEHRER¹, B., C. VON ROHDEN²,
J. ILMBERGER², & M. SCHULTZE²**

Quantification of erosive processes at the halocline of a meromictic lake

¹ *Helmholtz-Zentrum für
Umweltforschung - UFZ,
Brückstraße 3a, 39114
Magdeburg, Deutschland
bertram.boehrer@ufz.de*

² *Universität Heidelberg, Institut
für Umwelphysik, Im
Neuenheimer Feld 229, 69120
Heidelberg, Deutschland, E-mail
Johann.Ilmberger@iup.uni-
heidelberg.de*

Abstract

Meromixis is preserved at constant strength, if the effects sustaining stratification and erosive processes balance each other. We consider the salinity stratification in the lakes Wallendorfer See and Rassnitzer See in the former mining complex Merseburg-Ost of the Central German mining district. Both lakes are salt lakes which have been flooded with fresh water. The resulting salinity stratification was far from steady state, and was prone to show a temporal evolution. Regular measurements of conductivity profiles could document the erosion of the halocline during the deep circulation, while during periods of thermal stratification the sharp halocline continuously smoothed by turbulent diffusive processes. In both cases, the changes in the stability can be quantified, either from the change of the density profiles (i.e. change in potential energy) or from the turbulent transport coefficients at the halocline during the stratification period. The quantification of transports during the observational period and the comparison with the remaining stability, facilitate the prediction of the further evolution of the meromixis in both lakes.

VON ROHDEN, C.¹ & ILMBERGER, J.²

Vertical Transport in a Meromictic Mining Lake Studied with a SF₆- Tracerexperiment

¹ *University of Heidelberg, Im
Neuenheimer Feld 229, 69120,
Heidelberg, Germany. E-mail:
Christoph.vonRohden@iup.uni-
heidelberg.de*

² *University of Heidelberg, Im
Neuenheimer Feld 229, 69120,
Heidelberg, Germany. E-mail:
Johann.Ilmerberger@iup.uni-
heidelberg.de*

Abstract

We investigated vertical transport and groundwater coupling in a small mining lake in Lusatia, Germany. The lake shows a stable chemical stratification at a depth of ~1.5 m resulting in meromixis. The meromixis is assumed to be established and conserved by a closed iron redox circle at the transition zone (chemocline) between the oxic epilimnion and the anoxic water body below (monimolimnion). Vertical transport was estimated by injection of a SF₆-spike at the lake bottom and monthly sampling and measurement of its vertical spreading. SF₆-concentrations measured before spiking as well as SF₆ budgeting afterwards indicate an exponential groundwater exchange time in the range of 1 year. Based on SF₆-concentration changes we calculated vertical diffusion coefficients K_z applying the flux-gradient-method. The first results suggest that the vertical exchange is constrained to the heat conduction level. Within the chemocline region, a K_z -minimum with values tending to molecular diffusion ($\sim 10^{-9}$ m²/s) becomes apparent.

Introduction

Many lakes left from open lignite mining in East Germany tend to establish specific stratification pattern. Especially meromixis caused by chemical gradients is a rather common feature among mining lakes (e.g. Böhrer et al, 1998; Stevens and Lawrence, 1998; von Rohden and Ilmerberger, 2001). Mostly, groundwater is the main

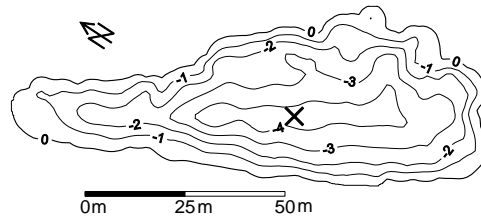


Figure 1 Lake Waldsee. Redrawn based on data from Cottbus University (BTU). The cross marks the sampling and measurement site.

source for the formation of those lakes. Consequently, filled (older) mining lakes are still recharged by groundwater, often at high rates. Due to the usually complex constitution of the surrounding geologic strata that partially are disturbed by mining activity, different types of groundwater with varying solute compositions are in contact with the lakes. This may result in stable chemical stratification, separating the water column into layers of different water types and limited exchange between them.

The investigated mining lake Waldsee in Lusatia, East Germany, is very small (~120×50 m, 4.8 m depth), meromictic since some 8 years with a chemocline varying its depth around 1.5 m. It is assumed that chemical interactions between the anoxic and iron rich monimolimnion and the oxic epilimnion support the meromixis in conjunction with an active groundwater coupling.

CTD-profiles with a vertical resolution of 2 cm (Fig. 1) document the seasonal development of the stratification. It is remarkable how the summer heating from the surface intrudes through the chemocline into the monimolimnion, enhancing stability during summer (thermocline within the monimolimnion), whereas in fall/winter cooling inverses temperature stratification which is stabilized by chemical gradients. These observations already

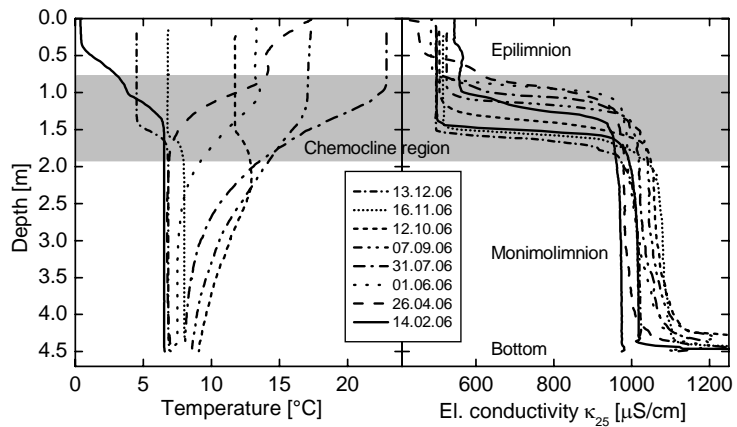


Figure 2 Temperature and conductivity in lake Waldsee (2006).

suggest that vertical exchange must be considerably reduced, at least within the chemocline region.

The quantification of vertical exchange in terms of effective diffusion coefficients and the estimation of the flushing with groundwater was the aim of this study. We used the anthropogenic trace gas SF₆ as conservative tracer for transport and for detecting groundwater inflow. Besides the chemical composition of the lake water, strong evidence for an active groundwater recharge comes from SF₆ data showing concentrations far below the recent solubility equilibrium (first profiles from the monimolimnion in spring 2006, see figure 3a) and from stable isotope data (Seebach et al., 2007). After injection of ~3 μmol SF₆ at the lake bottom (June 2006), we induced concentrations ~3 orders of magnitude higher than the background and observed the vertical spreading of this spike by monthly sampling for SF₆ at the deepest site with a resolution down to 10 cm within the chemocline. The temporal and vertical development of the SF₆-contour is caused by (i) the intensity of vertical (turbulent) diffusivity, (ii) the dilution of lake water by practically SF₆-free groundwater and (iii) the loss into the atmosphere by gas exchange. The temporal decline of the SF₆-content indicates the global tracer loss attributed to the discharge and the gas exchange. From that, effective renewal rates of Lake Waldsee can be drawn. Model calculations based on SF₆-balancing using the flux-gradient method (Jassby and Powell, 1975; von Rohden, 2002) including flushing with groundwater were applied on the measurement data. The results give a consistent picture, describing the interplay of vertical transport, groundwater coupling and gas exchange, if molecular diffusion is the governing transport process within the chemocline.

Results

Figure 3a shows three SF₆-profiles measured before injection of the spike on 1 June, 2006. The values are a factor of 3-4 lower than the equilibrium with the modern atmospheric mixing ratio (~2.5 fmol/l for ~6.3 pptv at 10°C). This demonstrates both the contact with older groundwaters and a reduced exchange of solutes through the chemocline at the scales of several years.

The SF₆-spreading after spike injection can be seen in figures 3b and 3c. In the first phase where stable stratification prevails throughout the whole water column (see figure 2), SF₆ is diffusively transported from the injection depth close to the bottom towards the chemocline. The chemocline acts as transport barrier. In November 2006, convective mixing occurred within the monimolimnion. This event homogenized the whole monimolimnion (figure 2),

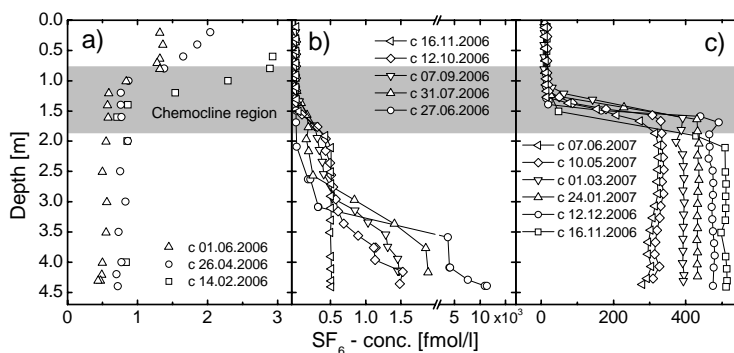


Figure 3 Measured SF₆-profiles. **a)** Background before spiking is lower than according to atmospheric equilibrium. **b)** First 5 spike profiles. SF₆ is redistributed upwards. Between 12 Oct. and 16 Nov a complete vertical mixing within the monimilimnion occurred. **c)** Starting with the 1 March profile, groundwater inflow is visible.

but did not significantly affect the chemocline. We address this to the strong inverse temperature profile, which makes the water column very sensitive to double diffusion processes within the chemocline and just below, inducing convection. This effect occurred frequently at least until the beginning of March 2007. The decrease of the SF₆-content is clearly visible. Starting with the profile of 4 April, the decreasing concentrations started to establish gradients in opposite direction in a depth below ~3 m. Only an inflow of groundwater can account for this, as diffusive processes cannot create these gradients.

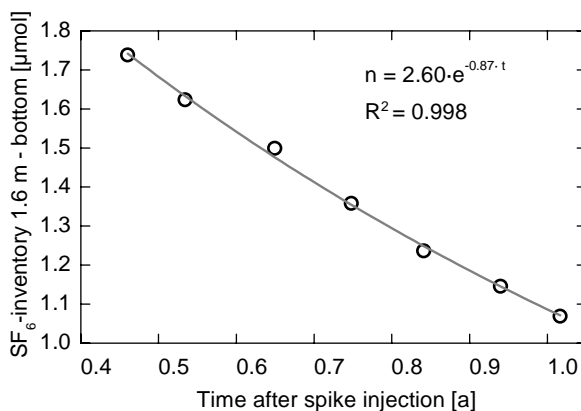


Figure 4 Temporal decrease of the SF₆-amount within the monimilimnion (lake bottom at ~4.5 m to the bottom side of the chemocline at ~1.6 m). A renewal rate of 1.1 a can be read off for the monimilimnion.

Results of the global SF₆-balance of the monimolimnion are presented in figure 4. An exponential fit yields a time constant of 0.88 a⁻¹. Assuming the SF₆-balance is dominated by groundwater flushing (see below), this corresponds to a monimolimnion exchange time of ~1.1 a. A similar number results from a fit to the balance of the whole lake.

Depth dependent vertical diffusion coefficients are evaluated applying the flux-gradient-method including a steady and evenly flushing throughout the whole water column. Flushing (renewal rates) are chosen as free input parameter in a way that molecular diffusion (10⁻⁹ m²s⁻¹) is the minimum vertical exchange in the chemocline (figure 5) where the stratification has its maximum. The resulting K_z-profiles give a plausible picture of the transport intensity. Molecular exchange within the chemocline is not obligatory but plausible. K_z according to the heat conduction level (10⁻⁷ m²s⁻¹) in the deeper monimolimnion during stratified periods is consistent to information from temperature data (not shown here). Because of convective mixing in late autumn and winter, K_z increases or is not evaluable here due to vanishing vertical gradients. The assumption of K_z higher than molecular in the chemocline requires unrealistic high gas exchange rates to close the SF₆-balance for periods at the beginning of the spike experiment.

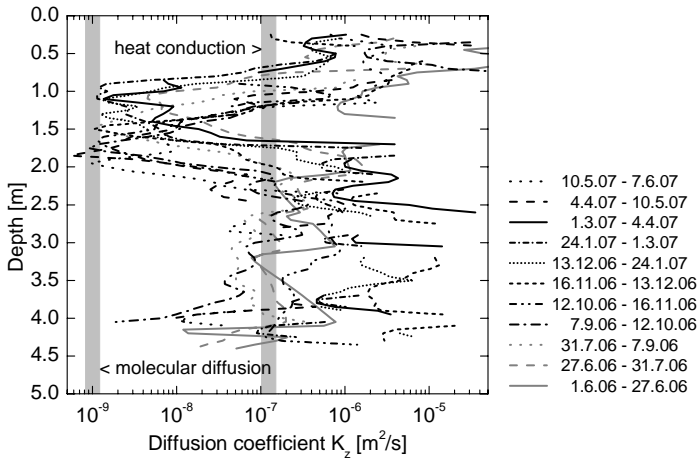


Figure 5 Effective vertical diffusion coefficients calculated with the flux-gradient-method from SF₆-profiles including a flushing with groundwater. Molecular diffusion is supposed to be the relevant transport process within the chemocline. During the thermally stratified season, transport as low as the molecular diffusion can become significant within the monimolimnion.

Acknowledgements

This work was funded by the German Research Foundation (DFG)

References

- BÖHRER B., HEIDENREICH H, SCHIMMELE M, SCHULTZE M. 1998. Numerical prognosis for salinity profiles of future lakes in the opencast mine Merseburg-Ost. *Intern. J. Salt Lake Res.* 7: 235-260.
- JASSBY, A, POWELL T. 1975. Vertical patterns of eddy Diffusion during stratification in Castle Lake, California. *Limnol. Oceanogr.* 20: 530-543
- STEVENS CL, LAWRENCE GA. 1998. Stability and meromixis in a water-filled mine pit. *Limnol. Oceanogr.* 43: 946-954.
- SEEBACH A, DIETZ S, LESSMANN D, KNÖLLER K. Estimation of lake – groundwater interactions in meromictic mining lakes by modelling isotope signatures of lake water. “*Isotopes in Environmental and Health Studies*”; Tayler & Francis Journals (submitted).
- VON ROHDEN C. 2002. Tracerstudie zur Quantifizierung des Vertikaltransports in meromiktischen Seen. PhD thesis, University of Heidelberg
- VON ROHDEN C, ILMBERGER J. 2001. Tracer experiment with sulfur hexafluoride to quantify the vertical transport in a meromictic pit lake. *Aquatic Sciences* 63: 417-431.

ILMBERGER, J.¹ & VONROHDEN, C.²

Investigation of Ground Water Interconnection and Vertical Transport in a Small Meromictic Mining Lake Using Background SF₆.

¹ *Institut für Umweltphysik,
University of Heidelberg,
INF 229, 69120 Heidelberg,
Germany. E-mail:
Johann.Ilmerger@iup.uni-
heidelberg.de*

² *E-mail:
Christoph.vonRohden@iup.uni-
heidelberg.de*

Abstract

In a joined project about meromixis, caused or supported by chemical processes, we studied the transport processes of a small mining lake (maximum depth 18 m) with a chemocline at a water depth of ~10 m. About monthly measured profiles of electrical conductivity, temperature and the man made background SF₆ were used for the investigations. From the electrical conductivity measurements different domains can be identified in the water column. The mixolimnion, down to ~10 m, and the Monimolimnion, which is subdivided into 4 regions: (1) the chemocline (~0.5 m thick, stability $N \sim 0.1$ 1/s), changing its depth by 1 m in a yearly course, (2) an apparently mixed region of about 1.5 m, (3) increasing conductivity over a range of ~2 m ($N \sim 0.03$ 1/s) and (4) a bottom layer of ~1.5 m mixed at the top and increasing towards the sediment.

In the mixolimnion SF₆ exhibits changing equilibrium concentrations in the course of the year due to the temperature dependent solubility.

The SF₆ concentrations just above the chemocline show gradients, while the electrical conductivity is well mixed there. This suggests a non ionic constituent which preserves stability.

The tracer SF₆ gives additional information about the monimolimnion. Its very low concentrations indicates that there has to be a water renewal with rather old (>30 a) ground water.

Introduction

The investigations are performed on a meromictic mining lake (Lake Moritzteich, Lusatia/East Germany). This lake (1000 m x

180 m, 18 m maximum depth), filled by groundwater more than 30 years ago, has an anoxic monimolimnion. The vertical transport at the chemocline is reduced due to stable density stratification, caused by chemical processes.

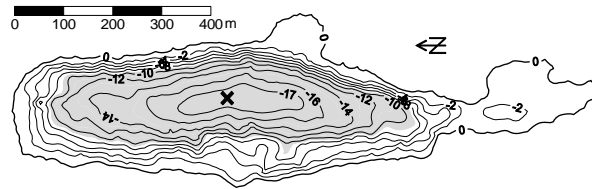


Figure 1 Bathymetry of Lake Moritzteich Lusatia/East Germany (UFZ Magdeburg).

Measurements (Monthly, over one annual cycle):

- a) temperature and el. conductivity profiles to describe temporal and spatial development of stratification structure
- b) anthropogenic conservative tracer sulfurhexafluoride SF₆ at „background level“.

Figure 2 shows the evolution of the atmospheric SF₆ concentration

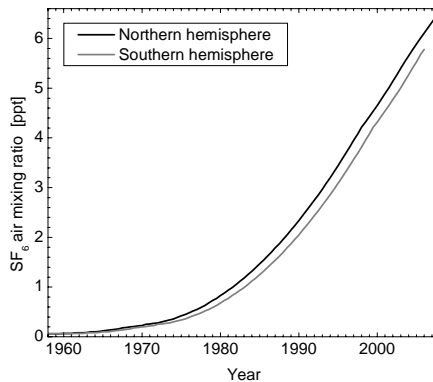


Figure 2 Atmospheric concentration of SF₆. (after Busenberg, 2006).

(background), starting at ~0.05 pptv about 1960. Thereafter the atmospheric concentration increased due to industrial use and release to the atmosphere.

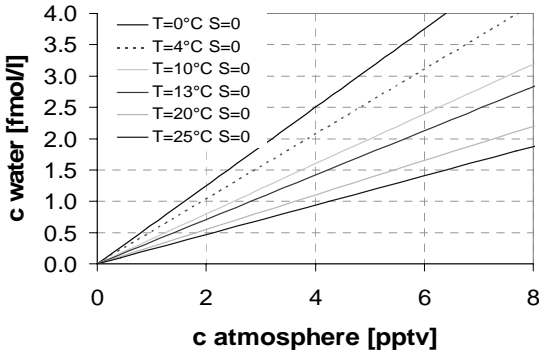


Figure 3 Temperature dependence of the solubility of SF₆ after Bullister et al. 2002.

The concentration of SF₆ in the surface water of lakes does not only depend on the atmospheric concentration, but also on the water temperature (see Fig. 3 after Bullister et al., 2002). For example at an atmospheric concentration of 6 pptv, which is about the recent concentration, equilibrated water contains 3.1 fMol/l at 4°C and only 1.4 fMol/l at 25°C.

Results

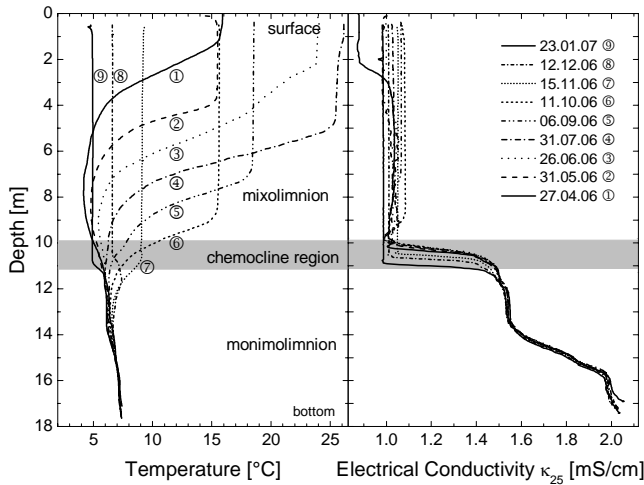


Figure 4 Lake Moritzteich. Profiles of water temperature (left) and electrical conductivity converted to 25°C (right), about monthly measurements from 27.4.2006 (1) to 23.1.2007 (9)

The mixolimnion temperature profiles (Fig.4 left) illustrate the usual changes in the course of the year: increasing temperature till late summer and thereafter decreasing as a result of convective mixing in fall and winter. In this region SF₆ varies because of the

change of the water temperature and the adjustment of the equilibrium concentration (Fig. 5). A special feature of the summer profile (26.6.06) is the increased concentration just above the chemokline, which is the left over from the last low temperature circulation.

Due to the temperature difference between mixo- and monimolimnion heat passes the chemokline region and the temperature of the monimolimnion increases. This heat transport, penetrating a few meters into the monimolimnion, must be on molecular diffusive level (heat conduction), otherwise the dissolved substances, represented by the conductivity, would display the same feature.

The right panel of figure 4 shows the electrical conductivity as representative of the dissolved substances. In the mixolimnion we find a more or less constant value.

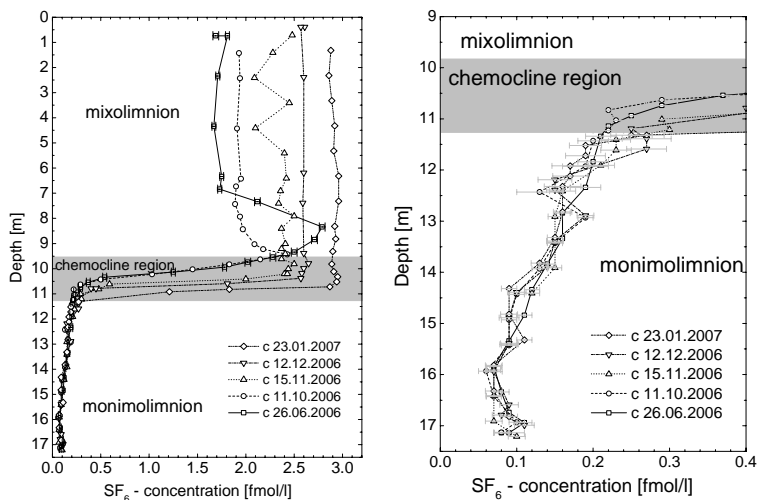


Figure 5 Sf6 back ground measurements to study vertical mixing and ground water exchange. Right panel: Zoom of the Monimolimnions low concentrations.

The depth of the chemokline varies about 1 m throughout the year. The gradient in the chemokline doesn't change, most probably due to the very low molecular diffusivity of matter and a permanent resharping caused by chemical processes (Fe dissolution /precipitation). In the chemokline region the SF₆ concentration drops from 2-3 fMol/l to values of ~0.2 fMol/l (Fig.5).

Below the chemokline we find a 1.5 m thick rather well mixed region, as a result of convective mixing because of double diffusive processes. This region is also influenced by groundwater, which can be seen from the tracer SF₆ in figure 5, displaying low and irregular concentration values.

Underneath the conductivity rises over a range of 2 m causing a stability of $\sim 0.03 \text{ s}^{-1}$. In this range the SF_6 concentration drops further to a value as low as 0.08 fMol/l which indicates more than 30 years old (ground) water. Measurements of stable isotopes (Seebach et al 2007) also confirm the influence of groundwater.

The bottom layer, $\sim 1.5 \text{ m}$ thick, shows a mixed top part and an increase towards the sediment. The SF_6 concentration displays a -so far not well understood- very slide but significant rise to 0.1 fMol/l towards the lake bottom.

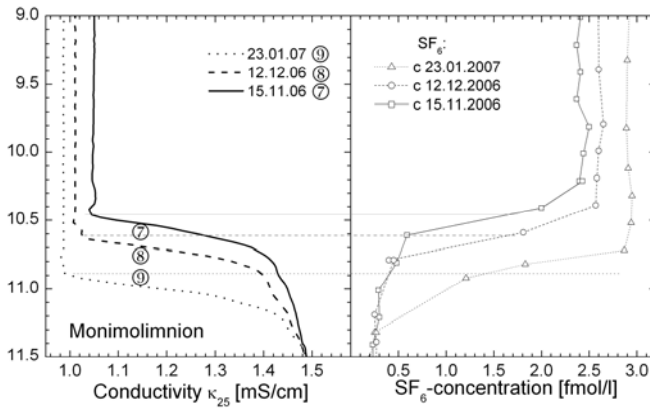


Figure 6 Vertical profiles of conductivity (left) and SF_6 (right).

The el. conductivity above the chemocline is well mixed (Fig. 6, left panel) whereas the SF_6 concentrations show a low level diffusive transport (Fig. 6, right panel).

Acknowledgements

The research is funded by the German science foundation (DFG).

References

BULLISTER, J. L., D. P. WISEGARVER AND F. A. MENZIA 2002. "The solubility of sulfur hexafluoride in water and seawater." *Deep-Sea Res.* 49: 175-187.

BUSENBERG E. 2006. http://water.usgs.gov/lab/software/air_curve/.

SEEBACH A, DIETZ S, LESSMANN D, KNÖLLER K. Estimation of lake – groundwater interactions in meromictic mining lakes by modelling isotope signatures of lake water. "*Isotopes in Environmental and Health Studies*"; *Taylor & Francis Journals* (submitted).

4 Turbulence

ZILITINKEVICH, S.¹

**A minimal energy- and flux-
budget (EFB) turbulence
closure model for stably
stratified sheared flows**

¹ *Finnish Meteorological Institute
Helsinki, Vuorikatu 15 A., 101,
Helsinki, Finland. E-mail:
Sergej.Zilitinkevich@fmi.fi*

Abstract

We propose a new turbulence closure model based on the budget equations for the basic second moments: turbulent kinetic and potential energies: TKE and TPE, which comprise the turbulent total energy: $TTE = TKE + TPE$; and vertical turbulent fluxes of momentum and buoyancy (potential temperature). Besides the new concept of the TTE, other key points are: non-gradient correction to the traditional formulation for the flux of buoyancy (potential temperature), and advanced analysis of the stability dependence of anisotropy of turbulence. The proposed model affords the existence of turbulence at any gradient Richardson number, Ri . Instead of the critical value of Ri separating the turbulent and the laminar regimes, the model includes its threshold value, between 0.2 and 0.3, which separates two turbulent regimes of essentially different nature: fully developed, chaotic turbulence at low Ri and weak, strongly anisotropic turbulence at large Ri . Predictions from the proposed model are consistent with available data from atmospheric and lab experiments, DNS and LES.

LORRAI, C.^{1*}, HUME, A.², MCGINNIS,
D. F.¹, BERG, P.², WÜEST, A.¹

Comparison of dissolved oxygen fluxes in natural waters from simultaneously deployed eddy-correlation devices

¹ *Eawag, Kastanienbaum, CH-6047, Switzerland. E-mail: claudia.lorrai@eawag.ch*

² *Department of Environmental Sciences, University of Virginia, Charlottesville, VA 22904-4123, USA*

Abstract

Currents influence near-sediment flow dynamics, turbulent transport of momentum and constituents (e.g. oxygen) and thereby the diagenetic processes in the upper sediments. We implement the new eddy-correlation technique to estimate local turbulent oxygen fluxes by correlating the fluctuating vertical velocity and dissolved oxygen concentrations. The eddy-correlation technique enables us to measure directly *in-situ* oxygen fluxes and turbulence at the same time and place. For the first time, we applied two similar eddy-correlation systems (one from the Swiss Federal Institute of Aquatic Science and Technology and one from the University of Virginia) deployed simultaneously in Lake Wohlen.

Introduction

A prime question in lakes and reservoirs concerns the flux paths between the stratified interior, through both the bottom boundary layer (BBL) and the sediment surface. With an acoustic Doppler velocity (ADV) meter coupled to a Clark-type oxygen sensor, turbulent dissolved oxygen (DO) fluxes can be determined using the eddy correlation technique (ECT; Berg et al. 2003; Berg et al. 2007). In this study, we present preliminary results of two simultaneously deployed EC devices in a riverine reservoir (Lake Wohlen, Switzerland).

The study was carried out as a collaboration between the University of Virginia (UVA) and the Swiss Federal Institute of Aquatic

Science and Technology (Eawag). As the application of the ECT to fresh water is a new technology, the test was designed to compare the EC devices in a quasi-steady system. Here, we present first results from this study.

Method

Theory: The ECT for DO in natural waters allows identifying turbulent eddy fluxes near the sediment-water interface, thereby inferring the sediment oxygen demand (or production). The components of the measured constituents, namely DO (C) and the vertical velocity (w), are separated by Reynolds decomposition into the average and the correspondent fluctuation, $w = \bar{w} + w'$ and $C = \bar{C} + C'$.

The fluctuations, w' and C' , are defined so that their time average equals zero. The equation describing the vertical oxygen flux driven by advection is $Flux = wC$ where w' and C' become equal to zero, if averaged over a time period substantially longer than the turbulent fluctuations. The average vertical velocity \bar{w} should be zero so we can calculate the turbulent flux as $Flux = w'C'$.

Study site: Lake Wohlen is a eutrophic run-of-the-river reservoir with a high sediment oxygen demand, near the City of Bern (Switzerland). Lake Wohlen has a surface area of 3.65 km², a maximum depth of 20 m and has a riverine character with a steady flow.

Device description: Both systems consist of an ADV (Vector, Nortek) and a Clark-type oxygen microsensor (fast Ox-10, Unisense for Eawag, custom for UVA), which has a short response time (<0.3 s for 90% reading).

Eawag system: The sensor is connected by wires to the amplifier. These wires are contained within a paraffin-filled rubber tube. The technology consists of a low noise current-to-voltage converter with a precision instrumentation in-housed designed pico-amplifier in series with a guard circuit.

UVA system: For the UVA EC device, the oxygen microsensor is connected directly to the amplifier. A Max Planck Institute for Marine Microbiology (MPI) amplifier is used for the oxygen signal.

Deployment: UVA and Eawag EC devices were mounted on the same tripod lowered near the shore in ~1 m deep water. The sensors were polarized in the lab with a PA2000 picoammeter (Unisense).

A temperature/DO logger (RBR TDO-2050) was fixed to the tripod at the same level as the oxygen microelectrodes.



Figure 1: (Left) The two eddy correlation systems mounted next to each other in the measurement site. (Right) A close up of the two systems.

Data Analysis: The data are analyzed using the user-friendly PC software package EddyFlux Version 1.3 beta (P. Berg, personal communication). The program calculates fluxes using raw velocity and DO data. It uses three independent ways to extract the fluctuating components of the velocity and the DO concentration (mean removal, linear detrending, and running averaging) and outputs among other parameters the cumulative fluxes and total fluxes. The program also allows coordinate rotation to correct the velocity for instrument tilt errors.

Preliminary Results and Discussion

Figure 2 shows the DO flux calculations for an 11 hour time series recorded by the Eawag system (upper panel) and UVA system (lower panel). Negative values represent fluxes into the sediment. Analysis of the data recorded by Eawag EC device indicates a net nighttime flux of $-7 \pm 2 \text{ mmol m}^{-2} \text{ d}^{-1}$. UVA's net nighttime flux is $-17 \pm 5 \text{ mmol m}^{-2} \text{ d}^{-1}$. Both calculated fluxes indicate DO production after sunrise, which is encouraging as, regardless of absolute values, the devices seem to have similar responses. The average production fluxes after sunrise are $5 \pm 5 \text{ mmol m}^{-2} \text{ d}^{-1}$ (Eawag) and $13 \pm 9 \text{ mmol m}^{-2} \text{ d}^{-1}$ (UVA).

It is possible that Eawag's fluxes are lower due to inadvertent filtering by the amplifier. Analysis of this, noise, and filtering issues are the subject of future work.

Due to the large variability in the DO data, it is most appropriate to detrend the data using a running average. Determining the appropriate averaging window for the flux calculations however is a critical task for the flux estimation. The number of data points used

in the running average must be large enough to contain all the turbulent contributions to flux but not too large as to include artifacts like sensor drift or non-turbulent changes (such as basis-scale waves). The running window size was determined by gradually increasing the length of the window and by repeatedly calculating the flux until it reaches a constant value.

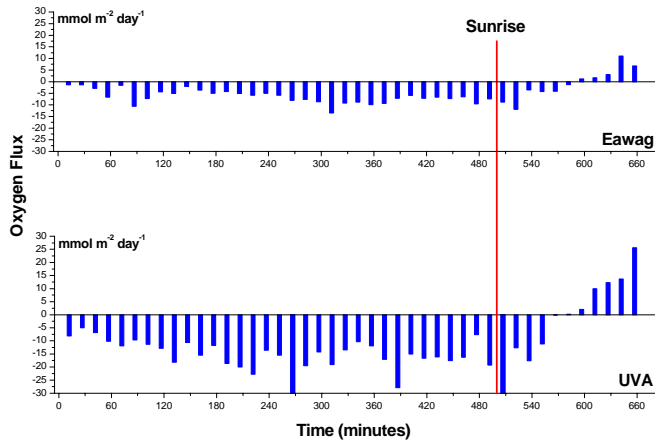


Figure 2: Dissolved oxygen flux estimates over time. Flux calculations were performed for time intervals of 15 minutes by filtering (running mean). Solid line marks time of sunrise in the region of Bern (Switzerland).

Figure 3 illustrates the dependency of the flux estimations on the averaging window size for Eawag (dashed line) and UVA (dotted line) 1 hour time series (see Berg et al. 2003 for details). Fluxes reach a maximum at 160 s (0.0063 Hz; Eawag) and 120 s (0.0083 Hz; UVA) before they level off (these frequencies are marked by solid lines; left for Eawag and right for UVA data). The cumulative cospectra agree well with the window-analysis. This is reassuring as the integrated cospectra give the flux.

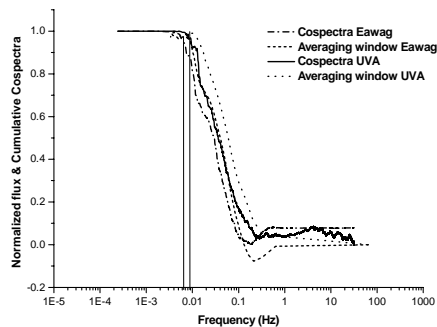


Figure 3: Time averaging window effect on the oxygen flux estimation for 1-hr long time series (same time series from Eawag and UVA data) and comparison with the corresponding cospectra.

The highest frequency turbulent contributions are approximately 0.5 Hz (2 s). The slope of both cospectra clearly illustrates the range of the contributing eddys (2 s - 160 s). The values shown are in good agreement with a separate study conducted in Lake Wohlen (McGinnis et al., submitted).

The contributing eddys are confirmed by determining the energy containing plots of the vertical velocity and DO data (energy containing plot is PSD x freq; Figure 4). The maximum timescale of turbulent eddies can be calculated from the shear velocity, which is

$$u_* = C_{1m}^{1/2} U_{1m}$$

where C_{1m} , the bottom friction coefficient, is taken as 1.5×10^{-3} (Wüest and Lorke 2003). The timescale is then calculated as D/u_* , where D is the mixing length. Using an average measured velocity of 2.2 cm/s and $D = 1$ m, the largest timescale expected is 1,200 s. Using our estimated times of 160 s (Eawag) and 120 s (UVA; Figure 3) yields a length-scale of about 0.5 – 0.6 m.

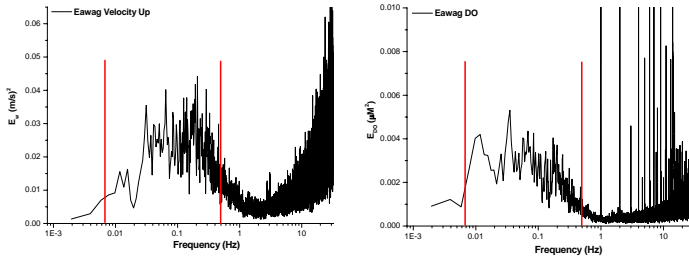


Figure 4: Energy containing spectral plot for 1-hr long time series of vertical velocity (left panel) and dissolved oxygen (right panel) recorded with the Eawag EC device. The part between the solid lines shows the range where turbulent eddys contribute to the signal.

The smallest calculated eddys are on the order of 4 mm with a lifespan of 10 s calculated by using the Kolmogorov length scale

$$L_K = (v^3 / \varepsilon)^{1/4}$$

with $\varepsilon = 1.5 \times 10^{-8} \text{ W kg}^{-1}$ and a kinematic viscosity of 1.5×10^{-6} . The time (10 s) is given by

$$\tau = (L_K^2 / \varepsilon)^{1/3}$$

Summary

The results shown here are a part of 4 long time series collected by simultaneous conducted measurements with the two eddy correlation devices from Eawag and UVA. The preliminary results

discussed in this paper are encouraging for the ECT, because both signals from UVA and Eawag devices showed the same reaction in terms of consumption and production. The response is quite similar and the time windows technique agrees well with the cospectra.

The difference of the estimated fluxes between Eawag and UVA time series is maybe caused by differences in the magnitude of the DO fluctuations due to filtering of the signal. The next steps will be to further investigate where this difference comes from and to better understand how to apply this promising method.

These results are a first step towards a routinely applicable EC device which gives the possibility to measure oxygen fluxes over the sediment of lakes and reservoirs in a non invasive way.

Acknowledgements

We thank L. Rovelli and T. Del Sontro for their great help in the field. The work was financially supported by the Swiss National Science Foundation (Grant: 200020-111763) and by EAWAG and UVA.

References

- BERG P., RØY P., JANSSEN F., MEYER V., JØRGENSEN B. B., HUETTEL M., AND DE BEER D. 2003. Oxygen uptake by aquatic sediments measured with a novel non-invasive eddy-correlation technique. *Mar. Ecol. Prog. Ser.*: 261, 75-83.
- BERG P., RØY H., WIBERG, P. L. 2007. Eddy correlation flux measurements – the sediment surface area that contributes to the flux. *Limnology and Oceanography*: 52:1672-1684.
- WÜEST A. AND LORKE A., 2003. Small-Scale Hydrodynamics in Lakes. *Ann. Rev. Fluid Mech.*:35: 373-412.
- MCGINNIS D. F., BERG P., BRAND A., LORRAI C., EDMONDS T. J., WÜEST A. Local oxygen fluxes estimates from eddy-correlation in a shallow riverine reservoir: towards routine method application, *Submitted to Geophysical Research Letters*
- BRAND A., MCGINNIS D. F., WEHRLI B., WÜEST A. Intermittency of turbulent oxygen flux into the bottom boundary of lakes as observed by eddy correlation, *submitted to Limnology Oceanography*

**MOHRHOLZ¹, V., H. U. LASS¹ & H.
PRANDKE¹**

Estimation of TKE dissipation rate in an inflowing saline bottom plume using a PC-ADP

¹ *Baltic Sea Research Institute
Warnemünde, Dept. of Physical
Oceanography and
Instrumentation, Seestraße 15
18119, Rostock, Deutschland. E-
mail: volker.mohrholz@io-
warnemuende.de*

Abstract

Inflowing high saline waters from the North Sea are the sole source for oxygen in the deep Baltic basins below the halocline. The depth layer which is finally ventilated by an inflow is determined by the density of the inflowing saline water and the actual stratification in the central basins. Along the pathway through the western Baltic turbulent mixing and differential advection causes an entrainment of ambient water and change the properties of the inflowing saline water. However, observations of mixing parameters in spreading dense bottom water plumes are scarce, since their occurrence is intermittent and not well predictable.

During a hydrographic survey in January 2006 the spreading of a newly formed saline bottom plume could be observed in the Arkona Sea. Two bottom mounted PC-ADPs were used to measure the near bottom current field of the dense plume with a high temporal (1s) and spatial resolution (5cm). In order to estimate the dissipation rate (ϵ) of turbulent kinetic energy (TKE) a structure function approach was applied to the beam velocity data of both devices. Contemporary measurements with an MSS-profiler and an ADV supplied independent data for the verification of the structure function method and additional measurements with standard CTD, near bottom towed ADCP and vessel mounted ADCP completed the data set. The estimated dissipation rates from the structure function approach fits surprisingly well with the values derived from the MSS profiler and the ADV. The dissipation rates ranged between $5e-6$ and $5e-8$ Wkg⁻¹ depending on the current regime and stratification. Inside the plume the dissipation rates exceeds that of the overlaying brackish water by two orders of magnitude.

Additionally, a long term deployment of an PC-ADP north of Kriegers Flak is presented, which supplied time series of current profile and TKE dissipation rate in the near bottom layer for a series of subsequent inflowing saline plumes.

UMLAUF¹, L., V. MOHRHOLZ¹, & L.
ARNEBORG²

Boundary layer effects in topographically constrained bottom gravity currents

¹ *Baltic Sea Research Institute
Warnemünde, Dept. of Physical
Oceanography and
Instrumentation, Seestraße 15
18119, Rostock, Deutschland. E-
mail: lars.umlau@io-
warnemuende.de*

² *Göteborg University, Earth
Sciences Centr, Box 460, 40530,
Göteborg, Sweden. E-mail:
laar@oce.gu.se*

Abstract

The structure and dynamics of frictionally controlled bottom gravity currents passing through a channel or constriction will be discussed. The focus will be on gravity currents for which rotational and frictional effects are of comparable importance, and result in a complex cross-channel secondary circulation that can be understood as a combination of thermal wind and Ekman effects. We will see that this secondary circulation may strongly distort the density structure in the interface and the interior of the gravity current, and therefore has considerable implications for the entrainment and the dynamical behavior. These effects will be discussed in the context of observations from the Baltic Sea, which will be compared to results from a simple numerical model.

BOUFFARD, D¹, **LEMMIN, U.**

Turbulent dissipation in the stratified Lake of Geneva forced by wind

¹ *Environmental Hydraulics Laboratory, Ecole Polytechnique Federale de Lausanne, Lausanne, Switzerland. E-mail: damien.bouffard@epfl.ch*

abstract

Vertical exchange processes are key to the understanding of physical and biological dynamics in stratified lakes or oceans. At present, fine scale field observations over time and space are still scarce. Here, the response of the stratified Lake of Geneva to strong wind forcing is analysed with a new experimental device which we developed to investigate the finescale flow structure in time and in space. The platform is equipped with a set of standard turbulence sensors for measuring velocity and temperature gradients and shear. It is displaced in the vertical by a bottom-resting winch and is cable-connected to the shore which provides real time access to the data, allowing to control the winch and to optimise the measurement strategy. In order to demonstrate the feasibility of the device, we present and discuss estimates of different parameters (the rate of dissipation of TKE ϵ , the vertical diffusivity K_z , the Richardson number Ri) in the vicinity of the thermocline during the wind event.

Introduction

The work presented here is a first step in a detailed investigation of the time and space evolution of the stability of the summer thermocline in response to wind forcing (shear). Large scale oscillations resulting from this external forcing in Lake Geneva (Switzerland) lead to long internal waves identified as internal Kelvin waves (Umlauf and Lemmin, 2005). In this paper, we focus on small scale mixing dynamics across strongly-stratified interfaces during Kelvin wave generation. We will briefly describe the new instrumentation and present results related to the turbulent dissipation and mixing in the thermocline in response wind forcing.

Instrumentation

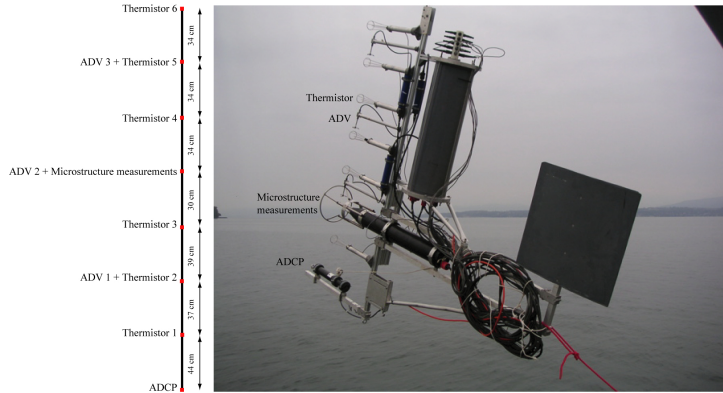


Figure 1: Photo of the platform developed at the EPFL

The results discussed here come from data collected in and around the summer thermocline during an intensive field campaign. Measurements were made from a new moored instrument platform recently developed at the Environmental Hydraulics Laboratory (EPFL-LHE). The structure consists of a vertical 2.5m high mast upon which different sensors have been mounted (10 high precision fast response thermistors, 4 Nortek 25 Mhz Acoustic Doppler Velocimeters, 1 turbulence package designed by Rockland Inc. with two airfoil probes and two fast response thermistors and 1 Nortek Aquadopp profiler operating with 10 bins of 0.25-meter size each and recording mean currents every 2 minutes. Fig. 1). A housing with the backup electronics and computers for data recording and communication has been fixed behind the sensors. The device can rotate freely into the direction of the current. The package is held in position by a cable that passes through a winch anchored on the lake bottom and connected to shore by a 1800 m long cable. By observing temperatures, velocities and pressure coming in real time from the instruments, the user can first take whole depth vertical profiles of all parameters by activating the winch and then precisely position the structure in the layer of interest. In order to put these data into a larger perspective, an RDI acoustic Doppler current profiler, operating with 50 bins of 1-meter size each and recording mean currents every 5 minutes, was moored on the lake bottom near the winch and gives velocity profiles of the whole water column. The study also included atmospheric data from a Swiss meteorological station at

Changins, located at less than 5 km distance.

Successful microstructure and velocity measurements require careful data treatment. Due to weak currents observed in lakes (0.05 to 0.3 m s^{-1}) the microstructure profiler operates near its limits leading to low signal-to-noise ratios (Lueck et al, 1997). Noise contamination is reduced and the spectra are corrected by standard processing methods (Levine and Lueck, 1999). Difficulties in velocity measurements are due to the low scatterer intensity in lakes which drastically increases noise. For variance calculations, one of the greatest difficulties is to eliminate corrupted data from the sample (Voulgaris and Trowbridge, 1998, Nikora and Goring, 1998). Different filtering methods have been tried to remove and replace spikes in the data. For despiking, three different filters are used: minimum/maximum threshold, acceleration threshold and wavelet denoising.

Turbulence related to strong wind forcing

The selected period for turbulence measurements in the stratified Lake of Geneva corresponds to a strong South-West wind forcing. The storm lasted only 7 h, but the average wind speeds was around 6 m s^{-1} . This energy input transformed an initial diffuse thermocline with a maximum stratification of about $1.1 \cdot 10^{-3} \text{ s}^{-2}$ into a sharp thermocline with a maximum stratification of $5 \cdot 10^{-3} \text{ s}^{-2}$. Wind stress induced strong shear with a mean flow of about 0.15 m s^{-1} in the mixed layer and a flow of about 0.05 m s^{-1} in the opposite direction in the metalimnion. An entrainment of about 1m (not presented here) was measured during the 7 h period. Since temperature gradients remained constant, this entrainment was corrected for in the analysis in order to be able to compare measurements over time. Here we focus on the fine scale structure in the thermocline and in the mixed layer just above the thermocline.

Figure 2 show an example of time evolution of velocity, temperature, temperature gradient, Richardson number (Ri), rate of dissipation of Turbulent Kinetic Energy (ϵ) and vertical diffusivity (K_z) which are the most relevant physical parameters in stratified flow. For this period, the device was placed at a 18.5 m depth in the upper part of this sharp thermocline. Results indicate significant temporal variability with ϵ and K_z varying respectively from $7 \cdot 10^{-9}$ to $1.3 \cdot 10^{-7} \text{ m}^2 \text{ s}^{-3}$ and from $4.2 \cdot 10^{-7}$ to $5.7 \cdot 10^{-6} \text{ m}^2 \text{ s}^{-1}$. Despite the pronounced stratification, shear was sporadically strong enough to produce low Richardson numbers. Local instabilities were associated with an increase of both dissipation and vertical diffusivity (between 45 et 50 min and at 58 min in Fig. 2). A mixing efficiency, Γ , can be estimated from $\Gamma = \frac{K_z N^2}{\epsilon}$. For the selected period pre-

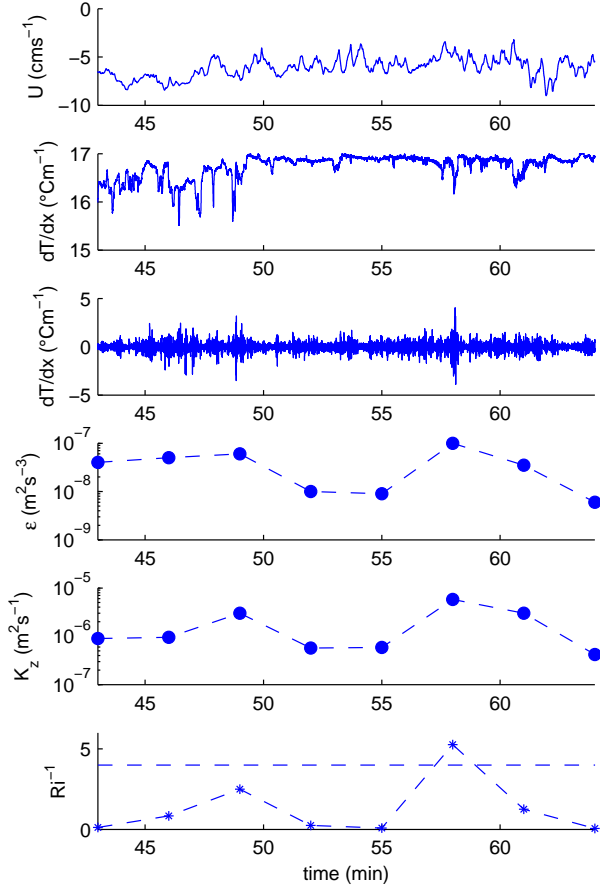


Figure 2: Time series of velocity, temperature, temperature gradient, dissipation, Richardson number and vertical diffusivity. The average rates of ϵ , Ri and K_z are estimated over 3 min periods (~ 20 m).

sented in Fig. 2, we found a mixing efficiency of about 0.16 ± 0.03 . While some instabilities can be observed in the upper part of the thermocline and in lower part of the mixed layer (Fig. 2), the lower part of the thermocline seem to be more stable (not shown).

Although Fig. 2 reveals significant temporal variability, we represent in Fig. 3 time averaged profiles of the same parameters. According to this averaging, the flow becomes marginally stable with $Ri(z) > 0.25$ in the thermocline layer. This mean stability may be explained by the weak time of persistence ($T^* \sim 12 Ri^{-\frac{1}{2}} N^{-1}$,

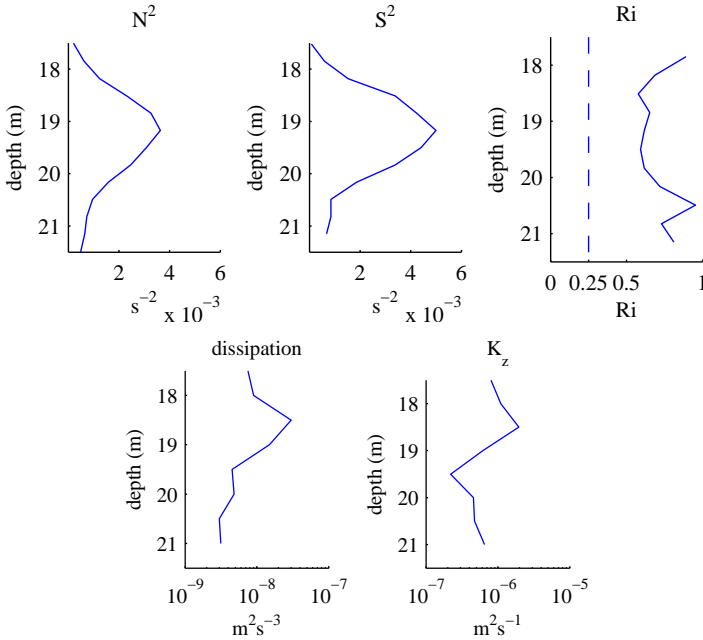


Figure 3: Vertical profiles of N^2 , S^2 , Ri , ϵ and K_z averaged over the whole measuring period

Thorpe, 1973) of turbulence after the onset of the instability in strong stratification. Taking a value of 0.25 as instability criteria for Ri results in a period of 320 s (5 min). This period is extremely short compared to the period of persistence of turbulence in a more "classical" thermocline: $T^* > 25$ min with $N^2 \sim 3 \cdot 10^{-4} \text{ s}^{-2}$. It is also interesting to observe that ϵ and K_z are reaching their maxima in the upper part of the thermocline.

Conclusions

We have analysed observations of turbulent dissipation during a period of strong wind in the vicinity of the thermocline with a new platform developed at LHE-EPFL. First results highlight the strong variability over time and space of turbulent mixing in response to wind forcing in a strongly stratified lake. High vertical diffusivity seems to be concentrate in the upper part of the thermocline during small scale instabilities events such as Kelvin-Helmholz billows. However, a more realistic accurate estimate of the energy transferred

by the shear to the mixing in the thermocline must take into account the time evolution of the turbulence. We are able to study this aspect with our new installation and we will extend the data analysis in that direction.

References

Levine, E. R. and R. G. Lueck, 1999: Turbulence measurement from an autonomous underwater vehicle. *Journal of Atmospheric and Oceanic Technology*, 16, 1533-1544.

Lueck, R. G., D. Huang, D. Newman, and J. Box, (1997): Turbulence measurement with a moored instrument. *Journal of Atmospheric and Oceanic Technology*, 14, 143-161.

Nikora, V. I. and D. G. Goring, (1998): ADV measurements of turbulence: can we improve their interpretation? *Journal of Hydraulic Engineering*, 124, 630-634.

Thorpe, S.A., (1973): Experiments on instability and turbulence in a stratified shear flow. *Journal of Fluids Mechanics*, 61, 731-751.

Umlauf, L. and U. Lemmin, (2005): Interbasin exchange and mixing in the hypolimnion of a large lake: The role of long internal waves. *Limnology and Oceanography*, 50, 1601-1611.

Voulgaris, G. and J. H. Trowbridge, (1998): Evaluation of the acoustic Doppler velocimeter for turbulence measurements. *Journal of Atmospheric and Oceanic Technology*, 15, 272-289.

ZUELICKE, C.¹

The impact of surface active films on waves and gas exchange

¹ *Baltic Sea Research Institute
Warnemünde, Dept. of Physical
Oceanography and
Instrumentation, Seestraße 15
18119, Rostock, Deutschland. E-
mail: christoph.zuelicke@io-
warnemuende.de*

Abstract

The formation of capillary-gravity waves (so-called ripples) on clear water is determined by the wind speed and the surface tension. The level of turbulence just beneath the surface regulates the thickness of the diffusive sublayer and consequently the gas exchange. The presence of surface active films increases the surface elasticity and damps the ripples. In an analytical model these effects are described with wave spectra and related gas transfer velocities.

**BONHOMME, C.¹ & TASSIN, B.¹, &
CUYPERS Y.¹ & POULIN M.**

**Mixing in the water body of a
deep meromictic lake: role of
double diffusive convection in
the dynamics of mixing**

¹ *CEREVE – Centre
d'Enseignement et de Recherche
sur l'Eau, la Ville et
l'Environnement, 6 et 8 avenue
Blaise Pascal, Cité Descarte
77455 MARNE LA VALLEE
Cedex 2, FRANCE. E-
mail: bonhomme@cereve.enpc.fr*

Abstract

Lake Pavin is a deep meromictic lake located in the middle of France. Lake Pavin is geothermally heated (+1°C at the bottom of the lake). Between 30 meters and 50 meters depth, the correlated increase of temperature and dissolved substances cause conditions favourable to double diffusive convection in the second part of year 2006: staircases on temperature and conductivity microstructure profiles are observed. The characteristic of the staircases are in agreement with empirical estimates of double-diffusive staircases thickness. Vertical dispersion coefficients (or K_z s) are estimated with local methods and compared to basin-wide vertical diffusivities. Diapycnal dispersion in the lake interior is increased by more than a factor 10 due to the apparition of double diffusive conditions. At the same time, basin-wide diffusivity is increased by a factor 2.

Introduction

In fresh water lakes, temperature gradients are small and the stability of the water column is low in the hypolimnion. Even if the thermocline acts as a barrier to the penetration of wind energy from the lake surface, about 0.3% of wind energy penetrates the thermocline in the form of TKE [Wuest et al., 2000]. However, other processes can greatly influence the mixing budget in the hypolimnion: mainly convection, sublacustrine intrusions or double diffusion processes. Lake Pavin has the particularity to be heated from the bottom. The destabilizing effect of the temperature is counterbalanced by a stabilizing effect due to dissolved substances gradient creating conditions favourable to double diffusive convection. In this study, we observe an enhanced mixing process in lake Pavin during the second part of year 2006, correlated with the apparition of conditions favourable to double diffusive convection.

Results

1. Conditions favourable to double diffusive convection in the second part of year 2006.

R_p as defined by [Walsh and Ruddick, 1995] provides a measure of the strength of the double-diffusive activity. The indicator R_p is the ratio of stabilizing forces due to temperature gradient and the destabilizing force due to the salinity.

Double-diffusion may occur when $R_p < 10$ and increases when R_p falls down to 1. R_p is here calculated with a 2 meters averaged window.

The water column is doubly stable until 45 meters depth in May 2006 ($R_p < 0$) and double diffusive between 45 and 55 meters depth (cf Figure 1, black line). In November 2006, we observe an extension of the double diffusive zone (red line). At this time of the year, double diffusion can occur between 35 and 55 meters.

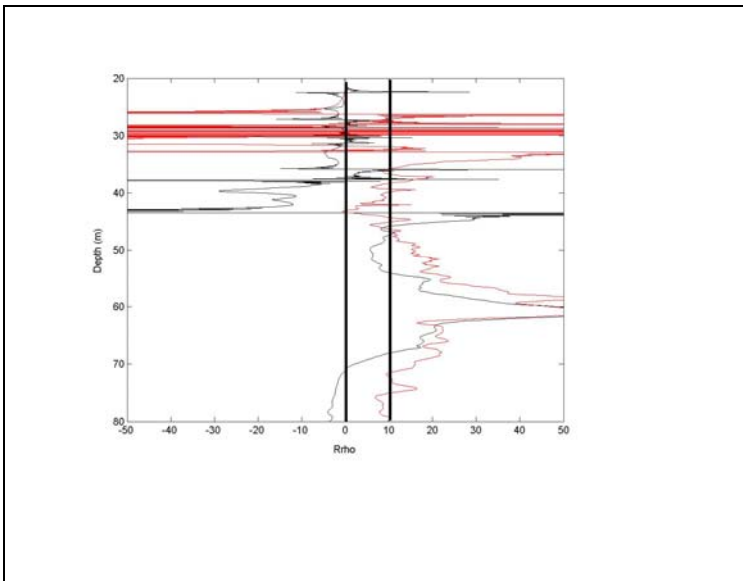


Figure 1 Evolution of R_p between May 2006 (black line) and November 2006 (red line) calculated with a 2 meters averaged window

2. Description of the staircases:

These staircases persist during several hours, they sometimes move up and down, sometimes split at time scale close to Brunt Vaisala period in this part of the water column.

Mean temperature gradients of 0.02°C delimit the interface between two staircases. The average thickness of a staircase is 2 meters.

Several semi-empirical equations have been proposed to estimate the average thickness H of the steps in double-diffusive staircases. The characteristics of the staircases are in agreement with these calculations.

As in the frame of the study of lake Nyos, the most reliable estimate seems to be the one by Fedorov [Schmidt, 2002].

3. K_z from fluxes at the interface between staircases

Double diffusion increases both vertical heat and salinity fluxes in the hypolimnion. Here we will use the estimations of Turner (1973) and Kelley (1990) and Fernando (1989) derived from laboratory experiments. It is important to consider that these formulations of fluxes are derived from the formulation of purely convective fluxes and are also valid if the process leading to the overturns is purely convective. K_z is then calculated using the local mean temperature gradient:

$$K_{zT} = \frac{F_T}{\left. \frac{\partial T}{\partial z} \right|_{z=z_0}}$$

K_{zT} (Turner) (m^2/s)	K_{zT} (Kelley-) (m^2/s)	K_{zT} (Fernando) (m^2/s)
1.41×10^{-6}	4.05×10^{-6}	2.0×10^{-6}

4. Kz from microstructure measurements

The vertical dispersion coefficient is calculated with the Batchelor fitting method of the spectrum of temperature fluctuations followed by the Osborn calculation of Kz [Luketina and Imberger, 1998] with γ mixing depending on double diffusive conditions. After having averaged, we obtain the profiles of Figure 3. In black, averaged Kz for May 2006 lies below averaged Kz for July (in blue) and September 2006 (in red) of about a factor 10. Values at the thermocline and at the chemocline are lower and are consistent with values that are usually published for the interior of lake body .

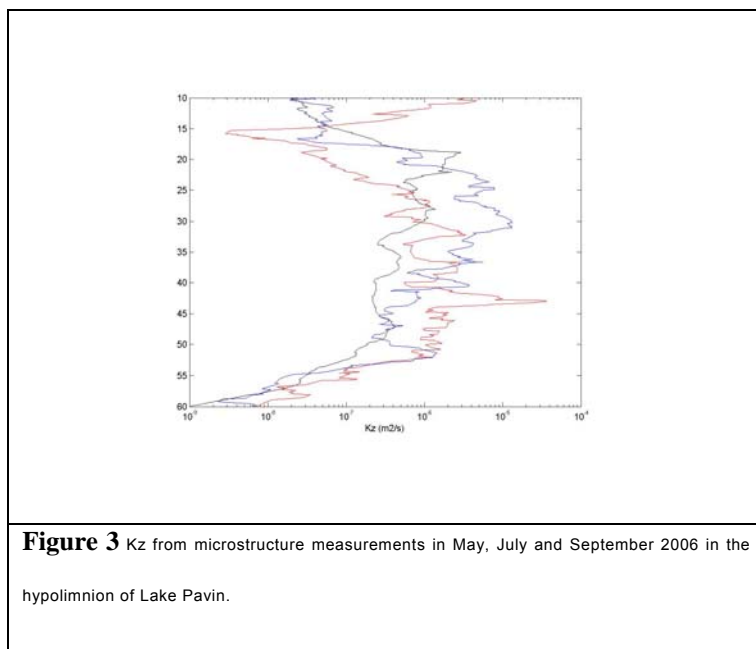


Figure 3 Kz from microstructure measurements in May, July and September 2006 in the hypolimnion of Lake Pavin.

5. Impact at the basin-scale.

Different methods show that local vertical diffusivity was increased in Lake Pavin in the second half of year 2006. The most interesting issue is now to quantify basin wide impact of such an increase in vertical dispersion. The method at the basin scale that will be used here is the heat budget method [Powell and Jassby, 1974].

This method permits to conclude the diffusivity at the basin-scale is increased by a factor 2 when double diffusive conditions occur, which is considerable for the transport of solutes in the hypolimnion of lake Pavin.

Acknowledgements

We thank D. Jezequel, A. Groleau and G. Michard (LGE, France) for fruitful discussions on this study. This work was supported by the ANR program METANOX.

References

- KELLEY D.E., 1990, Fluxes through diffusive staircases: a new formulation, *Journal of Geophysical Research* 95 3365-3371
- LUKETINA, D. and IMBERGER J., 1998, Determining Turbulent Kinetic Energy Dissipation from Batchelor Curve Fitting, *Journal of Atmospheric and Oceanic Technology*.
- POWELL T. and JASSBY A., 1974. The estimation of vertical eddy diffusivities below the thermocline in lakes. *Water. Resour. Res.*, 10, 191-198.
- SCHMID M., LORKE A., DINKEL G., TANYILEKE, WUEST A., 2004, Double-diffusive convection in Lake Nyos, Cameroon *Deep-Sea Research* 51 1097-1111
- WALSH D., RUDDICK B., 1995, Double-diffusive interleaving: The influence of nonconstant diffusivities, *Journal of Physical Oceanography* 25 348-358
- WUEST A., PIEPKE G. and VAN SENDEN D.C., 2000, Turbulent kinetic energy balance as a tool for estimating vertical diffusivity in wind-forced stratified waters, *Limnol. Oceanogr.*, 45 (6), 1388-1400

5 Numerical Modelling

G. KIRILLIN¹, S. GOLOSOV¹, D. MIRONOV² & C. ENGELHARDT¹

Climate warming and shallow lakes: the role of bottom sediments and water transparency

¹ *Leibniz-Institute of Freshwater Ecology and Inland Fisheries, Müggelseedamm 310, 12587 Berlin, Germany. E-mail: kirillin@igb-berlin.de*

² *German Weather Service FE14 Kaiserleistr. 29/35, D-63067 Offenbach am Main E-mail: Dmitrii.Mironov@dwd.de*

Abstract

The immediate effect of the climate warming on lake ecosystems consists in changing of the seasonal temperature pattern and, accordingly, the vertical density stratification. Simple 1D lake models should be, in principle, able to predict these changes, provided that reliable regional climate scenarios for the meteorological input are given. However, most existing models neglect the heat storage in lake sediments, which can play an essential role in distributing of the total heat amount in shallow lakes over the seasons. Our analysis includes 1D model experiments, based on long-term data from shallow lakes for 1961-2002 and regional climatic scenarios for the period until 2100. The modeling results demonstrate that heat storage in sediments is responsible for assymmetric seasonal distribution of climate-driven warming in lake with higher warming rate in spring and subsequent changes in mixing and ice regimes. Another factor affecting the mixing regime variability on climatic scales is the water transparency in upper layers. Its value is highly variable depending to a large degree on plankton biomass. The modeling results in couple with data from several shallow lakes suggest that even 10-20% changing of mean light extinction coefficient can lead to switching the seasonal mixing regime in a lake from polymictic to dimictic or vice versa. Thus, a reliable forecast of temperature and mixing conditions is questionable without a scenario for plankton dynamics in a lake.

**STIPS¹, A., E. GARCIA-GORRIZ² & K.
BOLDING^{1,2}**

Parameterizations of atmosphere-hydrosphere fluxes: An attempt to quantify uncertainty

¹ *Joint Research Center, Ispra
Establishment, 21020, Ispra,
Italien. E-mail:
adolfo.stips@jrc.it*

² *Institut de Ciències del Mar
CMIMA-CSIC, Barcelona, Spain.*

Abstract

Numerical simulations are an important tool for understanding and assessing the ecosystem in lakes and in the ocean. The atmosphere is the most important source of external forcing for these water bodies, thereby largely determining the internal dynamics.

Therefore the accurate parameterization of the heat, humidity and momentum flux at the atmosphere - hydrosphere interface is crucial to the successful simulation of the marine environment. This can be underlined by the example, that e.g. using not well adapted parameterizations for the Mediterranean Sea, the mean sea surface temperature in summer will be about 3-4 degC too high, with catastrophic consequences for the ecosystem, at least in the model. Comparing different published parameterizations for short wave radiation, latent heat flux and long wave radiation it is found that they can result in differences of up to about 50% under certain conditions. Sensible heat flux seems to be less critical and is anyhow of smaller magnitude. To make things worse, we must unfortunately state that we found in most examined models some coding errors in the air-sea interface routines, having more or less severe consequences for the fluxes. In summary, considering the large uncertainties that are apparent even in current air-sea flux parameterizations it must be concluded that specifically for doing multi-annual simulations it is necessary to carefully select and tune such methods that are appropriate for the region of interest.

DMITRII MIRONOV¹, ERDMANN
HEISE¹, EKATERINA KOURZENEVA²,
BODO RITTER¹ & NATALIA
SCHNEIDER³

Parameterisation of Lakes in Numerical Weather Prediction and Climate Models

*¹German Weather Service,
Offenbach am Main, Ger-
many. (Corresponding author:
dmitrii.mironov@dwd.de)*

*²Russian State Hydrometeoro-
logical University, St. Petersburg,
Russia.*

*³University of Kiel, Kiel, Ger-
many.*

Abstract

The application of the lake model FLake (<http://lakemodel.net>) to represent the effect of lakes in numerical weather prediction (NWP) and climate models is discussed. As a lake parameterization scheme, FLake is implemented into the limited-area NWP model COSMO and into the regional climate models CLM and RCA. It is on the way into the NWP model HIRLAM. First results from a numerical experiment with the coupled COSMO-FLake NWP system, including the complete COSMO model data assimilation cycle operational at the German Weather Service, are presented. Some challenging issues are discussed.

Introduction

Lakes significantly affect the structure of the atmospheric boundary layer and therefore the surface fluxes of heat, water vapour and momentum. In most numerical weather prediction (NWP) and climate models, the effect of lakes is either entirely ignored or is parameterised very crudely. In coarse resolution models, a large number of small-to-medium size lakes are indistinguishable sub-grid scale

features. These lakes become resolved scale features as the horizontal resolution is increased. Then, a physically sound lake model is required to predict the lake surface temperature and its time-rate-of-change. Apart from being physically sound, a lake model must meet stringent requirements of computational economy.

The application of the lake model FLake [1] to parameterise the effect of lakes in NWP and climate models is discussed. Much attention is focused on the implementation of FLake into the limited-area NWP model COSMO (formerly LM, [3]). FLake is a bulk model capable of predicting the vertical temperature structure and mixing conditions in lakes of various depth on the time scales from a few hours to many years. The model is based on a two-layer parametric representation of the evolving temperature profile and on the integral energy budget for the layers in question. The same concept is used to describe the temperature structure of the ice cover. Using the integral approach, the problem of solving partial differential equations (in depth and time) for the temperature and turbulence quantities is reduced to solving a number of ordinary differential equations for the time-dependent parameters that specify the evolving temperature profile. This approach, that relies on “verifiable empiricism” but still incorporates much of the essential physics, offers a very good compromise between physical realism and computational economy. FLake has been favourably tested against observational data through single-column numerical experiments. A detailed description of the model is given in [1]. Further information about FLake can be found at <http://lakemodel.net> or <http://nwpi.krc.karelia.ru/flake>.

Implementation of FLake into the limited-area NWP model COSMO

As a lake parameterization scheme, FLake is implemented into the limited-area NWP model COSMO. In order to be incorporated into COSMO, or into any other NWP or climate model, FLake requires a number of two-dimensional external-parameter fields. These are, first of all, the fields of lake fraction (area fraction of a given numerical-model grid box covered by the lake water) and of lake depth. A lake-fraction field is developed on the basis of the Global Land Cover Characterization data set with 30 arc sec resolution. Since no tile approach is used in COSMO, i.e. each COSMO grid box is characterised by a single land-cover type, only the grid boxes with the lake fraction in excess of 0.5 are treated as lakes. A data set containing mean depths of a number of European lakes and of a few lakes from other regions of the world is developed at the German Weather Service (DWD). The lake-depth external-parameter field is generated using that data set and the lake-fraction field.

Each lake is characterised by its mean depth. Results from single-column numerical experiments suggest that the use of a mean depth to the bottom is the best choice as far as the prediction of the water surface temperature and of the ice characteristics is concerned. These quantities are of prime importance in NWP and climate modelling. This choice is in fact consistent with the one-dimensional character of the lake model. For lack of better data, it is the only choice for most small-to-medium size lakes. Deep lakes are currently treated with the “false bottom”. That is, an artificial lake bottom is set at a depth of 50 m. The use of such expedient is justified since, strictly speaking, FLake is not suitable for deep lakes (because of the assumption that the thermocline extends down to the lake bottom). However, as the deep abyssal zones typically experience no appreciable temperature changes, using the false bottom one can expect FLake to produce satisfactory results.

Numerical experiment with the coupled COSMO-FLake NWP system

A numerical experiment, hereafter referred to as COFLEX, with the COSMO-FLake coupled system including the entire COSMO data assimilation cycle operational at DWD, is performed. The main goal with COFLEX is to see if the COSMO-FLake shows a reasonable performance with respect to the lake surface temperature (equal to the water temperature in the mixed layer or to the ice surface temperature if a lake is frozen), and to the lake freeze-up and melting. In order to save computational resources, the so-called LM1 numerical domain is used in COFLEX. That domain was operational at DWD until October 2005, prior to the operational implementation of the COSMO-EU whose numerical domain is much larger than the LM1 domain but the horizontal grid size is the same (ca. 7 km). A reader is referred to the COSMO web page, <http://www.cosmo-model.org>, for details of the COSMO model and its operational implementation at different NWP centres. Using the lake-fraction and the lake-depth external-parameter fields for the LM1 domain and a one-band exponential approximation of the decay law for the flux of solar radiation with the default value of $\gamma = 3 \text{ m}^{-1}$, the COSMO-FLake is run over a year, from 1 January to 31 December 2006. The surface fluxes of momentum and of sensible and latent heat are computed with the operational COSMO surface-layer scheme [2]. COFLEX is started on 1 January 2006, using the lake surface temperature from the COSMO sea surface temperature (SST) analysis as the initial condition and assuming no ice. The bottom temperature is set to the temperature of maximum density, and the shape factor with respect to the temperature profile in the thermocline is set to its minimum

value (see [1] for details of the temperature profile parameterisation used in FLake). The initial mixed-layer thickness is set to 10 m or to the lake depth, whichever is smaller. For lake grid boxes with the lake depth smaller than 10 m, mixing down to the lake bottom is assumed. Once a cold start is made, the COSMO-FLake runs freely, i.e. without any correction of the lake surface temperature and of the other FLake variables.

Preliminary analysis of the COFLEX results indicates a satisfactory performance of FLake in COSMO. Many lakes present in the LM1 domain are frozen and the ice melts in a reasonable time span. A detailed quantitative assessment of the simulated ice characteristics is difficult to make. A qualitative assessment is, however, possible on the basis of the available empirical information (see e.g. the World Lakes Database, <http://www.ilec.or.jp/database>, where data on the lake water temperature and on the duration of ice cover are given for a number of lakes). Examination of results from COFLEX suggests that the lakes that freeze up in reality do also freeze up in COSMO-FLake.

For three lakes, Lake Hjälmaren, Sweden, Lake Balaton, Hungary, and Lough Neagh, UK, the lake surface temperature predicted by COSMO-FLake (00 UTC values from the assimilation cycle), is compared with the lake surface temperature from the operational COSMO SST analysis (performed once a day at 00 UTC). Notice that in COFLEX the temperature from the routine COSMO SST analysis has no direct effect on the lake surface temperature that is now predicted by FLake. A substantial difference between the two temperatures is clearly seen in Figs. 1–3.

For Lake Hjälmaren and Lake Balaton, the difference is particularly striking during winter when it often exceeds ten degrees. Such a large temperature difference is brought about by the procedure used to determine the water surface temperature in the framework of the routine COSMO SST analysis. In case the observational data for a water-type COSMO grid box are not available, the surface temperature for that grid box is determined by means of interpolation between the nearest water-type boxes for which the surface temperature is known (from satellite data or from in situ measurements). Such procedure is not too harmful for sea points. Large horizontal gradients of the sea surface temperature are comparatively rare, so that the interpolated SST is expected to be a reasonably good approximation of the actual SST. In contrast to open sea, lakes are enclosed water bodies of a comparatively small horizontal extent. The lake surface temperature is a result of a complex interplay of physical processes in the lake in question. It has little or nothing to do with the surface temperature obtained by means of interpolation

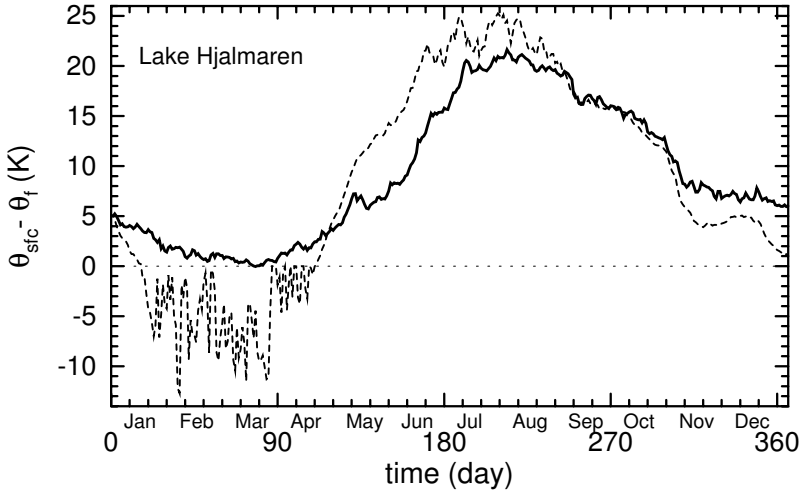


Figure 1: Lake surface temperature θ_{sfc} ($\theta_f = 273.15$ K is the fresh-water freezing point) in Lake Hjälmaren over the period from 1 January to 31 December 2006. Dashed curve shows the lake surface temperature predicted by FLake, and solid curve shows the temperature from the routine COSMO SST analysis. Curves are the results of averaging over the adjacent COSMO grid boxes that constitute the lake in question.

between the alien water bodies. Notice also that the COSMO SST analysis does not explicitly account for the presence of ice.

For many lakes the interpolation is likely to occur between the sea points. During winter, the above procedure yields a too high lake surface temperature that stays well above the freezing point even though the lake considered is frozen in reality. As clearly indicated by empirical data, both Lake Hjälmaren and Lake Balaton are frozen up over a long period of time (typically, over four and a half and over one and a half months, respectively), whereas the surface temperature from the routine COSMO SST analysis indicates that both lakes remain ice free. This proves to be the case for many other lakes in the model domain (not shown). The situation is not encountered if FLake is used to predict the lake characteristics. Since FLake allows the lake surface temperature to adequately respond to atmospheric forcing, lakes freeze up and the lake surface temperature, which is then equal to the ice surface temperature, drops in response to surface cooling.

An overestimation of the water (ice) surface temperature in the routine COSMO SST analysis may have far-reaching implications

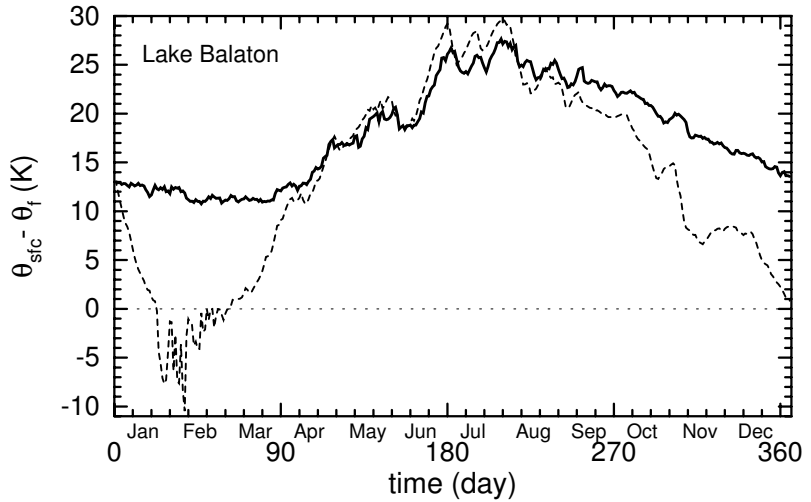


Figure 2: The same as in Fig. 1 but for Lake Balaton.

for the forecast quality. It leads to drastically increased surface fluxes of sensible and latent heat, particularly during winter. This in turn may result in the development of artificial cyclones over water bodies, leading to a considerable degradation of the COSMO performance. The situation will not occur if FLake is used to predict the lake surface temperature.

For Lough Neagh, the difference between the two temperatures proves to peak during summer. Again, the temperature from the COSMO SST analysis may result from the interpolation between the sea points. As the sea thermal inertia is high, the temperature from the SST analysis is likely to underestimate the actual lake surface temperature during summer. A considerably higher temperature is predicted by FLake as it allows the lakes to adequately respond to the summer heating.

Conclusions and outlook

The lake model FLake is incorporated as a lake parameterization scheme into the limited-area NWP model COSMO. Results from a numerical experiment with the coupled COSMO-FLake system, including the complete COSMO data assimilation cycle, indicate a good performance with respect to the lake surface temperature and to the freeze-up of lakes and the ice break-up. In particular, the use of FLake allows to do away with a significant overestimation of the lake surface temperature during winter that is typical of the routine

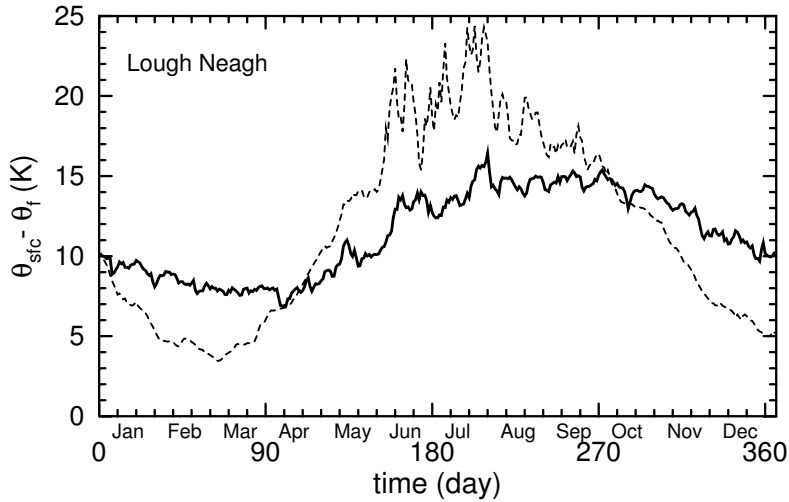


Figure 3: The same as in Figs. 1 and 2 but for Lough Neagh.

COSMO SST analysis. Work is underway at DWD to comprehensively assess the effect of FLake on the quality of the COSMO forecasts. Subject to successful verification of results from numerical experiments, FLake is expected to come into operational use.

Further development of FLake in terms of the model physics should address an extension of the temperature profile parameterisation to include the abyssal layer below the lake seasonal thermocline. What is even more important from an application standpoint is the extension of the lake-depth data base in order to eventually cover the entire globe. This should allow the application of FLake over an arbitrary numerical domain. Apart from the lake depth, it is advantageous to collect data on other lake characteristics, first of all, on the optical properties of the lake water.

One more challenging issue is the lake temperature spin-up following a cold start of FLake in an NWP or climate model. Lakes have a long memory. That is, erroneous initial conditions result in an erroneous heat content of the lake in question, leading to erroneous predictions of the lake surface temperature until the memory is faded. For stratified lakes this may last several months. Observations usually offer data on the water-surface temperature only, whereas the information about the entire temperature profile that is required for the FLake initialisation is lacking. A way out is to generate the so-called perpetual year solutions for a number of typical lakes present in a given numerical domain, using climatological mean meteorological data to specify atmospheric forcing. A per-

petual year solution is obtained by repeating a year-long simulation, using one and the same annual cycle of forcing, until a periodic “perpetual year” state is achieved. That is, running the model for one more year will not change the annual cycle of the lake-model variables. Although a perpetual year solution represents a climatological mean state of the lake in question, not the state of that lake at a particular date, it is a reasonable zero-order approximation that should considerably reduce the lake-temperature spin-up time. As the perpetual year solutions are generated through the stand-alone single-column FLake runs, the procedure is computationally inexpensive.

Acknowledgements. We thank Michael Buchhold, Thomas Hanisch, Peter Meyring, Van-Tan Nguyen, Ulrich Schättler and Christoph Schraff for discussions and for many helpful suggestions concerning the implementation of FLake into the COSMO model and numerical experiments with the coupled COSMO-FLake system. The work was partially supported by the EU Commissions through the projects INTAS-01-2132 and INTAS-05-100007-431.

References

- [1] Mironov, D. V. Parameterization of lakes in numerical weather prediction. Part 1: Description of a lake model. Technical Note, German Weather Service, Offenbach am Main, Germany, 2006.
- [2] Raschendorfer, M. The new turbulence parameterization of LM. *COSMO Newsletter*, No. 1:75–96, 2001.
- [3] Steppeler, J., G. Doms, U. Schättler, H. W. Bitzer, A. Gassmann, U. Damrath, and G. Gregoric. Meso-gamma scale forecasts using the non-hydrostatic model LM. *Meteorol. Atmos. Phys.*, 82:75–96, 2003.

BURCHARD¹, H., & L. UMLAUF¹

Impact of along-flow density gradients on sediment transport in estuaries (!), the Wadden Sea (!?) and in lakes (?)

¹ *Baltic Sea Research Institute
Warnemünde, Dept. of Physical
Oceanography and
Instrumentation, Seestraße 15
18119, Rostock, Deutschland. E-
mail: hans.burchard@io-
warnemuende.de*

Abstract

The hypothesis that the interaction between horizontal density gradients and tides significantly contributes to the accumulation of suspended particulate matter (SPM) in the Wadden Sea has recently been supported by numerical simulations. During winter, these density differences occur mostly due to freshwater run-off and net precipitation, during summer mostly due to differential heating. It has been demonstrated with idealised one-dimensional water column model simulations that the interaction of such small horizontal density gradients with tidal currents generate net onshore SPM fluxes. Major mechanisms for this are tidal straining, estuarine circulation and tidal mixing asymmetries. In tidal estuaries, these mechanisms have been identified as the major drivers of Estuarine Turbidity Maxima (ETMs) in the region of the upstream limit of the salt intrusion.

Three-dimensional model simulations in a semi-enclosed Wadden Sea embayment with periodic tidal forcing show that SPM with sufficiently high settling velocity is accumulating in the Wadden Sea bight due to density gradients. This is proven through a comparative model simulation in which the dynamic effects of the density gradients are switched off, with the consequence of no SPM accumulation. These numerical model results motivate future targeted field studies in different Wadden Sea regions with the aim to further support the hypothesis.

In stratified lakes, such density gradients along the major direction of oscillating shear flows occur near the sloping bed during internal seiches. It will be discussed with the aid of idealised numerical

simulations, whether these processes important for the SPM transport in the Wadden Sea may also be relevant for stratified lakes.

¹DEMCHENKO, N, ²CHUBARENKO, I.

**The transformation of one
type of littoral circulation to
another in a basin with
sloping bottom while passing
the temperature of maximum
density**

*^{1,2}P.P. Shirshov Institute of
Oceanology, Atlantic branch,
prospect Mira, 1, 236000,
Kaliningrad, Russia. E-mail:
ndemchenko@mail.ru*

Abstract

The present study is devoted to the investigation of transformation of one type of littoral circulation (gravity current) into another (subsurface jet) in water basin with inclined bottom while passing the temperature of maximum density (TMD) due to heating through the surface. On the base of laboratory experiments we conclude that (i) the thermal bar is a complicated phenomenon, consisting of the gravity current, subsurface jet and a compensating flow in the intermediate layer; (ii) it has two stages in its development: initial «slow» stage and subsequent «fast» stage; (iii) in the «slow» stage, the subsurface jet is very weak, horizontal density gradient between shallow and deep part is small and TMD–isotherm propagates faster than the subsurface jet; (iv) in the «fast» stage, due to increasing horizontal density gradient, the subsurface jet becomes evident and the TMD–isotherm is carried offshore by the «nose» of subsurface jet (v) the speed of propagation of the thermal bar in the «fast» stage is close to that of a convective jet.

Introduction

In spring period, shallow waters heat faster due to solar radiation than deeper ones (Kreiman, 1989; Farrow, 1995a,b). If water is still below the temperature of maximum density (exactly - 3.98 °C for fresh water), it leads to vertical convective mixing and formation of denser water cascade down-slope. When water temperature in the shallow-most part of the slope reaches the temperature of maximum density, a cell with stable vertical density

stratification appears there. This cell enlarges with time of heating, being bordered from offshore side by the isotherm of 4°C . When a horizontal density gradient has reached a certain threshold, a warm surface jet is generated from shallow to deeper part of the basin. This jet propagates towards the part, where vertical density stratification is still unstable, and slow denser water cascades still exist further down-slope. Some water volume in-between, associated with the 4°C -isotherm, is rather inertial: near the density maximum, temperature differences do not lead to considerable density gradients, and water motions are very weak. This very area is in fact what one calls “the thermal bar”, meaning a barrier for water mixing. In field, a dynamical front (line of convergence, with bands of foam, floating algae etc.) is associated with this area, which is called “the thermal bar” as well. This double meaning is a bit confusing, and we will use another terminology in this paper: we describe, separately, the propagation of the 4°C -isotherm (disregarding how water moves around) and the propagation of the nose of the surface jet. It is clear, that both of them are “associated” with the thermal bar, and have exact physical meaning, but do not coincide.

Laboratory modeling of (Kreiman, 1989) showed for the first time that the thermal bar has two phases of its propagation: initial «slow» phase and later «fast» stage. Numerical modeling has demonstrated (Farrow, 1995a,b) that the thermal bar is a complicated phenomenon. It was pointed out, that it consists of (i) a surface jet, (ii) gravity current and (iii) down-welling zone. Field data (Rianguin, 2002) demonstrated, that the thermal bar front is 3-dimensional surface with very small angle of inclination of the frontal division (is around 0.001), i.e. warm stratified waters are overlying colder quasi-isothermal waters. Thus, it is already proved by field data (Rianguin, 2002), that the thermal bar is not a sort of vertical «wall».

Results

In order to investigate water-exchange between shallow and deep part of a basin subject to cooling from the surface («autumn period»), a series of laboratory experiments were carried out in laboratory tank (the length of tank is 5 m, bottom slope 3-12 degree). In the beginning of every experiment, water was homogenized by intense mixing. During the experiments, the water body became stratified both in vertical and in horizontal: (i) in deep part of the basin, cold surface and bottom boundary layers were observed (dT up to 0.3°C), whilst the core part was well mixed; and (ii) water above the slope became significantly colder than that in deep part of the basin. The coldest water was on the top of

incline (dT up to $1.5^{\circ}C$). The flow pattern consists of a gravity current (with its flow-rate increasing down-slope, because new water masses permanently join it), a compensating flow toward to shallow part and slow compensating upward flow over the whole length of the tank. Velocity profile in deep part always had a significant maximum at the depth of the lower limit of the mixed layer (Chubarenko, et.al., 2005).

Flow structure was investigated by photographing the subsequent tracks from potassium permanganate crystals, which were dropped into the tank to produce vertical dyelines.

Track deformations were recalculated into velocity profiles and flow-rates. This way, about 60 series of photos were analyzed: for 3 locations, for 3 bottom slopes (3.7, 6.7, 12 degrees) and for different Ra number. We concluded, that (i) the highest speed of flow is observed always at the break point, where its thickness is also highest and makes up to $0.15 D$, (ii) the maximum observed speed of the gravity current was 10.8 mm s^{-1} – at the break point of the smallest slope of 3.7 degrees, and under moderate driving temperature difference of $T_w - T_a \sim 2^{\circ}C$, (iii) typical order of magnitude for the speed of bottom flow is $2-7 \text{ mm s}^{-1}$ for all bottom slopes, for the driving temperature difference up to $9^{\circ}C$, (iv) return flow in upper layer is 2-3 times slower, (v) the maximum of the return flow is located not at the surface, but below it, at the depth of $\sim 0.1-0.2 D$ (Chubarenko, et.al., 2005).

Laboratory experiments with heating from the surface («spring period») were performed in the same tank. The heating was carried out using by lamps or heat-exchange with the warm air.

During these experiments, water body got stratified in vertical and horizontal as well. The intensive heating using lamps caused the stratification close to the exponential one. More soft heating by exchange with warmer air caused the temperature decrease in upper layers as small as $0.04-0.062 \text{ }^{\circ}C \text{ cm}^{-1}$. Horizontal profiles of the upper layer temperature are self-similar; the temperature difference between shallow and deep part was more than $2.7^{\circ}C$. These conditions were chosen in order to investigate the main features of the motion when it is strong enough, and to extrapolate them to smaller buoyancy flux characteristic for the thermal bar conditions.

We concluded, that (i) the maximum of the return flow is located below the undersurface jet, with the maximum at the depth of $\sim 0.4-0.7 D$ (D is the depth of the tank), (ii) Vertical profile of the speed of the compensating flow is symmetric, with a

thickness 1.5-2 times larger, and a speed 2-5 times less than that of the undersurface jet, (iii) the typical profile consists of a narrow undersurface jet and a compensating flow, occurring directly below it, and a straight portion of the profile connecting their «noses».

The next set of laboratory experiments - with passing of the TMD - were performed in order to investigate temporal and spacial variations of the subsurface jet and the gravity current in presence of the TMD.

During one of the experiments, surface temperature was monitored using the array of thermistors in surface layer (1.5 cm) over the different depths (0.02, 0.04, 0.06, 0.1, 0.12, 0.145, 0.16 m).

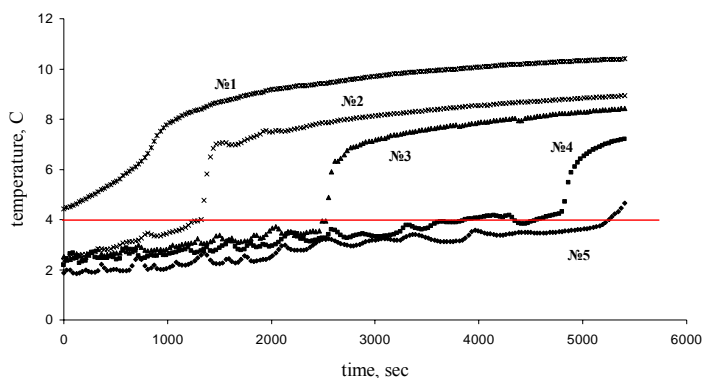


Figure 1 Increase of surface temperature for 5 locations of the thermistors in the laboratory tank (distances from the shore line are 26, 55, 80, 138, 168 cm). Horizontal line indicates the temperature of maximum density.

We conclude, that the temperature jump (Fig.1) occurs, when the subsurface jet reaches the location of the thermistors. When the subsurface jet arrives, the horizontal temperature gradients suddenly decrease.

At the beginning of the «fast» stage in shallow part of tank speed of the propagation of the subsurface jet was 0.23 mm s^{-1} , it increased up to $0.31 - 0.46 \text{ mm s}^{-1}$ over the different depths. At the end of the domain the speed of the subsurface jet was 0.46 mm s^{-1} . The 4°C -isotherm propagates with the same speed.

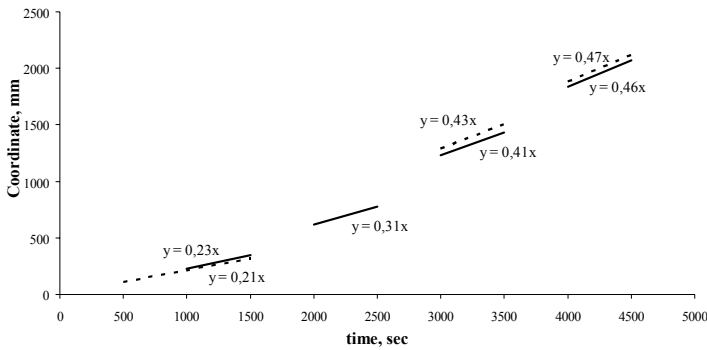


Figure 2 Speed of propagation of subsurface jet (black line) and 4°C -isotherm (dashed line).

We conclude, that the two phases of the thermal bar are connected with the following physical process: (i) the phase of intense vertical mixing over sloping bottom, characterized by the gravity current generation from the shallow to the deep area and the phase of the stable vertical stratification, characterized by generation of lighter water masses over the slope (ii) at the beginning of the process («slow» stage), horizontal gradient is rather small, the subsurface jet is weak and propagates slower than 4°C -isotherm; during the experiment, horizontal gradient increases, the subsurface jet is generated, carrying lighter waters to the deep part (iii) in the «fast» stage the subsurface jet accelerates twice in comparison to the beginning of this stage (vi) the convergence zone due to the presence of the temperature of maximum density was not observed; dynamical front of the thermal bar is associated with the «nose» of subsurface jet (v) the thermal bar is a complicated phenomenon, including the gravity current, (under)surface jet and compensating flow in the intermediate layer (vi) speed of propagation of the thermal bar front in “fast” stage is close to that of a convective jet.

Acknowledgements

I would like to express great thanks to Technical University of Eindhoven, Fluid Dynamics Laboratory, especially to Professor GertJan van Heijst, for the possibility to perform these experiments and to my supervisor Dr. Irina Chubarenko for her permanent support and help. This work is support by INTAS 06-100014-6508, RFBR №07-05-00850, 06-05-64138.

References

- CHUBARENKO, I., DEMCHENKO, N., HUTTER, K. 2005. Horizontal convection induced by surface cooling over incline: laboratory experiment Proc. International Conference «Fluxes and Structures in Fluids». Moscow, Russia. Pp. 27-29.
- KREIMAN K, D. 1989. Thermal bar based on laboratory experiments. *Oceanology*, 29. Pp. 695-697.
- RIANGIN P.I. 2002. *Lake Ladoga: Past, Present, Future*. Petrozavodsk. Pp. 355.
- FARROW, D.E. 1995a. An asymptotic model for the hydrodynamics of the thermal bar. *J.Fluid Mech.*, 289. Pp. 129-140.
- FARROW, D.E. 1995b. A numerical model for the hydrodynamics of the thermal bar. *J.Fluid Mech.*, 303. Pp. 279-295.

PODSECHIN, V.¹ FILATOV, N.², FRISK
T.¹, Terzhevik A.², BILALETDIN Ä.¹ &
PAANANEN A.¹

Modelling circulation and sediment dynamics in Kondopoga Bay, Lake Onega

¹ Pirkanmaa Regional Environment
Centre, POB 297, 33101,
Tampere, Finland. E-mail:
victor.podsetchine@ymparisto.fi

² Northern Water Problems Institute
KRC RAS, Aleksander Nevsky
str., 50, 185003, Petrozavodsk,
Republic of Karelia, Russia. E-
mail: nfilatov@nwpi.krc.kareliarut

Abstract

Kondopoga Bay is a large and deep water bay of Lake Onega (North-Western Russia). It is to a great extent isolated from the central open part of the lake. Over the last several decades the bay was under the heavy anthropogenic load from the Kondopoga paper-pulp mill. This led to a considerable pollution of the bay waters, accumulation of industrial wastes in bottom sediments and triggered eutrophication processes. A coupled hydrodynamic and sediment transport model COHERENS was applied to study the dynamics of suspended sediments, to determine the location of resuspension zones during stormy episodic events.

Introduction

Lake Onega (Onezhskoye Ozero in Russian) is the second largest lake in Europe after Lake Ladoga. The lake is located in the Karelian Republic, in the Leningradskaya and Vologodskaya regions of the Russian Federation. It is connected to the Baltic Sea via the river Svir (Syväri), Lake Ladoga and the Neva River and also to the White Sea via a channel. The lake surface area is 9693 km², volume is 291 km³, maximum depth is 120 m, mean depth is 30 m and mean residence time is about 14 years (Filatov et al., 1999). According to recent studies Lake Onega, as a whole, preserves its oligotrophic status (Filatov et al., 1999), but due to its high limnetic heterogeneity and very complicated shape and bathymetry (Fig. 1), different parts of the

lake experience different levels of anthropogenic load and react variously.

Pollution by industrial and communal wastewaters started from the middle of the last century, triggered eutrophication and affected negatively especially three largest bays of the lake: Kondopoga, Petrozavodsk and Bolshaya bays (Sabylina & Martynova, 2003). The annual discharge of wastewaters into the lake is about 0.12 km^3 and 83% (0.10 km^3) is discharged directly to the lake from the three main industrial centres on the western shore, namely Petrozavodsk (Petrozavodsk Bay), Kondopoga (Kondopoga Bay) and Medvezhjegorsk (Povenets Bay).

Kondopoga Bay is extended from southeast to northwest for a distance of 33 km. It has the surface area of 243 km^2 , and water volume is 4.3 km^3 (Belkina, 2005). The maximum depth is 82 m and the mean depth is 21 m. The Suna River, third large tributary of Lake Onega, drains into the bay. The mean annual inflow is 2.43 km^3 , the river brings annually about 3800 tons of suspended matter. Kondopoga paper-pulp mill, put into operation in 1929, is the main source of bay water pollution. The wastewater volume varied from 2.6 mln m^3 in 1948 to 70.3 mln m^3 in 1988 (Filatov et al., 1999). About 50 mln m^3 of wastewater is being discharged nowadays. It brings in average 3000 tons of suspended matter, 8 tons of oil products, 4 tons of methanon, 60 tons of P, 80 tons of N, 147 tons of chlorides, 9 tons of formaldehyde, 2000 tons of lignosulphonates (Belkina, 2005).

Mixture of silt with sand, clay and ore is typical for bottom sediments of Kondopoga Bay. More than two-thirds of the bed is occupied by grey-green clayey silts (Belkina, 2005). The concentration of suspended sediments decreases from 4 mg/l in the upper part of the bay to 1.7 mg/l in the southeastern area (Filatov et al., 1999).

The study of the suspended sediments dynamics has practical importance since it helps to quantify the pollution pathways in the bay.

Results

A coupled hydrodynamic and sediment transport model COHERENS (Luyten et al., 1999) was applied to study the dynamics of suspended sediments, to determine the location of resuspension zones during

stormy episodic events. The suspended sediment block describes sinking, resuspension to and from the fluff layer, advection and diffusion of single-fraction of suspended particulate matter. Results of numerical experiments will be presented and discussed.

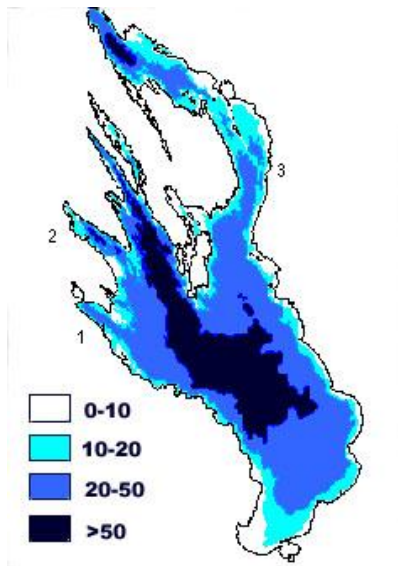


Figure 1 Bathymetric map of Lake Onega (source: Northern Water Problems Institute, KRC RAS, Petrozavodsk, Russia). 1 - Petrozavodsk bay, 2 – Kondopoga bay, 3 – Bolshaya bay.

Acknowledgements

The work has been carried out within the framework of the joint Finnish-Russian project, financially supported by the Ministry of the Environment, Finland.

References

- FILATOV N. N. (ED.), 1999. *Onezhskoe ozero, ekologicheskie problemy (Lake Onega. Ecological Problems)*. Petrozavodsk, Karelian Research Centre, Russian Academy of Sciences. 294 p. /in Russian/.
- LUYTEN P.J., JONES J.E. PROCTOR R., TAYLOR A., TETT P., WILD-ALLEN K., 1999. *COHERNS. A Coupled Hydrodynamical-Ecological Model for Regional and Shelf*

Seas. User Documentation. MUMM Report, Management Unit of the Mathematical Models of the North Sea, 914 p

SABYLINA A., MARTYNOVA N. 2003. Water chemistry changes in Lake Onega and it's basing during last fifty years. In: H. Simola, A.Yu. Terzhevik, M. Viljanen & I.J. Holopainen (eds). *Proceedings of the Fourth International Lake Ladoga Symposium 2002*. University of Joensuu. Publications of Karelian Institute 138. P.317-325.

BELKINA N. A. 2005. Retrospective Assesment of bottom deposits in Kondopoga Bay, Lake Onega. *Water Resources*, vol.32, No 6, pp. 629-639.

6 Thermo- and Hydrodynamics

MACCREADY, P.¹, BANAS, N. S.¹,
HICKEY, B. M.¹, AND DEVER, E. P.²

Energetics of a River Plume

¹ *University of Washington,
Seattle, WA, USA. E-mail:
parker@ocean.washington.edu*

² *Oregon State University,
Corvallis, OR, USA*

Abstract

Mechanical energy can be a compact way of describing the function of fluid systems. In this talk I detail the complete energy budget for a realistic numerical simulation of the Columbia River plume on the U.S. northwest coast. This is a complex system, where the small estuarine scales and the broader shelf scales are strongly coupled, and forcing from river flow, tides, and wind stress are all important. The energy budget is able to clearly quantify the important mixing processes in different parts of the domain, demonstrating the importance of tidal mixing in the estuary and wind mixing on the shelf. A key challenge however, both conceptually and numerically, arises from the open boundary on the shelf. In the volume integrated kinetic energy budget this boundary is the locus of both barotropic (tidal) and baroclinic (sometimes due to internal waves) pressure work on the system. The open boundary also allows the advection of potential energy into the domain, as the ocean stratification continually pushes against that created by river flow and tidal mixing near the estuary mouth. These terms may be large, difficult to calculate accurately, and of unfamiliar meaning. Overall, it appears that we still have much to learn about how to interpret energy budgets in such systems.

Introduction

In this talk I will explore the tidally-averaged mechanical energy budget within an estuary and coastal river plume. The motivation is to better understand how coastal upwelling works in the presence of freshwater input and tidal mixing due to an estuary. Classically, coastal upwelling has been understood as a wind forced process (e.g. Gill 1982 p 403-, Allen et al. 1995) with alongshore wind stress driving offshore surface Ekman transport and upwelling of deeper waters, particularly in the frictional bottom boundary layer. The addition of a freshwater source may be expected to increase

stratification and thus decrease upwelling – because greater energy would be required to lift deep water (Hickey et al. 2005). Conversely, enhanced tidal mixing may increase the vertical flux of nutrients to the euphotic zone. Thus from the start it is not clear how the presence of an estuary would affect coastal upwelling. In this work I do not give a complete answer to the above problem, but instead explore part of it. I focus on just the vertical turbulent mixing in the estuary and river plume, asking whether tides or wind is the more important forcing mechanism in different regions. Not surprisingly, I find that tides dominate in the estuary, while wind is more important in the far field plume. Interestingly, the net mixing in both places is comparable; indicating that a full understanding of water mass transformation must consider both the estuary and the shelf, and both types of forcing.

Results

The analysis is done using the Regional Ocean Modeling System (ROMS, Rutgers version 2.2) to perform a 3 month hindcast (June-August) of 2004 summertime circulation on the Washington and Oregon shelf, and in the adjoining Columbia River estuary. ROMS (Haidvogel et al. 2000) is widely used for coastal (e.g. Haidvogel 2005, Peliz et al. 2003) and estuarine (MacCready et al. 2002, Warner et al. 2005, Li et al. 2005) simulations. The simulation uses a stretched, spherical grid (Fig. 1) with ~500 m resolution in the estuary and plume region, telescoping to ~7 km in the far corners. The Columbia River beyond about 50 km from the coast is too small to model efficiently with this system, so we add a straight river channel 3 km wide and 3 m deep, extending about 300 km to the east. This allows tidal energy to propagate freely upstream, and almost no tidal energy gets to the eastern edge of the river channel. The model is forced with realistic river volume flux and temperature from a USGS gauging station. Tidal forcing at the open boundaries comes from the TPO06 global analysis. Surface wind stress and heat flux come from the regional MM5 numerical weather prediction model. Initial and open boundary conditions come from the NCOM 9 km resolution model of the California Current System. The model has been extensively tested against moored and ship-based observations, as documented in a submitted paper (MacCready et al. 2007) available at:

www.ocean.washington.edu/rise/papers_&_talks.htm

This work is done as part of the RISE program (River Influences on Shelf Ecosystems).

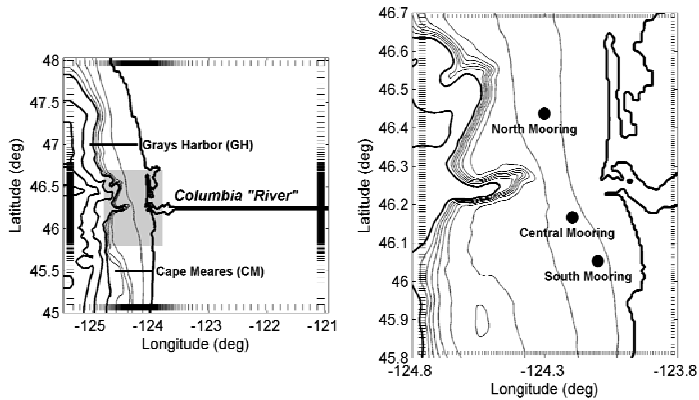


Figure 1 Left panel: the full domain of the numerical model, which includes the Washington and northern Oregon shelf and slope, and the Columbia River estuary. The resolution of the stretched grid is shown with tick marks at the edges. The Columbia River channel beyond 50 km from the coast is replaced by a straight channel which absorbs tidal energy. Locations (GH and CM) of CTD sections are shown. Bathymetry contour intervals are 100 m (thin lines) and 500 m (thick lines). The bay to the north of the Columbia River mouth is Willapa Bay. The right panel is a close up of the gray region, showing the locations of 3 moorings from the 2004 summer RISE program. Thin lines show isobaths on the shelf at 50 m intervals. Grid resolution is ~500 m in this area.

Typical model fields are plotted in Figure 2. The water leaving the estuary on ebb can have practical salinity of 15 or lower (Jay and Smith 1990c). The region within ~1 tidal excursion of the mouth (say 20 km) will be referred to as the “near field plume.” There the plume dynamics are strongly tidal, with a prominent surface front and nonlinear internal wave generation (Nash and Moum 2005, Orton and Jay 2005). Farther out on the shelf the plume is typically 3-20 m thick and loosely identified with surface salinity < 31 (Barnes et al. 1972, Landry et al. 1989, Hickey et al. 1998). Ambient seasonal currents and seasonal wind stress tend to push the plume up the length of the Washington coast in winter, and offshore to the southwest in summer (Hickey et al. 2005). The plume away from the mouth is subject to a variety of types of forcing. Local winds are important in surface boundary layers and in generating alongshelf currents on the shelf. However coastal trapped waves have been shown to be important in the plume region (Battisti and Hickey, 1984). On the inner shelf local wind forcing predominates (Oke et al. 2002). Flow on the outer shelf in this region is part of the California Current, flowing southward.

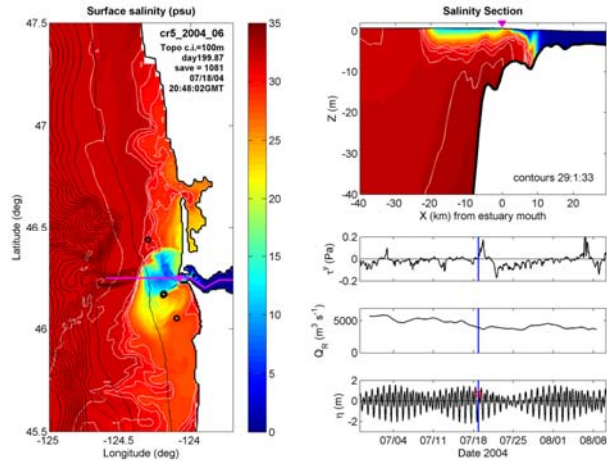


Figure 2 Typical fields from the numerical simulation. The left panel shows a map of surface salinity just before the start of a downwelling-favorable wind event. The windstress, riverflow, and tidal height are plotted versus time in the lower right panels. A salinity section across the shelf and into the Columbia River estuary is plotted in the upper right, following the magenta line in the map at left.

The volume integrated mechanical energy budget is shown in the equation in Figure 3. The volume integral extends from the seafloor to the free surface. We also average each term over several tidal cycles. Selected terms are plotted in Fig. 4, shown as integrals over each horizontal grid cell, so these are effectively vertically-integrated. We present only the forcing terms (WIND and the tidal part of the PRESSURE WORK), and the turbulent dissipation and mixing terms. The wind forcing (Fig. 4a) is generally positive, and shows the largest values in river plume regions. These are the places where the surface flow responds most directly to the wind. The convergence of tidal pressure work is plotted in Fig. 4b. We may expect the field to be positive where energy is being lost from the barotropic tide, and this is evident in both the Columbia River estuary and Willapa Bay. Farther offshore, particularly over the continental slope, there are regions of barotropic pressure work divergence (negative convergence), which is a surprising result. It is possible in principle to have barotropic pressure work divergence (e.g. across a stationary hydraulic jump), however there is also the possibility of errors in the energy calculation. Nevertheless, the overall level of error in the budgets is found to be reasonable. The dissipation (Fig. 4c) is negative definite, and strongest in the

estuaries. Irreversible mixing (Fig. 4d) is strongest near the Columbia River mouth, where strong dissipation and stratification coincide. Mixing is also apparent over the continental slope.

$$\begin{aligned}
 \frac{d}{dt} \left[\int_V KE_V dV + \int_{A_0} \frac{1}{2} \rho_0 g \eta^2 dA + \int_V \rho' g z dV \right] &= \text{(STORAGE)} \\
 - \int_{A_{OPEN}} (KE_V + \rho' g z) \mathbf{u} \cdot \hat{\mathbf{n}} dA &\text{ (ADVECTION)} \\
 - \int_{A_{OPEN}} (\rho_0 g \eta + p') \mathbf{u} \cdot \hat{\mathbf{n}} dA &\text{ (PRESSURE WORK)} \\
 + \int_{A_0} (u\tau^x + v\tau^y) dA &\text{ (WIND STRESS)} \\
 - \int_{V^+} \rho_0 K_M (u_z^2 + v_z^2) dV - \int_{A_0} \rho_0 C_D |\mathbf{u}^3|_{z^+} dA &\text{ (TKE PRODUCTION)} \\
 - \int_V g K_D \frac{\partial \rho'}{\partial z} dV &\text{ (BUOYANCY FLUX)}
 \end{aligned}$$

Figure 3 The volume integrated mechanical energy equation (both kinetic and potential energy). Names of the various terms are given in parentheses on the right.

Then volume integrals may be taken over larger regions: the estuary, the near field plume, and the far field plume. In terms of forcing, tidal pressure work was greatest in the estuary, whereas the wind was most important in the far field plume, as one might expect. In the near field plume both processes may be important. While net dissipation, particularly in the bottom boundary layer, was greatest in the estuary, the net buoyancy flux was distributed over all three regions. This highlights the difficulty of determining net budgets of buoyancy flux observationally, because the more dispersed, weaker, and episodic mixing in the wind-driven plume may not be neglected. The mixing efficiency is greatest, 20%, in the far field plume region, and is only 3% in the estuary. In part this represents the fact that some of the estuary volume was often unstratified, but it also reflects the fact that the river plume is a stratification feature that is particularly susceptible to wind driven mixing.

Finally, in order to understand the energetics of such a system (or eventually its role in the biological function of a coastal upwelling region) it is clear that we must consider the estuary, plume, and shelf as a single larger system. Only then will we be able to properly tell the story of how deep waters find their way to the surface.

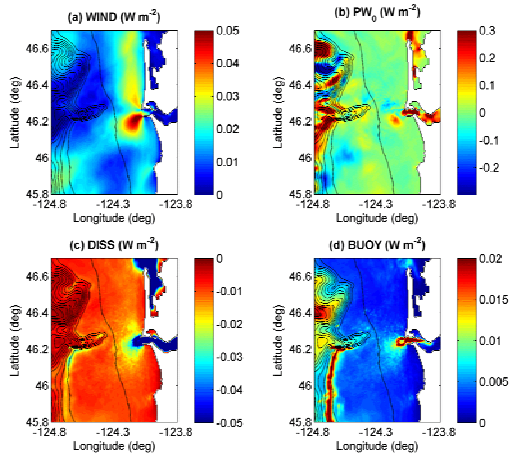


Figure 4 Selected fields from the time-averaged, vertically integrated, mechanical energy budget. These are averaged over the upwelling period indicated in Fig. 2. The wind stress term is plotted in (a). The tidal pressure work convergence term is plotted in (b). Dissipation (like TKE production) and buoyancy flux are plotted in (c) and (d). Isobaths are contoured every 100 m.

Acknowledgements

This work was generously supported by NSF grant OCE 0239089. The author would like to sincerely thank the many people who contributed to the ideas and analyses in this work, including Antonio Baptista, David Darr, Emmanuel di Lorenzo, Mike Foreman, Rob Hetland, David Jay, Steve Lentz, and Scott Tinis.

References

PLEASE REFER TO MACCREADY ET AL. (2007) WHICH MAY BE DOWNLOADED FROM THE URL GIVEN ON PAGE 2.

GALE, E. & PATTIARATCHI C.

Hydrodynamics of Intermittently Closing and opening Lakes and Lagoons

*University of Western Australia,
35 Stirling Highway, 6009
Crawley Western Australia
E-
mail: Chari.pattiaratchi@uwa.edu
.au*

Abstract

Coastal lakes with intermittent, restricted or choked inlets, the exchange and subsequent flushing, with the ocean, can become limited and therefore significant in defining the water quality. To examine the exchange and flushing characteristics of intermittently open coastal lakes, two field sites were chosen for a comparative study, with the main difference being the waterway size. The exchange and flushing characteristics were then examined through the use of field data analysis and numerical modeling, and the results illustrated that different processes were dominating the exchange and subsequent flushing, in the two lakes. Tidal processes were found to dominate within the smaller lake, which led to a short flushing timescale (days), and sub tidal processes dominated the larger lake, resulting in a much longer flushing timescale (months). A closer examination of the larger lake identified the dominating sub tidal process as a process defined as spring tidal setup, which is driven by the fortnightly variation in tides and friction within the inlet, and promotes the net advection of waters into and out of the lake on a fortnightly timescale. Numerical modeling was employed to examine the importance of spring tidal setup against different sub tidal forcing (changes in mean sea level and variations in local wind) and the results showed that the exchange, in all of the model runs, was still dominated by the spring tidal setup.

Introduction

Intermittently open shallow coastal lakes, also known as Intermittently Closing and Opening Lakes and Lagoons (ICOLLs) are an important sub category of coastal lagoon, due to their limited exchange with the ocean and their lack of river inflow. These specific characteristics make ICOLLs particularly vulnerable to the

trapping of nutrients and contaminants (Roy et al. 2001). In addition, the occurrence of high nutrient loads in these shallow, well lit systems favour the development of substantial biomass of attached and floating macro algae. When an ICOLL is open to the ocean, exchange through the inlet channel is often restricted due to its shallow nature. Therefore it is beneficial to try and understand some of the processes and timescales associated with the exchange and flushing of intermittent coastal lagoon systems in order to provide better management. Along the southeast coastline of Australia there are over 135 estuaries of which 45% are intermittently open (Pollard, 1994) and within this sub category approximately 72% are artificially opened (DNR, 2004). The resulting frequency and duration of the opening events can vary between and within ICOLLs, with frequencies ranging from 2- 3 times per year, to once every 2 years, whilst the duration can vary from weeks to months.

This paper examines two ICOLL systems located on the east coast of Australia, both of which are artificially opened, primarily for flood mitigation purposes. The paper will illustrate how these two systems, which appear quite similar in appearance, can act quite differently with regards to their flushing and exchange characteristics. The format of the paper will be split into two sections, the first will examine the exchange characteristics and the second section will examine the flushing characteristics, and then the results will be drawn together at the end by the conclusions.

Study Sites

The two field sites that were chosen for this study were Wamberal Lagoon (Figure 1) and Smiths Lake (Figure 2). Wamberal Lagoon is a small ICOLL system, with a waterway area less than 1km². The lagoon opens quite frequently (2-3 times per year on average), but rarely stays open to the ocean for longer than 2 weeks at any one time. The field data collection involved the deployment of a Nortek Acoustic Doppler Current Profiler (ADCP) at the bed, near the inlet channel and measured horizontal velocities every 10 minutes, with an averaging interval of 1 minute and a vertical spacing of 0.2 m. During the same time period two CTD probes were also deployed at the same location, one at the bed and one at the surface, suspending by a buoy. The CTD's recorded information at 30 minutes intervals, with an averaging interval of 5 minutes. The second field site,

Smiths Lake, is a larger ICOLL system, with a waterway area of approximately 11km². The lake opens less frequently (once every 18 months on average) and stays open between 1-4 months. The field data collection involved a similar field set up to that at Wamberal Lagoon.



Figure 1 Wamberal Lagoon.



Figure 2 Smiths Lake.

Results

The harmonic analysis for Smiths Lake highlighted the low frequency tidal constituents as potentially dominant processes driving water level fluctuations. Therefore spectral analysis of the water levels (3.5 months of data) was undertaken, to quantify the low frequency forcing within the lake. The beginning and end of the water level record were removed due to potential interference from the changing inlet geometry. It should be noted though, that changes in the inlet geometry might still be affecting the following analysis. The analysis was also undertaken on the offshore tidal water levels, to gain an understanding of local and remotely forced processes. The analysis confirmed the dampening of the high frequency forcing (O1, K1 and M2) within the lake, whilst also re-producing the peak in the low frequency band at 15 days. Whilst the low frequency peak at 15 days may be driven by the MSf tidal constituent, as highlighted in the harmonic analysis, it may also be due to the action of tidal pumping or spring tidal pumping, all of which have a similar frequency. The specific process producing this peak was investigated further through Fourier analysis (Figure 3). The area under each of the peaks in the spectral analysis indicated that that only 2 % of the energy coming into the lake was from tidal forcing (cf. 96 % in the ocean) and approximately 87.5 % was derived from the lower frequency forcing as opposed to only 4 % in the ocean, defining it as a much more significant process than the high frequency tidal forcing. A closer examination of the sub tidal lake water levels from the 17th July to the 10th August 2003 showed a fortnightly variation of approximately 0.5 m. This was much greater than the combined amplitude of all the identified tidal constituents (0.2 m) and suggested that another source of sub tidal forcing may be present within the lake.

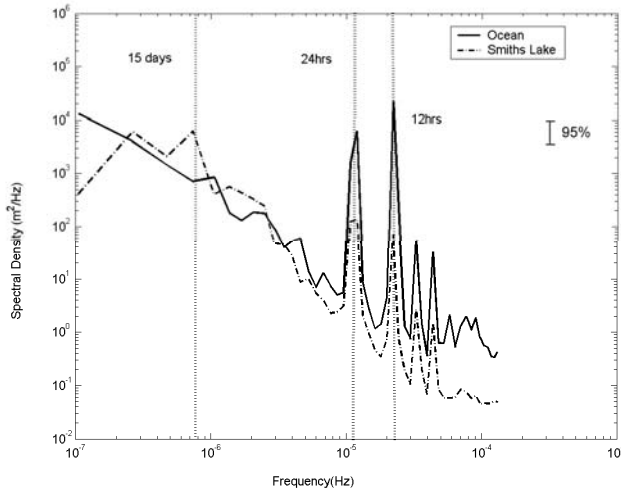


Figure 3 Spectral density plots of water level fluctuations within Smiths Lake (solid line) and the ocean (dotted line) over a 6-week period in 2003.

To examine the influence of the spring tidal pumping, on the exchange, at a longer timescale, a T-S diagram covering data from the 16th July – 10th August 2003, was plotted for the surface and bottom waters (Figure 4). The surface water mass changed in salinity from (1) to (2) (Figure 4) during the neap (21st) to spring (28th) tides, with a gradual increase in salinity. During the following spring (28th) to neap (4th) tides, the water masses (2) and (3) returned half way back to (1) and during the following neap (4th) to spring (11th) tides the water composition changed very little. The variation in response within the lake, over the two neap spring cycles appeared to correspond to variations in the mixed, semi diurnal tidal signal from the ocean.

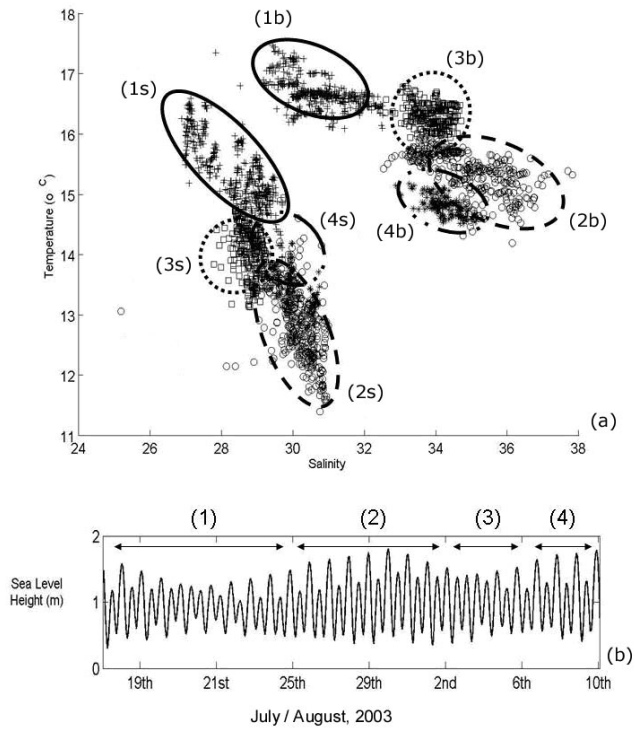


Figure 4 (a) T-S plot of the surface and bottom waters within Smiths Lake, covering data from the 16th July to the 10th August, 2003. The water masses are identified by the numbering (1) through to (4), and the surface waters are identified with an s, and the bottom waters are identified with a b, (b) Sea level height for the corresponding period, including the timing of the water masses identified by the numbering 1 through 4 above.

The first set of neap tides (~ 21st July) had a smaller diurnal inequality, when compared to the second set of neap tides (~ 4th August), which suggested that the variations in diurnal inequality, influenced by the proximity to the solstice, promoted variations between the fortnightly cycles. The process of spring tidal pumping, however, was the dominant process in exchanging waters with the ocean.

Acknowledgements

The research for this paper was undertaken whilst the first author was a postgraduate student at the University of Western Australia. The author was funded by an APA (I) scholarship from the Australian Research Council Government and the Department of

Natural Resources, N.S.W. The author would also like to thank a number of people (they know who they are) who helped in the collation of field data and the modelling work.

References

- DNR (2006) Department of Natural Resources web site
http://www.dnr.nsw.gov.au/care/water/estuaries/inventory/index_ns.html
- DNR, (2004). Discussion Paper: ICOLL Management Guidelines. Department of Natural Resources, N.S.W. Australia
- GALE, E.J. (2006) The hydrodynamics of Intermittently Closing and Opening Lakes and Lagoons (ICOLLs). PhD Thesis submitted to the University of Western Australia.
- GALE E., PATTIARATCHI C.B. and RANASINGHE R. 2006. Vertical mixing processes in Intermittently Closed and Open Lakes and Lagoons, and the dissolved oxygen response. *Estuarine, Coastal and Shelf Science*, 69, 205–216.
- GALE E., PATTIARATCHI C.B. and RANASINGHE R. (2007). Processes driving circulation, exchange and flushing within intermittently closing and opening lakes and lagoons, *Marine and Freshwater Research*. (in press).
- HINWOOD, J., MCLEAN, E. and TREVETHAN, M., (2005). Spring Tidal Pumping. In the Proc. Coasts and Ports Conference: Coastal Living – Living Coast, Adelaide, South Australia, Australia, 601-606.
- MASSELINK, G. and HUGHES, M. (2003) Introduction to Coastal Processes and Geomorphology. Hodder Arnold Publishing.
- POLLARD, D.A. (1994). Opening regimes and salinity characteristics of intermittently opening and permanently open coastal lagoons on the south coast of New South Wales. *Wetlands (Australia)* 13, 16-35
- ROY, P.S., WILLIAMS, R.J., JONES, A.R., YASSINI, I., GIBBS, P.J., COATES, B., WEST, R.J., SCANES, P.R., HUDSON, J.P., NICHOL, S. (2001). Structure and function of south – east Australian estuaries. *Estuarine, Coastal and Shelf Science* 53:351 – 384.

SCHMID, M.¹, BUDNEV, N.M.²,
GRANIN, N.G.³, SCHURTER, M.¹,
STURM, M.¹ & WÜEST, A.¹

Advective deep-water renewal in Lake Baikal

¹ *Swiss Federal Institute of
Aquatic Science and Technology
(Eawag), CH-6047
Kastanienbaum, Switzerland.*

E-mail: martin.schmid@eawag.ch

² *Irkutsk State University, Applied
Physics Institute, blvd. Gagarin
20, Irkutsk 664003, Russia*

³ *Limnological Institute of the
Siberian Division of the Russian
Academy of Sciences, P.O. Box
4199, Irkutsk 664033, Russia*

Abstract

From March 2000 until March 2007, moorings equipped with thermistors and current meters were deployed in different configurations in the South Basin of Lake Baikal. Advective deep-water intrusions of cold surface water were regularly observed in the temperature time series from the near-bottom thermistors of these moorings. The observations indicate that the strongest deep-water intrusions generally take place in December or January. They seem to originate from wind-induced downwelling along the steep northern shore of the South Basin and can be much larger than the previously estimated typical values of 10 km³, filling a significant fraction of the deepest 100 to 200 m of the South Basin volume.

Introduction

Lake Baikal is the world's deepest lake and the largest reservoir of liquid fresh surface water. It is divided into three basins of similar size the deepest of which is the Central Basin with a maximum depth of 1642 m, followed by the South Basin (1461 m) and the North Basin (904 m). Whereas the top 200 to 300 m of the water column are reached by seasonal convective mixing, the deep water of the lake is permanently stratified. Nevertheless, the water is oxygenated down to the deepest reaches, and oxygen penetrates up to several cm into the sediment (Maerki *et al.*, 2006). This is only

possible thanks to a very efficient deep-water formation which leads to oxygen renewal times in the deep water of only around 10 years (Weiss *et al.*, 1991). This high rate of deep-water renewal is important in many respects, e.g., for the recycling of nutrients (Müller *et al.*, 2005), and for the oxidation of methane within the sediments and the water column, which as a consequence is not emitted from the lake (Schmid *et al.*, 2007). Several studies have shown that the efficient deep-water renewal in Lake Baikal is caused by both a very high vertical diffusivity on the order of $10^{-3} \text{ m}^2 \text{ s}^{-1}$ within the permanently but very weakly stratified deep water, and an advective flux of surface water down to the bottom of the individual basins (Kipfer *et al.*, 2000; Ravens *et al.*, 2000). Especially in the South Basin, advective deep cold intrusions with a typical volume of about 10 km^3 were regularly observed (Wüest *et al.*, 2005). They usually occur around the time of convective surface mixing in June and December/January. Here we present some recent observations of such intrusion events from the South Basin of Lake Baikal.

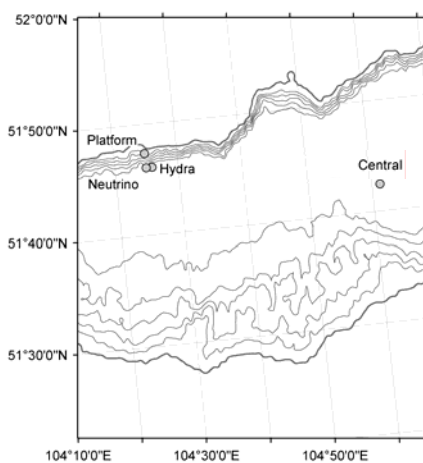


Figure 1 Positions of the moorings within the South Basin of Lake Baikal.

Moorings were installed at several locations in the South Basin of the lake (Fig. 1). The moorings were equipped with thermistors of different types (Vemco minilog, RBR TR-1000, TR-1050, and TR-2050), registering temperatures at least every hour and covering the full depth of the lake. Some of the moorings were also equipped with Aanderaa current meters, either near the surface or near the bottom of the lake. The registered data were retrieved and the configurations of the moorings were adapted once every year. At the site “Neutrino”, near the neutrino telescope, a mooring was installed for the whole period between March 2000 and March 2007.

Within the framework of the CONTINENT project (Oberhänsli and Mackay, 2006), moorings were installed in the center of both the South (March 2001 to July 2003) and the North Basin (July 2001 to July 2003). During these years, the “Neutrino” mooring was maintained with a reduced configuration. From March 2004 to March 2007, two additional moorings were deployed near the “Neutrino” mooring: the “Hydra” mooring, situated about 1 km east of the “Neutrino” mooring at a similar depth, and the “Platform” mooring, situated on a small flat area at a depth of 550 m within the steep slope between the “Neutrino” mooring and the northern shore of the South Basin.

Results

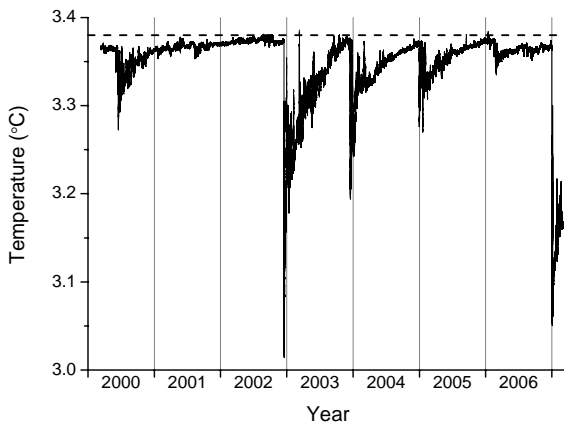


Figure 2 Observed temperatures 2 m above the bottom at the “Neutrino” mooring in the South Basin of Lake Baikal from March 2000 to March 2007. The horizontal dashed line indicates the “background” temperature of 3.38 °C.

Fig. 2 shows the observed signal at the bottom of the “Neutrino” mooring. The “background” temperature at this depth was around 3.38 °C, which was also the temperature typically observed at 1000 m depth. A first strong intrusion in June 2000 cooled the deep water at the mooring site by 0.1 °C. In the following two years, no major intrusions were registered at the “Neutrino” mooring. In contrast, the deepest thermistor of the “Central” mooring, which was located about 40 m deeper, showed cooling events of short duration and with amplitudes around 0.05 °C both in June and in December 2001. In December 2002, a very strong intrusion cooled the deep water down to almost 3.0 °C. This intrusion was simultaneously observed at the “Central” Mooring (Fig. 3). A first small peak on 14 December, visible only at the “Central” mooring, was followed by the main intrusion registered first on 15 December at the “Central” and 15 hours later at the “Neutrino” mooring. On 17 December, an

cooling was detected in all thermistors within the deepest 200 m of the “Central” mooring. During the next few weeks, the temperature at the “Central” mooring intermittently switched back to the background temperature, while it remained constantly at low levels at the “Neutrino” mooring. These observations indicate that the source of this intrusion was near the northern shore of the South Basin (but at another location than the “Neutrino” mooring) and filled a large part of the deepest reaches of the South Basin with cold water. However, obviously a significant fraction of the deep water remained at the background temperature and was only slowly mixed with the cold intrusion water. The border between these two water masses must have been near the “Central” mooring, which was then alternately located within both of them.

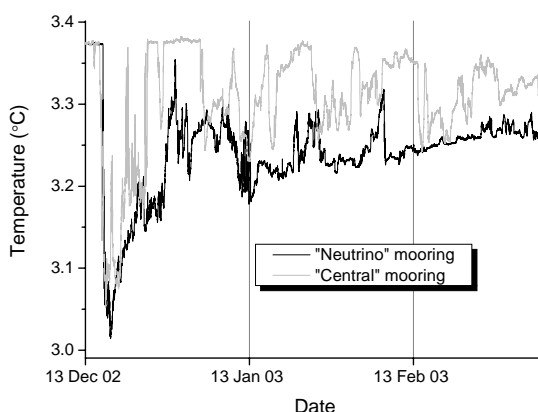


Figure 3 Observed temperatures 2 m above the bottom at the “Neutrino” (black line) and the “Central” (grey line) moorings in the South Basin of Lake Baikal from 13 December 2002 to 10 March 2003.

Subsequently, progressively weaker cooling events were registered annually around the turn of the year. In 2006, the major cooling only occurred in the second half of February, even though a first short signal was already observed on 16 December 2005. Finally, in January 2007, a very strong cooling event took place (Fig. 4) similar to that observed 4 years before. Compared to the intrusions with estimated volumes around 10 km^3 presented by Wüest *et al.* (2005), these two events were of much larger amplitude and duration, and they must have filled a significant part of the volume of 180 km^3 below 1300 m depth in the South Basin.

Interestingly, the flow direction of the intrusions was not always the same. Fig. 4 shows the bottom temperatures of the two moorings “Neutrino” and “Hydra” for the intrusion of January 2005. The two signals correspond very well to each other, and it is obvious that the

same water masses were observed. However, the first intrusion arrived almost a full day later at the “Neutrino” mooring, which is located about 1 km west of “Hydra” (Fig. 1). This means that the water masses were flowing slowly westwards, along with the surface currents that usually flow in this direction at the northern coast of the South Basin. A similar time lag indicating a westward flowing intrusion was also observed in February 2006, while in January 2007, the signal arrived one day earlier at the “Neutrino” mooring than at the “Hydra” mooring, indicating an eastward flow. After each cooling event, the temperature signal exponentially decayed back towards the background temperature with a time constant on the order of 4 to 6 months. This means that the intruded water masses were completely mixed into a background water mass of significantly larger volume within one year. This time constant seemed to be rather independent of the strength of the cooling.

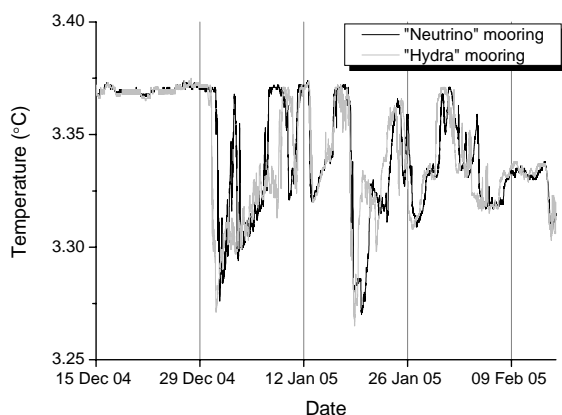


Figure 4 Observed temperatures 2 m above the bottom at the “Neutrino” (black line) and the “Hydra” (grey line) moorings in the South Basin of Lake Baikal from 15 December 2004 to 15 February 2005.

To be able to predict changes in the rates and occurrence of this deep-water renewal in a changing environment, it is necessary to know the mechanisms causing it. Since the observed intruding water is colder than any other water masses in the deep part from the lake, it must obviously stem from the near-surface layer. Wüest *et al.* (2005) proposed that the most likely mechanism should be a coastal downwelling triggered by Ekman transport towards the shore due to wind blowing from the east. As a next step an in-depth analysis of the temperature time series of all thermistors from the “Neutrino”, “Hydra” and “Platform” moorings and the available meteorological data will be performed to check whether there are sufficient indications to confirm this hypothesis.

Acknowledgements

The authors would like to thank J. Chavanne, G.V. Domogatsky, R. Gnatovsky, S. Lovtsov, A.I. Panfilov, Y.M. Parfenov †, M.I. Rosanov, B.A. Tarashansky, E.G. Vologina and A.A. Zhdanov for their invaluable support during field work and fruitful scientific discussions. This research was supported by Eawag research funds (VERTEX), by the EU-project CONTINENT (grant EVK2-CT-2000-00057), by RFBR (grants 05-02-16593, 07-05-00948) and by the RF Ministry of Science and Education (grant RNP.2.2.1.1.7334 "Research-Educational Center Baikal").

References

- KIPFER, R., M. HOFER, F. PEETERS, D. M. IMBODEN, V. M. DOMYSHEVA. 2000. Vertical turbulent diffusion and upwelling in Lake Baikal estimated by inverse modeling of transient tracers. *Journal of Geophysical Research-Oceans* 105:3451-3464.
- MAERKI, M., B. MÜLLER, B. WEHRLI. 2006. Microscale mineralization pathways in surface sediments : A chemical sensor study in Lake Baikal. *Limnology and Oceanography* 51:1342-1354.
- MÜLLER, B., M. MAERKI, M. SCHMID, E. G. VOLOGINA, B. WEHRLI, A. WÜEST, M. STURM. 2005. Internal carbon and nutrient cycling in Lake Baikal: sedimentation, upwelling and early diagenesis. *Global and Planetary Change* 46:101-124, doi:10.1016/j.gloplacha.2004.11.008.
- OBERHÄNSLI, H., A. W. MACKAY. 2006. Introduction to "Progress towards reconstructing past climate in Central Eurasia, with special emphasis on Lake Baikal". *Global and Planetary Change* 46:1-7.
- RAVENS, T. M., O. KOCSIS, A. WÜEST, N. GRANIN. 2000. Small-scale turbulence and vertical mixing in Lake Baikal. *Limnology and Oceanography* 45:159-173.
- SCHMID, M., M. DE BATIST, N. GRANIN, V. A. KAPITANOV, D. F. MCGINNIS, I. B. MIZANDRONTSEV, A. I. OBZHIROV, A. WÜEST. 2007. Sources and sinks of methane in Lake Baikal: A synthesis of measurements and modeling. *Limnology and Oceanography*, in press.
- WEISS, R. F., E. C. CARMACK, V. M. KOROPALOV. 1991. Deep-water renewal and biological production in Lake Baikal. *Nature* 349:665-669.
- WÜEST, A., T. M. RAVENS, N. GRANIN, O. KOCSIS, M. SCHURTER, M. STURM. 2005. Cold intrusions in Lake Baikal - direct observational evidence for deep water renewal. *Limnology and Oceanography* 50:184-196.

FEISTEL, R.¹

Thermodynamics of Water, Vapour, Ice and Seawater

¹ *Baltic Sea Research Institute,
Seestrasse 15, D-18119,
Warnemünde, Germany. E-mail:
rainer.feistel@io-
warnemuende.de*

Abstract

With the 1995 Release of the International Association for the Properties of Water and Steam (IAPWS) on the thermodynamic properties of fluid water, a development commenced towards a new generation of thermodynamic descriptions for the different phases of water and seawater. The next consistent step has been the recent IAPWS Release on ice in 2006.

In cooperation with the Working Group 127 of the Scientific Committee on Oceanic Research (SCOR) and the International Association for the Physical Sciences of the Ocean (IAPSO), a new salinity scale extending the current one of 1978, and a new joint equation of state, replacing the one of 1980 (EOS-80) is currently being developed for seawater.

These new formulations will be perfectly consistent with each other, cover wider ranges of temperatures, pressures and salinities, include all thermodynamic properties (e.g. enthalpy or chemical potential) and thus permit the very accurate determination of various mutual phase transitions and mixed-phase systems like e.g. sea ice or evaporation equilibria.

Introduction

In a joint effort, the SCOR/IAPSO Working Group 127 on Thermodynamics and Equation of State of Seawater together with the International Association for the Properties of Water and Steam (IAPWS) are aiming towards a new international standard for the description of seawater properties, equally applicable in oceanography, limnology and planetary sciences as well as for the specification of technical constructions like power stations or desalination plants.

This new formulation is designed to be

1. consistent with the international standard of fluid water
2. consistent with the international standard of ice
3. expressed in terms of absolute salinity, consistent with the latest IUPAC atomic weights
4. based on a seawater composition model to appropriately account for regional anomalies
5. formulated as a single comprehensive thermodynamic potential function rather than an incomplete collection of independent correlation equations for particular properties
6. expressed in the temperature scale ITS-90
7. extended in its range of validity in temperature and salinity

On its meetings 2006 in Warnemünde and 2007 in Reggio di Calabria, WG 127 has specified various tasks and has made a number of decisions in this direction with the aim of releasing officially a new recommended seawater formulation by the fall of 2008 (SCOR 2006, 2007).

In this paper, several aspects of this programme will be briefly explained and related background problems discussed.

Results

1. Adoption of IAPWS-95 for fluid pure water

WG 127 decided that the intended formulation of seawater will consist of a primary standard, and in addition, secondary, tertiary etc standards derived from it. The primary standard is given by the IAPWS-95 formulation as a Helmholtz function, $f(T, \rho)$, expressed in temperature, T , and density, ρ , (Wagner & Pruß 2002, IAPWS 1996), in combination with the saline part of a Gibbs function, $g(S, T, P)$, depending on absolute salinity, S , temperature, T , and pressure, P (Feistel 2003, 2008). This definition is highly accurate and strictly consistent in its properties, but the code is relatively slow and complicated to be used in practice. Therefore, from the primary standard, various particular secondary standard equations (“wrappers”) need to be derived, for example, equations that are valid in restricted parameter ranges or are designed for improved computational speed. Since IAPWS-95 includes the vapour

properties, quantities like vapour pressure or evaporation enthalpy are available for seawater from this formulation, too.

2. Adoption of IAPWS-06 for ice

WG 127 decided that the international standard of ice (IAPWS 2006, Feistel & Wagner 2006) is to be a part of the seawater formulation for the accurate computation of freezing points and sea ice properties like the freezing enthalpy or the brine salinity. The Gibbs function of ice also permits the determination of precipitation/sublimation equilibria under atmospheric and even cosmic conditions (Feistel & Wagner 2007).

3. Definition of a new Reference Salinity Scale

WG 127 has developed and submitted a manuscript on the Reference Composition of Seawater and on the definition of Reference Salinity (Millero et al. 2007). The new independent salinity variable, Reference Salinity, is intended to be used as the concentration variable for future thermodynamic functions of seawater, as an SI-based extension of Practical Salinity, as a reference for natural seawater composition anomalies, as the currently best estimate for Absolute Salinity of IAPSO Standard Seawater, and as a theoretical model for the electrolyte “seawater”.

From a practical point of view, the value of the Reference Salinity S_R can be related to the Practical Salinity S that is now commonly used by $S_R = (35.164\ 86/35) \text{ g kg}^{-1} \times S$.

The Reference Composition model is a detailed stoichiometric specification sufficiently close to standard seawater from the North Atlantic, with respect to which chemical anomalies of seawater or limnic waters can properly be quantified (Millero et al. 2007)

4. Development of a new saline Gibbs function

Seawater with high salinity and/or high temperature is found in the brine pockets of cold sea ice, in tropical estuaries, or in desalination plants. For concentrated, cold seawater up to saturation (about 110 g kg^{-1}), the first Gibbs function was derived from Pitzer equations for each of the particular sea salt components (Feistel & Marion 2007). This method can be applied to arbitrary ionic solutions.

The saline Gibbs function developed for the intended new standard is mainly derived from seawater measurements and is valid to salinity 120 g kg^{-1} and temperature $80 \text{ }^\circ\text{C}$ (Feistel 2008).

Acknowledgements

The concepts presented in this paper were developed by the SCOR/IAPSO WG 127 in cooperation with the working group TPWS of IAPWS.

References

- IAPWS 1996. *Release on the IAPWS Formulation 1995 for the Thermodynamic Properties of Ordinary Water Substance for General and Scientific Use*. The International Association for the Properties of Water and Steam, Fredericia, Denmark, September 1996. Internet: <http://www.iapws.org>
- IAPWS 2006. *Release on an Equation of State for H₂O Ice Ih*. The International Association for the Properties of Water and Steam, Witney, UK, September 2006. Internet: <http://www.iapws.org>
- FEISTEL R. 2003. A new extended Gibbs thermodynamic potential of seawater. *Progr. Oceanogr.* 58: 43-114.
- FEISTEL R. 2008. A Gibbs function for seawater thermodynamics for -2 °C to 80 °C and Salinity up to 120 g kg⁻¹. *Progr. Oceanogr.*, in preparation
- FEISTEL R, MARION GM. 2007. A Gibbs-Pitzer function for high-salinity seawater thermodynamics. *Progr. Oceanogr.*, DOI: 10.1016/j.pocean.2007.04.020, in press. Internet: <http://www.sciencedirect.com/science/journal/00796611>
- FEISTEL R, WAGNER W. 2006. A new equation of state for H₂O ice Ih. *J. Phys. Chem. Ref. Data* 35: 1021-1047.
- FEISTEL R, WAGNER W. 2007. Sublimation pressure and sublimation enthalpy of H₂O ice Ih between 0 and 273.16 K. *Geochim. Cosmochim. Acta* 71: 36–45
- MILLERO F J, FEISTEL R, WRIGHT DG, MCDUGALL T J. 2007. The composition of standard seawater and the definition of the reference-composition salinity scale. *Deep-Sea Res.* submitted
- SCOR 2006, 2007. *WORKING GROUPS REPORTS. SCOR/IAPSO WG 127 on the Thermodynamics and Equation of State of Sea water*. Progress as at 31 July 2006. Progress as at 27 June 2007. Internet: <http://www.scor-int.org>
- WAGNER W, PRUB A. 2002. The IAPWS formulation 1995 for the thermodynamic properties of ordinary water substance for general and scientific use. *J. Phys. Chem. Ref. Data* 31: 387-535.

**TERZHEVIK A.¹, GOLOSOV S.², MITROKHOV A.¹,
PALSHIN N.¹, POTAKHIN M.¹, ZDOROVENNOV R.¹,
ZDOROVENNOVA G.¹**

Some features of the vertical dissolved oxygen structure in shallow ice-covered lakes

¹ *Northern Water Problems Institute, Russ. Acad. Sci., Aleksander Nevsky 50, 185030 Petrozavodsk, Russia. E-mail:*

ark@nwpi.krc.karelia.ru

² *Institute of Limnology, Russ. Acad. Sci., Sevastyanov str. 9, 196109 St. Petersburg, Russia.*

E-mail: sergey_golosov@mail.ru

Abstract

Winter studies of the dissolved oxygen (DO) distributions in Lake Vendyurskoe, which can be considered as a typical representative of shallow mesotrophic lakes, reveal some features that appear every season. Those include the development of the anaerobic zone in deeper parts of the lake and a sharp decrease of DO in the bottom layer along the slope. From observational data, oxygen fluxes at the water-sediment interface are estimated. It is shown that the thermal regime in ice-covered lakes may affect the vertical DO structure.

Introduction

In the framework of research performed, several field campaigns were conducted in Lake Vendyurskoe (Fig. 1a) located in southern Karelia, Russia (latitude 62°10'-62°20'N, longitude 33°10'-33°20'E). The lake can be considered as relatively small, with the total area of 10.4 km² and volume of 5.5·10⁷ m³ (Litinskaya and Polyakov 1975), and shallow with a mean and maximal depth of 5.3 and 13.4 m, respectively. It belongs to the catchment area of the Suna River inflowing into Lake Onega. The lake hollow is of the glacial origin, being elongated from west to east, with length of seven and width of 1.5 km. The inflow/outflow is small and can be neglected in estimates of the volume exchange, which is mostly influenced annually by precipitation and groundwater flow. Water transparency, according to the Secchi disk estimates, is 3-4 m. The lake status can be considered as mesotrophic. Bottom sediments are composed by sand at shallow (2-3 m) depths and by brown and dark-brown silts in deeper parts. The silt thickness reaches 0.4-1.0

m (Litinskaya and Polyakov 1975). The organic matter content varies from 10% in sand to 30-50% in silty bottom sediments in the shallow north-western part of the lake.

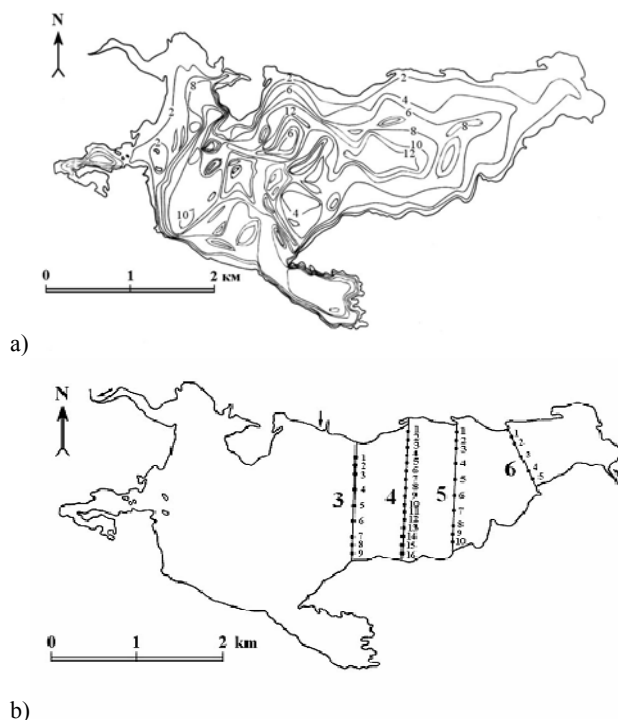


Figure 1. Bottom topography of Lake Vendyurskoe (a) and location of measurement stations (b).

Organic matter (OM) in lake water is mostly of allochthonous origin. Formation of OM in the lake usually does not reach high values. Destruction transcends production, i.e. not only autochthonous but also a part of allochthonous OM is oxidised (Kovalenko 1985). Formation and destruction of OM, its coagulation and sedimentation affect the oxygen regime of the lake. Concentration of dissolved oxygen (DO) and its spatial-temporal dynamics is affected by physical processes related to the gas exchange through air-water and water-bottom interfaces and also by currents (transport) and mixing within a water column.

In 2001-2006 winters, detailed field studies of DO dynamics in Lake Vendyurskoe have been performed by the oxygen meter OXI-

340 (for water temperatures lower than 5°C, accuracy about ±0.5% of measured value). The space step interval was 0.5 m for the water column bulk, and 0.1 m for the near-bottom layer. In April 2006, measurements with the space step interval of 0.01 m were performed in the vicinity of the water-bottom interface to evaluate the oxygen transfer. During some surveys, water samples were collected to perform the BOD estimates.

Results

The maximal DO saturation in Lake Vendyurskoe occurs in autumn due to strong wind mixing and low water temperatures. For example, on 10-11 November 2004 in the central part (depth 10 m) the water temperature was 3°C with the DO content 12.6-12.7 mg·l⁻¹ and saturation of 94-95%, and in the eastern part (depth 7 m) the water temperature was 2.8°C with the DO content 12.7-12.8 mg·l⁻¹ and saturation of 94-96%. The similar DO distribution was observed on 25 November 2003 (3.8-4.0°C, 94-96%). On 9 November 2005 the water temperature in the eastern (St. 6-3, depth 3.6 m) and central (St. 4-9, depth 11.0 m) parts was 4°C from surface to bottom. The DO content varied from 12.1 (surface) to 11.9-12.0 mg·l⁻¹ (bottom), with saturation of 94-95%.

Thus, we can assume that to the moment of ice cover formation the DO content in the lake reaches its maximal values (about 95% of saturation). In 2003 the ice cover was formed on 20 November, with water temperature of 1.5°C in the central part and of 0.8°C in the near-shore areas and with corresponding calculated values of 95% DO saturation of 13.3 and 13.6 mg·l⁻¹, respectively. In 2004, the ice cover was formed on 18 November, with water temperature of 1.8°C in the central part and of 1.4°C in the near-shore areas. Corresponding calculated values of 95% DO saturation are 13.2 and 13.4 mg·l⁻¹, respectively.

Winter 2001-2002. Measurements performed in November 2001 demonstrated the high DO content in surface waters (11.-11.7 mg·l⁻¹) and somewhat lower values in near-bottom layers. In December 2001, DO content in the near-shore areas was practically homogeneous in vertical (10.0-11.5 mg·l⁻¹, 60-75% of saturation). At the “deep” station (4-9), the vertical distribution was rather different. The DO content in the upper 8-m layer was equal to ~10 mg·l⁻¹ (70-76%), and below it sharply lowered, being about 0.1 mg·l⁻¹ in the vicinity of bottom. In January-February 2002, the DO content of shallow waters was about 70% of saturation, with a sharp decrease up to zero close to the bottom. In deeper parts of the lake DO content was >70% of saturation in the upper 6-m layer, with a gradual decrease to the values <2% in bottom layers. In March, the

DO content of shallow waters was slightly lower, but in deeper parts of the lake it changed basically to worse. At the depths 1.5 m from the bottom, DO saturation was less than 20%, and the last 1-m layer was characterised by practically full DO absence, see Fig. 2. In April, 50% saturation coincided with the 6-m depth (10% lower than in March).

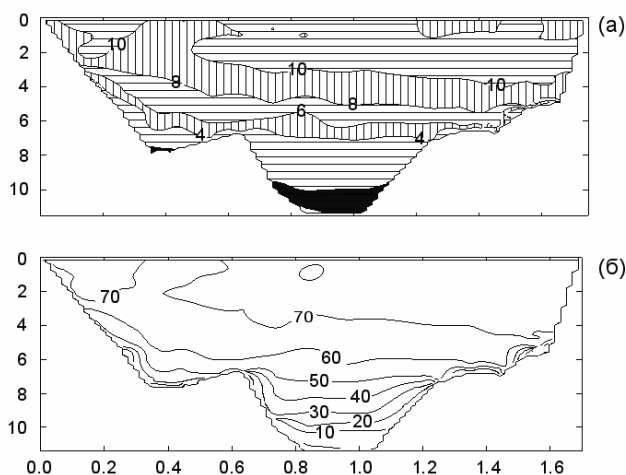


Figure 2. Spatial distribution of absolute (upper panel) and relative (lower panel) DO concentration along the cross-section 4 on 22 March 2002. X-axis represents distance from the northern shore, km; Y-axis stands for depth, m.

2002-2005 winters. Because of shortage of financing, measurements in these seasons were performed in December 2002, and then only in April 2003-2005. During 2002-2003 winter, the DO content was extremely low. In December 2002 surface waters were characterised by $8 \text{ mg}\cdot\text{l}^{-1}$ (less than 60% of saturation). As in December 2001, vertical inhomogeneity of the DO content tended to a decrease towards bottom was developed. In the vicinity of bottom it was close or equal to zero. In April 2003, the DO content in surface waters was about $5\text{-}7 \text{ mg}\cdot\text{l}^{-1}$ (40-50% of saturation). The thickness of the anaerobic zone was the highest for years in consideration, although the temperature profile was similar to observed. The profiles registered in April 2004-2005 demonstrate the DO distribution in vertical similar to that from previous years, i.e. a sharp decrease of DO in the very vicinity of bottom at stations located along the slope and presence of very low DO content in bottom layers over local hollows.

Typically, the development of any non-conservative substance C in time can be described as,

$$\frac{\partial C}{\partial t} + u \frac{\partial C}{\partial x} + v \frac{\partial C}{\partial y} + w \frac{\partial C}{\partial z} = (D_t + D_m) \frac{\partial^2 C}{\partial z^2} + S. \quad (1)$$

Here, u , v , and w are current vector components along corresponding axes; D_t and D_m stand for turbulent and molecular diffusivities, respectively; $S = \gamma C$ is a term describing sources and/or sinks of non-conservative substance; γ is the substance consumption rate.

Results of measurements show that main changes in DO concentrations occur mostly in vertical (Fig. 2). Besides, there are no sources of energy for the turbulence development during the ice-covered period (Malm et al. 1998). Thus, we can consider advective and turbulent terms as negligible, and Eq. 1 can be re-written as,

$$\frac{\partial C}{\partial t} = D_{eff} \frac{\partial^2 C}{\partial z^2} + \gamma C, \quad (2)$$

or

$$H \frac{\partial C}{\partial t} = D_{eff} \frac{\partial C}{\partial z} + \gamma CH \quad (3)$$

where H is depth; D_{eff} effective diffusivity, which may differ from molecular value. In Eq. 3, the left-hand term in our case represents DO content change in time, the first right-hand term stands for the DO flux, and the second for the biochemical DO consumption, including destruction of organic matter and bacterial activity in the vicinity of the water-sediment interface.

Let us estimate which process determines DO content change in time for Lake Vendyurskoe by means of the scale analysis. We introduce the following representative values: time $t = 10^7$ s; depth $H = 5.3$ m; $D_m = 2 \cdot 10^{-9} \text{ m}^2 \cdot \text{s}^{-1}$; seasonal DO change $\Delta DO = 5 \cdot 10^{-3} \text{ kg} \cdot \text{m}^{-3}$; DO consumption rate $\gamma = 10^{-7} \text{ s}^{-1}$ (Golosov et al. 2007). Applying these values to Eq. 3, it shows that DO content change in time is mostly controlled by biochemical DO consumption.

From observational data, estimates of DO content change during winter were received being based on calculations of the DO volume in the whole lake (Table 1), and comparison of vertical profiles registered during winter (Fig. 3). For winters 1999-2000 and 2003-2004, which were fully covered by observational data from the

thermistor chains, we have a possibility to define the date of the ice cover formation and to re-construct the initial DO profile by calculating the 95% level of saturation under the known water temperature of the water column, see Fig. 3b. Table 1 clearly demonstrates that the highest rate of change occurs in the beginning of the ice-covered period. After the first month, the rate drops down drastically and then it gradually gets smaller. A slight difference between estimates for periods including the first month of the ice-covered period is likely determined by the initial temperature. In general, they can be considered as related to the mean depth of the lake.

It was shown (Petrov et al. 2006) that during the first month of the ice-covered period effective thermal diffusivity is two orders of magnitude higher than a molecular value, see Table 2. Vertical displacements of the ice cover that may invoke barotropic seiches (Malm et al. 1998; Petrov et al. 2007) and the temperature gradients that may lead to the development of baroclinic seiches, are the strongest in the beginning of the ice-covered period. In turn, seiche activity may induce stirring and convective instability in the vicinity of the water-sediment interface (Engelhardt et al. 2006; Lorke et al. 2005). These mechanisms are likely explanations of a higher heat release. Mackenthun and Stefan (1998) found out that sediment oxygen demand linearly depends on the flow velocity above the sediments and water temperature. As the DO gradient across the water-sediment interface is always negative, see Fig. 4 as a typical pattern, the DO flux is directed into the sediment, being at least one order of magnitude higher than a molecular value during the first-four-week period.

Because of lack of observational data, we can not confirm dependence of DO change rate on bottom temperature, but we can assume that it exists. Fig. 3 clearly demonstrates such dependence on depth, and from previous studies we know that the larger depth, the higher bottom temperature in shallow ice-covered lakes (Petrov et al. 2006).

To evaluate whether results from the analysis of observational data registered in Lake Vendyurskoe can be considered as typical for moderate shallow lakes, we have performed the classification procedure based on morphometric factors (lake area F_l , length L , average width B , oblongness factor $K_o=L/B$, mean depth D , maximal depth D_{max} , and factor of the basin shape D/D_{max}). As it comes from the factor analysis performed for more than 100 lakes, the lake in study represents about 30% of lakes in consideration. This allows us to assume that results achieved represent DO

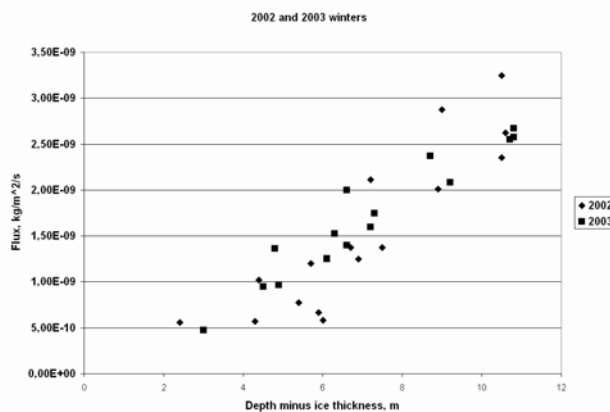
dynamics in shallow mesotrophic and/or eutrophic lakes of glacier origin.

Table 1
Estimates of dissolved oxygen content change through winter

Period between surveys	Δt , days	Layer	ΔDO , ton	$\Delta DO/\Delta t$, t·d ⁻¹	$\Delta DO/\Delta t/A^*$, 10 ⁹ ·kg·m ⁻² ·s ⁻¹
Winter 2001/02 г.					
16.11.01–02.12.01	16	0.5-bottom	38.6	2.41	2.7
02.12.01–26.01.02	55	0.5-bottom	40.8	0.74	0.8
26.01.02–23.03.02	56	0.5-bottom	26.9	0.48	0.5
Period from ice cover formation to mid-April					
20.11.03–21.04.04	152	0.5-bottom	256.7	1.69	1.9
18.11.04–19.04.05	152	0.44-bottom	236.9	1.56	1.7
05.12.05–18.04.06	134	0.5-bottom	251.8	1.88	2.1
December – third decade of April					
02.12.01–23.04.02	142	0.5-bottom	134.6	0.95	1.1
23.12.02–21.04.03	119	0.5-bottom	109.4	0.92	1.0

* Lake area A=10.4 km²

a)



b)

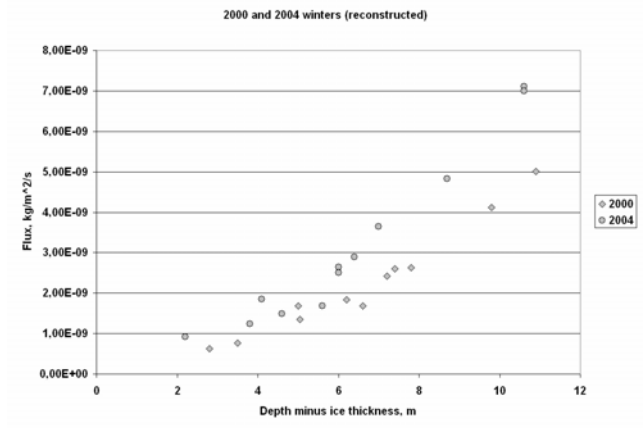


Figure 3. Estimates of dissolve oxygen content change for different seasons: a) stands for periods from December to mid-April; b) for periods from the ice cover formation to mid-April.

Table 2

Effective thermal diffusivity estimates for locations of different depth (MLT – mixed layer thickness), taken from (Petrov et al. 2006).

Season	Depth of location, m	Weeks from ice cover formation	MLT, m	$10^5 \cdot \lambda_{eff}, m^2 \cdot s^{-1}$
1999-2000	11.3	1	5.0	6.6
	11.3	2	4.5	3.8
	11.3	3	4.0	2.9
	11.3	4	3.8	2.3
	9.45	1	5.0	3.3
	9.45	2	3.5	2.9
	6.7	1	4.5	0.8
	6.7	2	3.5	0.8
	6.7	3	3.0	0.8
	6.7	4	2.5	0.7

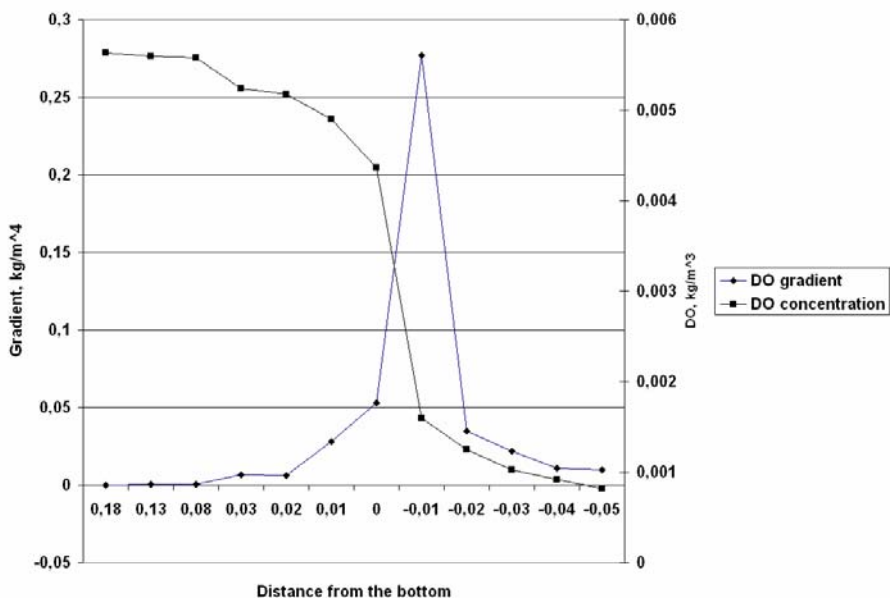


Figure 4. Vertical profiles of DO gradient and concentration. Positive values of X-axis stand for water, negative for bottom sediments.

Acknowledgements

This study is performed under financial support from the Russian Academy of Sciences, Russian Fund of Basic Research (project 07-05-00351), European Commission (projects INTAS-97-0734, INTAS-05-100007-431), Lund University, Sweden.

References

- ENGELHARDT C., GOLOSOV S., CASPER P., HUPFER M., KIRILLIN G., 2006. Seiche-induced convection in upper sediments. In: F. RUEDA VALDIVIA, (Ed.), *Proc. 10th European Workshop on Physical Processes in Natural Waters*, 59-68, Spain, Granada University.
- GOLOSOV S., MAHER O. A., SCHIPUNOVA E., TERZHEVIK A., ZDOROVENNOVA G., KIRILLIN G., 2007. Physical background of the development of oxygen depletion in ice-covered lakes. *Oecologia*. 151: 331-340. DOI: 10.1007/s00442-006-0543-8.
- KOVALENKO V.N., 1985. Chlorophyll content and production processes in lakes of different trophic status. In: *Organic matter and nutrients in waters of Karelia*. Pp. 165-177, Petrozavodsk. (In Russian)

- LITINSKAYA K.D., POLYAKOV Yu.K., 1975. Lakes of Vendyurskaya group – Uros, Rindozero, Vendyurskoe. In: *Water resources of Karelia and their use*. Pp. 57-66, Petrozavodsk.
- LORKE A., PEETERS F., WUEST A., 2005. Shear-induced convective mixing in bottom boundary layers on slopes. *Limnol. Oceanogr.* 50: 1612–1619.
- MACKENTHUN A.A., STEFAN H.G., 1998. Effect of flow velocity on sediment oxygen demand: Experiments. *J. Environ. Eng.*, 124: 222-230.
- MALM J., TERZHEVIK A., BENGTSSON L., BOYARINOV P., GLINSKY A., PALSHIN N., PETROV M., 1998. A field study on currents in a shallow ice-covered lake. *Limnol. Oceanogr.*, 43: 1669-1679.
- PETROV M., TERZHEVIK A., ZDOROVENNOV R., ZDOROVENNOVA G., 2006. The Thermal Structure of a Shallow Lake in Early Winter. *Vodnye Resursy*, 2: 135-143. (*Water Resources*, in Russian and in English).
- PETROV M., TERZHEVIK A., ZDOROVENNOV R., ZDOROVENNOVA G., 2007: Water motions in a shallow ice-covered lake. *Vodnye Resursy*, 34: 113-122. (*Water Resources*, in Russian and in English).

GOLOSOV S^{1,3}, ZVEREV I¹, TERZHEVIK
A.YU², G KIRILLIN³, C ENGELHARDT³

On the effective thermal diffusivity in ice-covered lakes

1Institute of Limnology, Russ. Acad. Sci., 196105 St.

Petersburg, RUSSIA; E-mail: sergey_golosov@mail.ru

2Northern Water Problems Institute, Karelian Scientific

Centre, Russ. Acad. Sci., Petrozavodsk, RUSSIA; E-mail:

ark@nwpi.krc.karelia.ru

3 Leibnitz Institute of Freshwater Ecology and Inland

Fisheries, D-12561 Berlin, GERMANY

E-mail: kirillin@igb-berlin.de

Abstract

Numerous observational data on the thermal regime of ice-covered lakes show that re-distribution of the heat storage between the bottom sediment and water takes place during winter. It results in a so-called effect of the “under-ice lake warming” that strongly influences on different aspects of the lake ecosystem behaviour. Based on the analysis of field data collected in three freezing lakes, it is revealed that the vertical heat transfer during the ice-covered period is governed by the processes of higher intensity comparing the molecular diffusivity. The phenomenon was studied using simple parameterised model based on the self-similar representation of the vertical temperature profile in water column and in sediments. Empirical dependence of the thermal conductivity on the magnitude of the near-bottom vertical gradient of temperature is revealed in the course of the observational data analysis and numerical model runs.

Introduction

The numerous observational data on the thermal regime of the ice-covered lakes (Kuzmenko, 1976, 1984; Bengtsson et al., 1995; Malm et.al., 1997) show that redistribution of the heat storage between the bottom sediment and water takes place during winter, which may last for five-six months. It results in a so-called effect of the under-ice lake warming. Fig. 1 presents observational data on the vertical distribution of the water temperature in Lake Vendyurskoe (Russia) in November 1995 – April 1996 (Malm et.al. 1997), which demonstrate the mentioned effect.

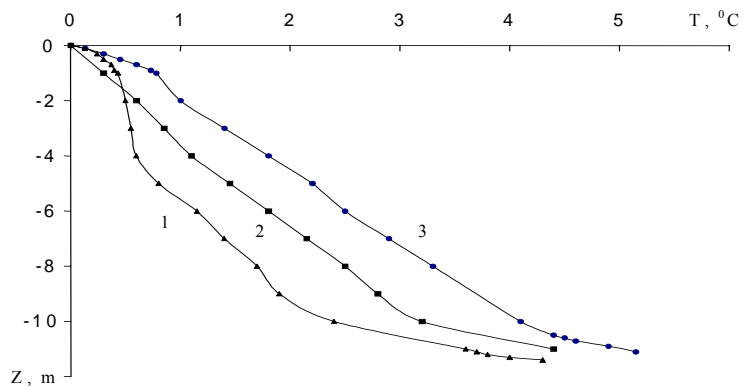


Fig.1. Variability of the vertical temperature distribution during ice-covered period in Lake Vendyurskoye: 1 – November 1995, 2 – December 1995, 3 – March 1996 (data from Malm et.al. 1997).

Materials and data processing

The phenomenon mentioned above was studied using the data collected in two Russian and one German ice-covered lake. Data from Russian lakes were collected in Northwestern Russia (Leningradskaya Oblast, and Republic of Karelia) during the winter surveys in 1974-75 (Lake Krasnoe, 60° N, maximal depth 14 m) and in 1995-96 (Lake Vendyurskoe, Karelia, 64° N, maximal depth 12.5 m). The average duration of the ice-covered period in Northwestern Russia is five to six months; the ice may reach 0.6-0.8 m of thickness. The morphometric parameters of lakes differ rather strongly. The basin of Lake Krasnoe is trough-shaped, whereas the shape of Lake Vendyurskoe is irregular. German Lake Muggelsee is located in Berlin (53° N, maximal depth 7 m). Steady ice cover has an episodic character. In the case of ice appearance the ice-cover duration not exceeds few weeks. Ice reaches 10-15 cm of thickness.

Data on water and sediments temperature collected in all lakes differ rather strongly too. Thus, data from Lake Krasnoye represent a set of vertical temperature distributions measured in water column and in a so-called thermal active layer (4-5 metres) of sediments every month during the winter 1974-75. It should be noted that the temperature at the lower boundary of the thermal active layer of sediments is close to constant for the whole year. Below, this fact will be of top position at the field data processing. Data from Lake Vendyurskoe consists of detailed measurements of temperature in the water column and in 10 centimetres of the upper layer of sediments at 11 stations of the regular cross-section along the lake.

The frequency of measurements was once or twice a month. And finally, the data from Lake Mueggelsee represents vertical temperature profiles measured during the winter 2005-06. The measurements were performed in the 10-centimetric near bottom layer of water and in the upper 10-centimetric layer of sediments. The spatial and the time resolution between measurements were 2 cm and 5 minutes correspondingly. The patterns of the temperature distributions from the lakes are presented in Fig. 2

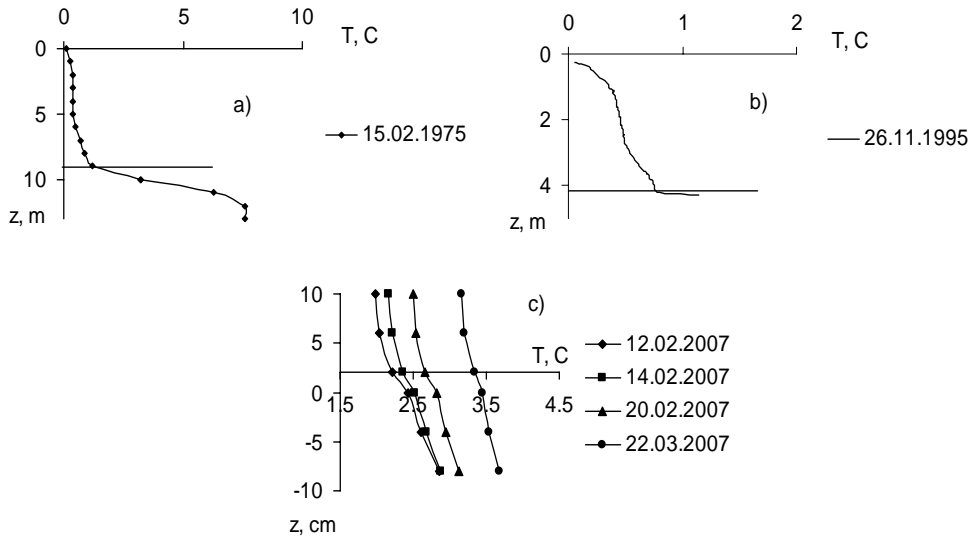


Fig.2 Patterns of vertical temperature profiles obtained in the lakes under study: a) Lake Krasnoye, b) Lake Vendyurskoe and c) Lake Mueggelsee (daily averaged). Horizontal line marks the water-bottom interface.

The under ice water warming mentioned above takes place due to heat redistribution between sediments and water column. It allows assuming that heat fluxes in the upper sediments and in the near bottom water should be equal to each other. The common feature for all temperature profiles is the evident bend in temperature curve at the immediate boundary between water column and sediments. In other words, the vertical temperature gradients in the water-sediments vicinity differ rather strongly. The heat transfer in the upper sediments can be realised only by the molecular diffusivity. In that case the temperature curve bend at the water-sediments interface can be generated only in the presence of the more effective mechanism of vertical heat transfer in the near bottom water. In terms of heat fluxes, thermal diffusivity and temperature gradients it can be written as follows,

$$\begin{aligned}
Q_W &= -\lambda_{eff} \frac{dT_w}{dz}, \\
Q_S &= -\lambda_m \frac{dT_S}{dz}
\end{aligned}
\tag{1}$$

Here Q_W , Q_S , dT_W/dz and dT_S/dz are the heat fluxes and the temperature gradients in the near bottom water (W) and in the upper sediments (S) correspondingly, λ_{eff} and λ_m are the effective and molecular coefficients of thermal diffusivity in water. It should be noted that the water content in the upper layer of sediments is close to 95-98%. So, the coefficient of the molecular diffusivity in the upper sediments can be assumed of equal value with the water one ($\lambda_m = 1.3 \cdot 10^{-3} \text{ cm}^2\text{s}^{-1}$). Taking into account the equality of heat fluxes Q_W and Q_S , the formula for the definition of λ_{eff} can be easily derived from (1),

$$\lambda_{eff} = \gamma_m \cdot \frac{dT_S / dz}{dT_W / dz}
\tag{2}$$

All vertical temperature distributions obtained from three lakes under study were processed in terms of the formula (2). The results of processing are presented in Fig. 3 as a dependence of the effective coefficient of thermal diffusivity λ_{eff} [cm^2s^{-1}] on dimensionless temperature ratio $T_D / (T_L - T_D)$, where T_L is the temperature at the lower boundary of the thermal active layer of sediments (T_L is constant, see above), T_D is the current temperature at the water-bottom interface.

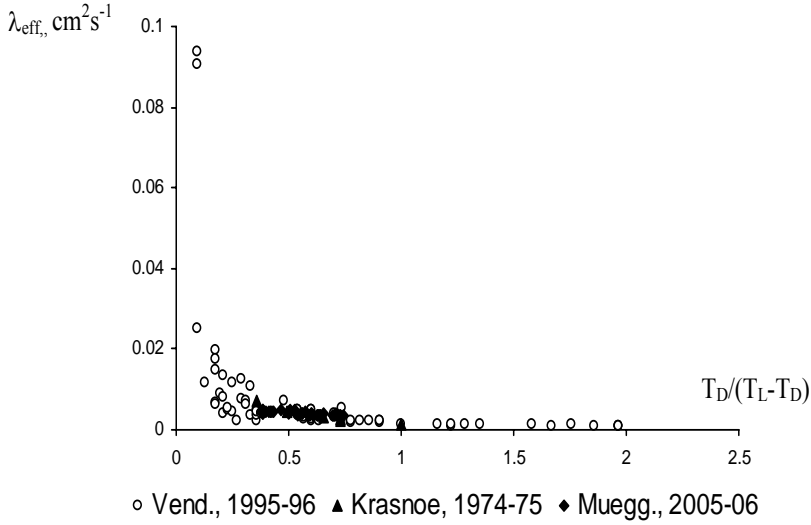


Fig. 3 Effective coefficient of thermal diffusivity in dependence on dimensionless temperature ratio.

Results presented in Fig. 3 show that at certain values of the temperature ratio the magnitude of λ_{eff} is in two orders higher comparing to molecular heat transfer. Moreover, all empirical data are located on the same curve independently on particular lake conditions. The empirical approximation for the data presented in Fig. 3 was obtained as follows,

$$\lambda_{eff} = 0.001 \cdot \left(\frac{T_D}{T_L - T_D} \right)^{-1.005} \quad (3)$$

The coefficient of proportionality in (3) in fact is very close to the value of the coefficient of molecular thermal diffusivity in water $\lambda_m = 1.3 \cdot 10^{-3} \text{ cm}^2\text{s}^{-1}$. The exponent in the right side in (3) is equal to -1 . So, we have the right to rewrite the formula (3) in form,

$$\lambda_{eff} = \lambda_m \cdot \frac{T_L - T_D}{T_D} \quad (4)$$

Now the effective coefficient of thermal diffusivity in the near bottom zone is an implicit function of time and can be calculated in

dependence on the temperature of the water-bottom interface. The numerous observational data on the thermal regime of the ice-covered lakes (Kuzmenko, 1976, 1984) show that T_L varies within a very narrow range in different lakes. Its value is close to 7-8 C at 4.5 – 5 metres of the thermal active layer thickness.

Main equations and parameterizations of the model

The model of the phenomenon of under-ice lake warming in details was described in Golosov et . al., 2003. Below just main equations and parameterisations of the model will be remembered. Thus, Fig. 2 schematically represents a vertical thermal structure of the ice - water - sediments system in absence of snow on the ice surface. In adopted notations, the vertical co-ordinate axis is directed from the ice surface ($z=0$) towards the lower boundary of the thermal active layer of bottom sediments ($z=L$) where the temperature is constant during the whole year and is equal to T_L ; l stands for ice thickness, the upper boundary of which has a temperature T_s ; the temperature of the lower boundary of ice ($z=l$) during the whole ice-covered period equals to that of water freezing, $T_f=0^\circ\text{C}$. In the very vicinity from the lower boundary of ice, a thin layer (δ) is located, within which heat transfer is accomplished on a molecular level; D is a water-bottom interface with temperature T_D .

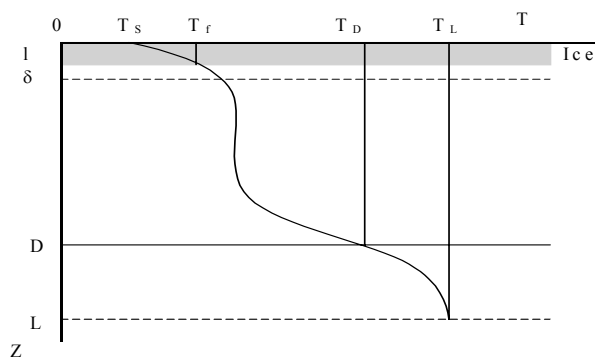


Fig 4. Schematic representation of the vertical temperature profile in an "ice-water column-sediments" system.

Equation of heat conductivity for the considered domain $0 \leq z \leq L$ is,

$$\frac{\partial T}{\partial t} = -\frac{\partial Q}{\partial z} \quad (5)$$

where t is time; z is depth; T is water temperature; Q is vertical kinematic heat flux.

The vertical temperature profile in the considered domain is presented as the following parametric concept,

$$T(z) = \begin{cases} T_S - (T_S - T_f) \cdot f_1\left(\frac{z}{l}\right) & \text{at } 0 \leq z \leq l \\ T_f + (T_D - T_f) \cdot f_2\left(\frac{z-l}{D-l}\right) & \text{at } l \leq z \leq D \\ T_D + (T_L - T_D) \cdot f_3\left(\frac{z-D}{L-D}\right) & \text{at } D \leq z \leq L \end{cases} \quad (6)$$

Dimensionless functions $f_1(\xi_1)$, $f_2(\xi_2)$ and $f_3(\xi_3)$, where $\xi_1 = (z/l)$, $\xi_2 = (z-l)/(D-l)$ and $\xi_3 = (z-D)/(L-D)$ are dimensionless depths, describe the vertical temperature distribution in ice, water and bottom sediments, respectively, and satisfy the obvious boundary conditions,

$$f_1(0) = f_2(0) = f_3(0) = 0; f_1(1) = f_2(1) = f_3(1) = 1; f_3'(1) = 0. \quad (7)$$

The last condition (7) for the function $f_3(\xi_3)$ follows from definition of the active layer of bottom sediments, according to which the vertical temperature gradient for $z = L$ is close to zero. From here, we consider only a problem of joint evolution of temperature profiles in water and sediments, described by the second and third equations in (6).

After integrating Eq. (5) with respect to z twice, first from l to D using the second equation in (2), then from D to L using the third equation in (6) we obtain the following differential equations,

$$\frac{dT_D}{dt} (D-L)\alpha_2 = -Q_D + Q_l + T_D\alpha_2 \frac{dl}{dt} - T_D(D-L) \frac{d\alpha_2}{dt} \quad (8)$$

$$\frac{dT_D}{dt}(L-D)(1-\alpha_3) + (T_L - T_D)(L-D)\frac{d\alpha_3}{dt} = Q_D \quad (9)$$

$$\alpha_2 = \int_0^1 f_2(\xi_2) d\xi_2; \quad \alpha_3 = \int_0^1 f_3(\xi_3) d\xi_3.$$

Eqs. (8) and (9) include five unknown parameters: bottom temperature T_D ; heat fluxes Q_D and Q_I through water-bottom and water-ice interfaces, respectively; and also parameters α_2 and α_3 , which are integrals accordingly from functions $f_2(\xi_2)$ and $f_3(\xi_3)$. To calculate the development of ice thickness, any of numerous models describing the interaction between a lake and atmosphere can be used (e.g. Patterson and Hamblin 1998; Rumyantsev *et al.* 1986). The value of the water-ice heat flux Q_I is negligible comparing the other terms of Eq. (8), so it can be excluded out of further consideration. To enclose system of equations (8)-(9), we need two additional relations, namely expressions for functions $f_2(\xi_2)$ and $f_3(\xi_3)$.

According to (7), the function $f_2(\xi_2)$ has two time-constant boundary conditions, $f_2(0) = 0$ and $f_2(1) = 1$, which are insufficient to define its time dependence. Two additional boundary conditions for function $f_2(\xi_2)$ can be determined from the speculations on the character of the temperature distribution in the vicinity of water-ice interface. As mentioned above the layer of molecular diffusion in at the water-ice interface is very thin, so the temperature profile can be assumed as linear within this layer. In terms of the parameterisation (6) it means that the first derivative of the function $f_2(0)$ is equal to 1, e.g. $f_2'(0) = 1$. As the first derivative is constant the second one should be equal to 0, e.g. $f_2''(0) = 0$. A time-dependent boundary condition for the derivative of function $f_2(\xi_2)$ can be set up at the interface water-sediment ($\xi_2 = 1$). Usually, the upper layer of bottom sediments has high porosity (~95%) and water saturation (95-98%). This allows considering its heat-conducting capacity close to that of bottom water. Taking into account the second equation in (6), the heat flux through the water-sediment interface (1) can be written as,

$$Q_D = -\lambda_{eff} \cdot \frac{T_D}{D-l} \cdot \frac{df_2}{d\xi_2} \quad \text{at} \quad \xi_2 = 1$$

or

$$f_2'(1) = -\frac{Q_D \cdot (D-l)}{\lambda_{eff} \cdot T_D} = A \quad (10)$$

where λ_{eff} is effective thermal conductivity in water. The value of λ_{eff} can be estimated from the relation (4). Thus, the function $f_2(\xi_2)$ has five boundary conditions,

$$f_1(0) = 0; f_1(1) = 1; f_1'(0) = 1; f_1''(0) = 0; f_1'(1) = A \quad (11)$$

The last condition in (11) defines variability of $f_2(\xi_2)$ in time. According to (11), $f_2(\xi_2)$ can be expressed as a forth-degree polynomial with time-dependent coefficients,

$$f_2(\xi_2) = \xi_2 + (1-A) \cdot \xi_2^3 + (A-1) \cdot \xi_2^4 \quad (12)$$

According to (7), $f_3(\xi_3)$ has three boundary conditions that are not dependent on time, $f_3(0)=0$, $f_3(1)=1$, $f_3'(1)=0$. To describe time dependence of function $f_3(\xi_3)$, we need additional boundary condition analogous to the condition (11). By repeating considerations led to (6) and taking into account the third equation in (6), the forth boundary condition can be written as,

$$Q_D = -\lambda_m \cdot \frac{(T_L - T_D)}{(L-D)} \cdot \frac{df_3}{d\xi_3} \quad \text{at} \quad \xi_3 = 0$$

or

$$f_3'(0) = -\frac{Q_D \cdot (L-D)}{\lambda_m \cdot (T_L - T_D)} = B \quad (13)$$

Here λ_m is the coefficient of the heat molecular diffusivity in water (see above). This boundary condition, in much the same as (7), defines variability of $f_3(\xi_3)$ in time. Now a desired function can be expressed as a third-degree polynomial with time-dependent coefficients,

$$f_3(\xi_3) = B \cdot \xi_3 + (3-2 \cdot B) \cdot \xi_3^2 + (B-2) \cdot \xi_3^3 \quad (14)$$

Thus, the system of equations (8), (9), (12) and (14) with additional formula (4) is closed and represents a simple model describing evolution of heat distribution between bottom sediments and water during the ice-covered period.

Model verification

The model was applied to reconstructing of the winter dynamics of the temperature profile in Lake Krasnoe. Calculations were performed for ice-covered period 1964-65. Results of reconstruction are presented in Fig. 5. As it follows from Fig. 5 agreement between measured and calculated data is fairly well. The present version of the model in contrast to the previous one is capable to describe much more wide range of variability of the vertical temperature profiles. Thus, the model computes the point of temperature extremum within the thermal active layer of sediments.

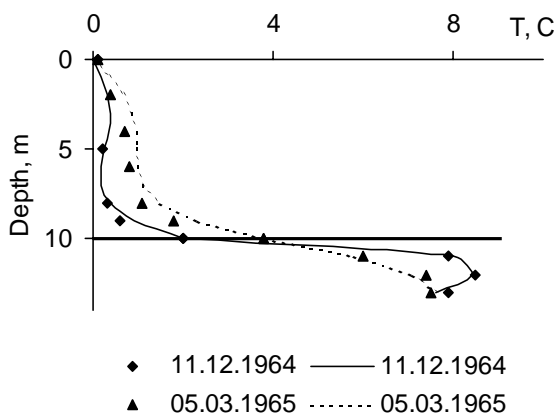


Fig. 5 Temporal dynamics of the vertical temperature profile in water column and sediments in Lake Krasnoe during the winter 1964-65. Points represent measured values of temperature, lines are modeled profiles. Solid horizontal line marks the water-bottom boundary.

Acknowledgements

The present study is supported by the German Foundation of the Basic Research (DFG, Project KI-853/3-1 in frames of the program „AQUASHIFT“), the Russian Academy of Sciences, and particularly by the Russian Basic Research Foundation (RBRF, Project N 07-05-00351).

References

- BENGTSSON L., MALM J., TERZHEVIK A., PETROV M., BOYARINOV P., GLINSKY A., PALSHIN N., 1995, A field study of thermo- and hydrodynamics in a small Karelian Lake during late winter. *Sweden, Lund Univ., Rep. № 3185*, 72 p.
- GOLOSOV S., ZVEREV I., TERZHEVIK 2003 A. Thermal Structure and Heat Exchange in Ice-WaterColumn-Sediment System *In: Terzhevik, A. (ed.):*

Proceedings of the 7th Workshop on Physical Processes in Natural Waters, 132-140.

KUZMENKO L.G. 1976, Thermal regime of lake water column and sediments. In *Biological productivity of Lake Krasnoye. Leningrad, "Nauka" Publishing House*, p. 18-36 (in Russian).

KUZMENKO L.G. 1984, The seasonal structure of lakes thermal states. In *The features of water quality formation in lakes of different types at Karelian Isthmuth. Leningrad, "Nauka" Publ. House*, pp. 45-60 (in Russian).

MALM J., TERZHEVIK A., BENGTSSON L., BOYARINOV P., GLINSKY A., PALSHIN N., PETROV M., 1997. Temperature and hydrodynamics in Lake Vendyurskoe during winter 1995/1996. *Sweden, Lund Univ., Rep. № 3213*, 203 p.

PATTERSON J.C., HAMBLIN P.F. 1988. Thermal simulation of a lake with winter ice cover. *Limnol. Oceanogr.* 33, pp. 323-338.

RUMUANTSEV V.A., RAZUMOV E.V., ZILITINKEVICH S.S. 1986, Parameterized model of seasonal temperature changes in a lake (application to the problem of Lake Sevan), *Leningrad, Institute of Limnology RAS*, 74 p. (in Russian).

7 Physical-biological Coupling

**RUEDA, F. J.¹ A. HOYER², A. RIGOSI,
J. VIDAL, C. ESCOT, A. BASANTA, E.
MORENO-OSTOS, I. DE-VICENTE, V.
AMORES, & L. CRUZ-PIZARRO**

**The role of physics in driving
the functional structure of
phytoplankton communities:
observations from an
autonomous profiling platform**

¹ *Universidad de Granada, Dept.
Civil Engineering & Instituto del
Agua, C/Ramón y Cajal 4, 18071,
Granada, Spanien. E-mail:
fjrueda@ugr.es*

² *Universität Münster,
Moltkestr.26, 48151 Münster,
Deutschland. . E-mail:
ahoyer@uni-muenster.de*

Abstract

Ramon Margalef's Mandala describes the composition of phytoplankton communities, the relative abundance of component species, and their evolution (succession) as the result of a nutrient-turbulence balance. If we accept Margalef's Mandala as a valid interpretation of succession in freshwater ecosystems, one necessarily concludes that the analysis and understanding of the functional structure of phytoplankton communities and its evolution needs to be grounded on the knowledge of the physical processes of transport and mixing determining turbulence levels and nutrient distribution in the water column. To advance in the knowledge of the physical-biological coupling in water bodies, we have installed an autonomous profiling platform that gathers information on meteorological variables, water physical and biological variables. We will present and analyze some of the data gathered at that platform.

**HOYER, A.¹ & Vidal, J.¹ & Escot,
C.² & Basanta, A.² & Moreno-
Ostos, E.^{1,3} & Rueda, F.¹**

**The seasonal evolution of the
functional structure of the
phytoplankton community in a
Mediterranean reservoir:
influence of external
perturbation**

¹ *Instituto del Agua de la
Universidad de Granada,,
C/Ramón y Cajal,4, 1807,1
Granada, Spain. E-mail:
fjrueda@ugr.es*

² *Empresa Municipal de
Abastecimiento y Saneamiento de
Aguas de Sevilla, S.A. EMASESA,
Sevilla, Spain. E-mail:
cescot@emasesa.es*

³ *Departamento de Ecología y
Geología. Universidad de
Málaga. Campus Universitario
de Teatinos. 29071. Málaga.
Spain. E-mail: quique@uma.es*

Abstract

It is now widely accepted that phytoplankton communities in lakes and reservoirs, their functional structure and their seasonal evolution (succession), are the results of a nutrient-turbulence balance. Therefore, the analysis and understanding of microalgae succession, and in general, the functioning of aquatic ecosystems, needs to be grounded on the knowledge of the physical processes of transport and mixing determining turbulence levels and nutrient distribution in the water column. Our general goal is to study the role played by external forcings driving mixing and transport processes in determining the seasonal evolution of phytoplankton communities, their abundance and structure in a Mediterranean water supply reservoir located in southern Spain. We will show that the phytoplankton community composition (in terms of functional groups) is mainly determined by habitat conditions. Further, we will demonstrate that seasonal changes in the phytoplankton community are triggered by exogenous perturbations.

Introduction

Margalef's Mandala (e.g. Margalef 1997) describes the composition of phytoplankton communities, the relative abundance of component species, and their evolution (succession) as the result of a nutrient-turbulence balance. Based on a long series of intensive studies in temperate natural lakes and experimental enclosures Reynolds (1997) showed that species pertaining to what is referred to as a functional group occupy the same region in two-dimensional plot of energy limitation (parameterized as the ratio of the depth of the mixed-layer z_{mix} to the depth of the euphotic zone z_{eu}) vs. resource limitation (parameterized by the concentration of nutrients in the water column). The environmental conditions (i.e. energy or resource levels) to which phytoplankton responds are, to a large extent, determined by the occurrence and intensity of transport and mixing processes in the water column. These processes, in turn, are driven by exogenous fluxes of mass and energy (thermal and mechanical) that occur either through the free surface or through inflow or outflow sections (Imboden and Wüest 1995).

Reynolds' theory has been applied to summarize information on seasonal succession and diversity of phytoplankton and to propose general patterns for temperate lakes, for temperate rivers and for subtropical systems (e.g. Hambright and Zohary 2000). Limited information, however, has been generated on phytoplankton succession in Mediterranean reservoirs and the influence of external forcing as drivers of such processes (Moreno-Ostos 2004). Although Reynolds' phytoplankton theory is grounded on extensive data sets, and is widely accepted as a valid interpretation of succession, its usefulness for Mediterranean reservoir still needs to be proven. Our general goal is to study the seasonal evolution of phytoplankton communities, their abundance and structure in El Gergal reservoir, taken as a prototypical example of Mediterranean lentic ecosystem (e.g. George and Rouen 1997). In particular, we will determine whether the functional groups of phytoplankton appear to have similar environmental requirements as defined in Reynolds (1997). We will also show through a series of case examples that changes in the functional composition of phytoplankton community are triggered by exogenous perturbations in the nutrient-energy state. Our work is based on an extensive data set collected during a 5 year period in El Gergal reservoir (Seville, Spain). The data set includes meteorological variables collected at hourly intervals; weakly temperature profiles; nutrient concentrations, abundance and composition of the phytoplankton community analyzed from samples collected at discrete depths and at nearly weekly intervals; and hydraulic information recorded at daily intervals.

Results

Phytoplankton community: abundance and composition.

The phytoplankton community in El Gergal consists of eleven functional groups. Only groups H_1 , Y , Z , and B formed seasonal maxima of abundance during the study period. The growth of group H_1 (*Aphanizomenon* sp. and *Anabaena* sp., atmospheric nitrogen-fixing Cyanobacteria) is promoted by surface warming and thermal stratification, high light levels and nutrient supplies. Algae of group Y (naked, biflagellate algae) are adapted to a wide range of habitats, which makes them almost ubiquitous, though they are relatively more abundant in moderately enriched waters. They are adapted to low insolation levels and but they are not affected, due to their motility, by the level of mixing in the water column. The functional group Z includes picocyanobacteria of small unit size ($<10 \mu\text{m}^3$ in volume), which prevents them from sinking out rapidly. They tend to be persistent as long as they remain ungrazed (Reynolds 1997, 2002). The Diatoms of group B (*Cyclotella*, *Melosira* and *Synedra*) mainly live in vertically mixed enriched lakes. Their negative-buoyancy makes their population dependent on turbulence for suspension and, thus, sensitive to mixing depth and to the seasonal onset of near surface density stratification (Reynolds 1997). Of all the groups forming seasonal maxima, group H_1 dominates the community for longer periods of time, with the largest number of cells per volume.

Phytoplankton dominance under limiting conditions

(*energy and nutrient limitation*) - Figure 1 shows the energy ($Z_{\text{mix}}/Z_{\text{eu}}$) and nutrient (P- PO_4 max) conditions that favour the growth and dominance of functional groups identified in El Gergal. The position of the functional groups identified in El Gergal in the two-dimensional energy-nutrient domain appears to follow the expected behaviour defined by Reynolds (Reynolds 1997). Group B , for example, appears in regions of high light limitation ($Z_{\text{mix}}/Z_{\text{eu}} > 8$), which is consistent with its adaptation to low light intensities and its' relaying on turbulence for suspension (Reynolds 2002). Group Y , not present in the habitat template, coincides with group B , but occupies the whole range of the ratio $Z_{\text{mix}}/Z_{\text{eu}}$, which is consistent with its ability to grow both under mixing as well as stratification. Group H_1 dominates at average concentrations of phosphate, while group Z appears at low phosphate concentration and low $Z_{\text{mix}}/Z_{\text{eu}}$.

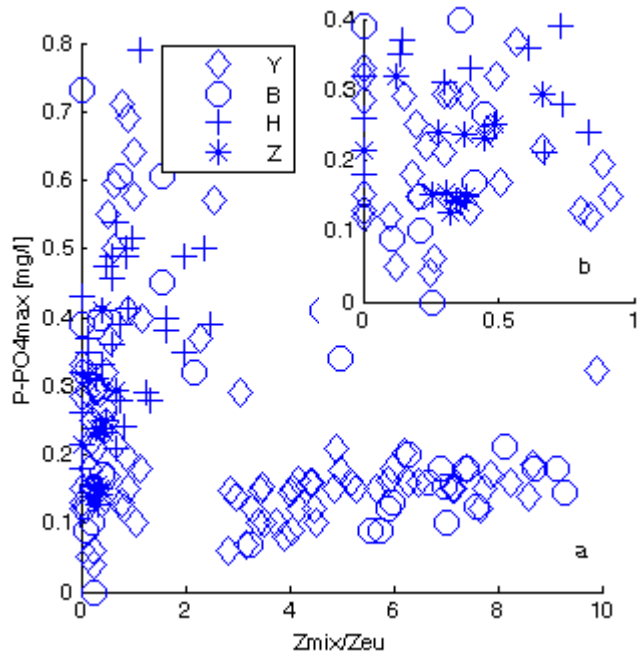


Figure 1 The distribution of four phytoplankton functional groups in relation to nutrient (P-PO₄max) and light (Z_{mix}/Z_{eu}) conditions. a) overview b) detailed view of the range P-PO₄max 0-0.4 and Z_{mix}/Z_{eu} 0-1.

Phytoplankton seasonal succession. The seasonal succession of the phytoplankton functional groups (not shown) follows, in general, the sequence $B \rightarrow X_1/Y \rightarrow F \rightarrow Z/H_1 \rightarrow L_M$, similar to the sequence observed in the small eutrophic lake Crose Mere (e.g Reynolds 1973). This successional trend, however, is interrupted and re-started (at different stages depending on the year) by exogenous perturbations (events), which modify significantly the environmental conditions in the water column.

External forcing and phytoplankton community change. Exogenous perturbations of the environmental conditions in the water column was associated to changes in the withdrawal regime or wind forcing. Abrupt changes in the abundance and composition of the phytoplankton community occurred in response to those perturbations. Changes in the composition of the community were characterized using the index of community change ICC, calculated as in Reynolds (1984). Large ICC values represent abrupt changes, where several genders declined simultaneously and others increased rapidly (Reynolds 1984). Vertical bars in Fig. 2 represent periods of

time when the magnitude of the variables being represented exceeded a threshold value. For L_N that threshold value is 1; for the outflow discharge vertical bars define when water was being withdrawn. For ICC and abundance vertical bars mark periods of time when the ICC > 0.14 and the abundance of the dominant functional group exceeded 80 cells/ml. Long periods of time with no withdrawal were followed by long periods when the abundance of certain groups was large (see for example August 2001 in Fig.2a-e). During those periods, ICC was always low indicating that the community was dominated by one single group (in August 2001, for example the dominant group was H_I). For the successional event presented in Fig. 2b, corresponding to June 2003, the peak in abundance occurred after the interruption of withdrawal. The dominant group in this case was also H_I . This peak, however, was short. The decline in phytoplankton abundance was driven by the injection of energy either by strong winds (Fig. 2f) or the withdrawal (Fig. 2h), which was reinitiated shortly after it stopped.

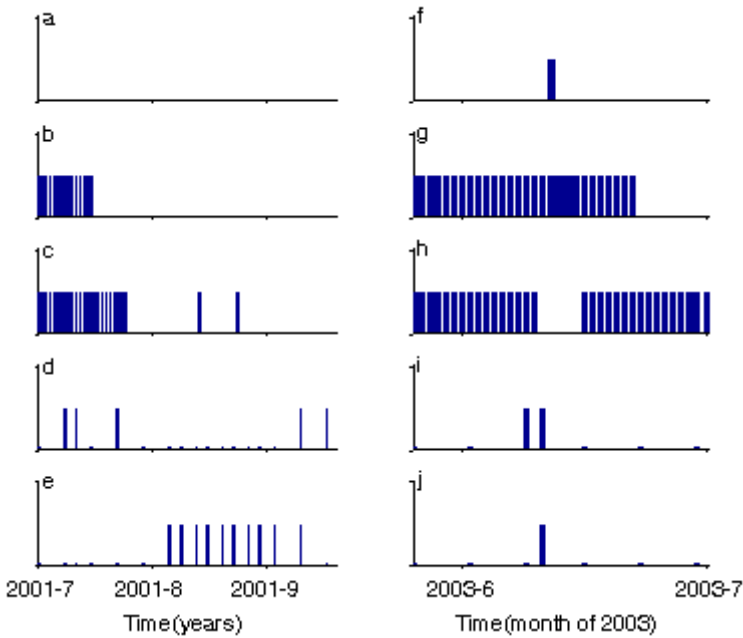


Figure 2 Events of external forcings and phytoplankton community change in the summer of 2001 (left) and in spring of 2003 (right). a, f) Predicted upwelling ($L_N < 2$); b, g) water withdrawal from the upper outlet; c, h) water withdrawal from the lower outlet; d, i) change in the phytoplankton composition (Index of community change, > 0.14); e, f) seasonal maxima of phytoplankton abundance (> 80 cells/ml). See text for further information.,

Acknowledgements

Data used in this work was collected by EMASESA, as part of its routine water quality monitoring program. The analysis work is part of the project CGL2005-04070/HID (Ministerio de Educación y Ciencia).

References

- IMBODEN D. M, WÜEST A. 1995. Mixing mechanisms in lakes. In: ZILERMANN A, IMBODEN D, GAT J. (ED). *Physics and Chemistry of Lakes*. Pp.83-138, Springer, Berlin.
- GEORGE, D.G., M.A. ROUEN. 1997. The development of an automated network of water quality monitoring stations in a series of European lakes. UE-LIFE93/UK/3167 Final Report.
- HAMBRIGHT K D., ZOHARY T. 2000. Phytoplankton species diversity control through competitive exclusion and physical disturbance. *PLimnol. Oceanogr.* 45(1): 110-122.
- MARGELEF, R. 1997. *Our biosphere*. Institute of Ecology.
- MORENO-OSTOS E.. 2004. *Spatial dynamics of phytoplankton in El Gergal reservoir (Seville, Spain)*. Ph.D. thesis, Universidad de Granada.
- REYNOLDS C. S. 1973. The phytoplankton of Crose Mere, Shropshire. *J. PBr. Phycol. J.* 8: 153-162.
- REYNOLDS C. S. 1984. *The ecology of freshwater phytoplankton*. Cambridge University Press, Cambridge.
- REYNOLDS C. S. 1997. *Vegetation Processes in the Pelagic. A model for Ecosystem theory*. ECI, Oldendorf.
- REYNOLDS C. S. 2002. Towards a functional classification of the freshwater phytoplankton. *J. Plankton Res.*24(5): 417-428.

ROSKOSCH, A., & HUPFER, M. &
NÜTZMANN, G. & LEWANDOWSKI, J.

Investigation of flow velocities
and rates in burrows of
Chironomus plumosus (L.)
(Diptera: Chironomidae) in
lake sediments

¹ *Leibniz-Institute of
Freshwater Ecology and Inland
Fisheries, Müggelseedamm 310,
12587 Berlin, Germany.
E-mail: roskosch@igb-berlin.de*

Abstract

The impacts of macrozoobenthos in lake sediments on hydraulic and biogeochemical processes are largely unknown. For further examination it is indispensable to specify the water exchange across the sediment-water interface due to bioirrigation caused by tube-dwelling macrozoobenthos species.

The goal of our studies was to characterize and quantify the flow velocities and flow rates in the burrows of *Chironomus plumosus* larvae. The hydrodynamic measurements were realized with flow velocity, diffusivity and oxygen micro-sensors, particle tracking velocimetry, conductivity and colour tracer experiments.

The experiments have shown that *C. plumosus* (L.) is not pumping continuously. We observed pumping, resting and feeding periods. During pumping periods the maximum flow velocities in the burrows were approximately 15 mm s^{-1} , and perfusion rates of 15 ml h^{-1} can be assumed.

Our studies show in detail how and how much water and oxygen are transported from the surface water into the burrows and the surrounding sediment by of *C. plumosus* (L.). The pumping activities will have a huge impact on hydrodynamic as well as biogeochemical processes in lake sediments. It is still difficult to evaluate the reliability of the different measurement methods.

Introduction

Macrozoobenthos living at the sediment-water interface affects its sediment environment by bioturbation, bioirrigation, ingestion, digestion, defecation, excretion, secretion and resuspension

(Lewandowski & Hupfer, 2005a; 2005b). These activities result in considerable effects on biogeochemical turnover of nutrients e.g. phosphorus-retention, in impacts on microorganism numbers and species compositions in the sediment and, not least, in an enormous influence onto the hydrodynamic exchange processes between pore water and the overlying water body.

In this study we investigate the impacts of a tube-dwelling macrozoobenthos species on hydrodynamic transport and water exchange due to bioirrigation in lake sediments. Our goal is to characterize and quantify mean perfusion rates, maximum flow velocities and pumping periods in the burrows of *Chironomus plumosus* larvae. These hydrodynamic data will be very important for our further investigations with regard to nutrient cycling and release in lake sediments. Moreover, the deliverables will establish the basis to develop a reactive transport model which will help us to understand the interaction between macrozoobenthos activities and biogeochemical processes in lake. Another goal of our studies is to compare different measurement techniques to find out which of them can be used to answer the different hydrodynamic questions best and to evaluate the potential error of the different methods.

Material and Methods

All experiments were performed with 3rd and 4th instar of *C. plumosus* (L.) collected from the sediments of Lake Müggelsee (Berlin, Germany). Chironomidae are non-biting midges which are highly abundant all over the world. The larvae of *C. plumosus* live in sediments and dwell u-shaped burrows up to 15 cm deep through which they pump water to provide oxygen for respiration and phytoplankton for food.

To observe the behaviour of the chironomids some larvae were put inside transparent u-shaped Tygon tubes (inner diameter 3.2 mm) with a similar geometry as natural chironomid burrows. The activities of the larvae could be monitored and recorded with a digital video camera. Other chironomids were put in u-shaped Plexiglas tubes (inner diameter 10 mm) filled with sediment. In that case every larva had to dig its burrow along the course of the tube, consequently the length of the burrow is known. Compared to the Tygon tubes the inner surface of the burrow is more natural but the extension of the surrounding sediment is quite limited. A third group of chironomids was added into u-shaped tubes made from wire gauze which were filled with and placed in sediment. In this case the larvae could also build burrows inside the tubes but the

effects of the pumping activities on the surrounding sediment were less disturbed than in the previous case. A fourth group of chironomids was not forced to build a special burrow geometry. They were just put into mesocosms filled with sediment and could freely build their burrows. Sediment and water used for our investigations was taken from Lake Müggelsee.

Perfusion rates, maximum flow velocity and pumping periods were investigated with different measurement techniques. To determine the perfusion rates a conductivity experiment was performed. A sediment filled Plexiglas tube with a chironomid inside was placed in a water filled Plexiglas box with two separated chambers (Fig. 1). Sodium chloride (NaCl) was added to the water of the chamber containing the burrow inlet. Changes in conductivity were measured online with a conductivity meter (WTW). Maximum flow velocities can be determined with colour tracers. Eosin yellowish was added above a burrow inlet. The time the tracer needed until it could be visually observed at the outlet was timed. Particle image velocimetry (PIV) is a technique in which a planar laser light sheet is pulsed twice, and images of fine particles moving in the light sheet can be recorded on a video camera. Movement patterns of added particles allow determining the flow velocity of the water (Goharzadeh et al., 2005; Stoehr & Khalili, 2006). With PIV flow velocities above burrow inlets and outlets were estimated. Another technique we used to study the hydrodynamics in chironomid burrows and the surrounding medium were flow velocity and diffusivity micro sensors (Unisense). The principle of the measurement is to detect how fast a gas sphere of a tracer gas (H_2) around the sensor tip is eroded (Brand et al., 2007). The sensor handling, especially the calibration procedure, was adapted to our applications. With the diffusivity sensors transport rates inside the sediment were measured, whereas flow velocity and oxygen micro-sensors (Unisense) were placed in burrow inlets and outlets to detect flow velocities and pumping periods. The oxygen micro-sensor is based on diffusion of oxygen through a silicone membrane to an oxygen reducing cathode (Revensbech, 1989). Every time shift between oxygen increase at inlet and outlet was used to estimate flow velocities during pumping periods (Fig. 2 in Results and Discussion). Pumping and resting periods were calculated from oxygen increase and decrease at the burrow inlet.



Figure 1. Experimental setup of the conductivity experiment: a u-shaped tube filled with sediment is placed in a water filled Plexiglas box which is divided into two chambers; both chambers are stirred continuously; a Tygon tube ensures the reflux of water to avoid water level differences; in one chamber chloride concentrations are enriched and in the other chamber the increase of chloride concentrations due to chironomid activity is measured with a conductivity electrode (not shown).

Results and Discussion

Chironomids living inside the transparent Tygon tubes give us detailed information about the activities of the larvae. To provide itself with oxygen and food *C. plumosus* is worming very uniformly. After some minutes of pumping the larvae stop worming and start grazing bacteria from the burrow walls. During this feeding periods which also take some minutes the chironomids move around inside the tube and even turn around. These movements might cause some irregular water flow through the burrow. After grazing the larvae return to the pumping position and start worming again. Before pumping *C. plumosus* sometimes spin a conical net across the burrow to catch phytoplankton out of the water flow. Afterwards they eat the net with the entrapped food (filter feeding). Usually there is also a resting period in-between moving and pumping intervals.

By means of oxygen sensors in a natural burrow surrounded by wire gauze we determined pumping periods of 7.2 ± 3.2 (standard

deviation, n=13) min and non-pumping periods of 5.5 +/- 1.4 min (n=13) (Fig. 2), but not all data are evaluated yet. In comparison Polerecky et al. (2006) stated pumping periods of 5.4 +/-1.7 min and resting intervals of 9.2 +/- 5.8 min with planar oxygen optodes.

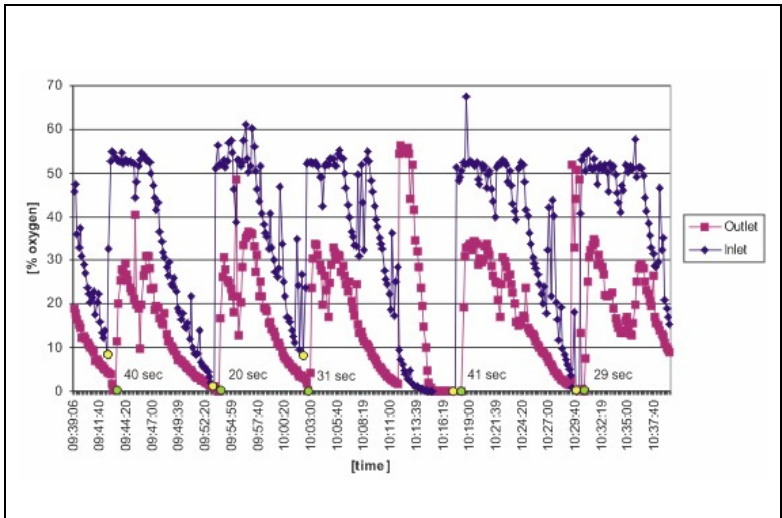


Figure 2. Example for oxygen measurements at burrow inlet and outlet to determine pumping periods and resting periods. Pumping and resting periods were calculated from the oxygen increase and decrease at burrow inlet. The time shift between oxygen increase at inlet (yellow spots) and outlet (green spots) is used to estimate flow velocities in chironomid burrows (see Tab. 1).

The results of the different measurement techniques are shown in Table 1. Since our investigations are not completed yet Table 1 should only be seen as a preliminarily result.

Table 1. Results of flow measurements conducted with different measurement techniques. Maximum flow velocities are given for pumping periods only whereas mean perfusion rates take pumping and resting periods into account. * measured value, ** calculated value, for calculation 2 mm is assumed as burrow diameter.

Measurement technique	Experimental setup	Mean perfusion rate (mL h ⁻¹)	Maximum flow velocity (mm s ⁻¹)
Determination of maximum flow velocities			
flow sensor	Tygon tube used as an artificial burrow; measurement in the outlet	1.00**	0.09*
flow sensor	natural burrow in a mesocosm; measurement in the outlet	3.00**	0.27*
colour tracer	burrow in a tube filled with sediment; discharge rate	160**	14.11*
colour tracer	natural burrow surrounded by wire gauze; discharge rate	166**	14.67*
oxygen sensor	natural burrow surrounded by wire gauze; displacement between inlet and outlet (Fig. 2)	70.2**	6.21*
PIV	flow velocity above inlet and outlet of a natural burrow	$\leq 23^{**}$	$\leq 2^{*}$
Determination of perfusion rates (mean values)			
conductivity	burrow in a tube filled with sediment; experimental setup Fig. 1	13.4*	1.2**

The determined flow velocities show drastic differences between the different measurement techniques. Our measurements with flow sensors might be incorrect since flow velocities might be too high for the highly sensitive sensors. The measurements with colour tracer might have resulted in very high maximum rates because the larvae might have been disturbed by the addition of the tracer and started to “clean” their burrows. In such a case *C. plumosus* can pump very intensive for a brief period of time. In other observations with colour tracer we found flow velocities around 3 mm s⁻¹ (34 mL h⁻¹) which are fitting with the magnitude of data from oxygen sensor (6.21 mm s⁻¹) and PIV (2 mm s⁻¹) measurements. Especially PIV measurements are not completed yet. We are going to determine flow velocities in the specified setups, and have to calculate mean perfusion rates from the data set. In literature Kießner et al. (2004) observed a flow rate of merely 3.8 mL h⁻¹ for *C. plumosus* with tracer technique. Leuchs (1986) evaluated the ventilation activity of *C. thummi* and determined 1.0 mL h⁻¹.

Conclusions

Summarizing, the present study confirms the influence of bioirrigation caused by chironomid larvae in lake sediments. Our measurements revealed much higher flow velocities than reported previously (e.g. Kißner et al., 2004). *C. plumosus* can be found in amounts up to 10,000 individuals m⁻² sediment. Calculations assuming only 1,000 chironomids m⁻² and perfusion rates of 13 mL h⁻¹ (Tab. 1) result in an amount of water pumped through the sediment of 312 L m⁻² d⁻¹. This value shows the impacts of *C. plumosus* in an impressive way. Further studies are necessary to validate the different measurement techniques and to confirm the detected flow velocities and perfusion rates.

Acknowledgements

Our studies wouldn't have been possible without the help of Arzhang Khalili and Mohammad Reza Morad from MPI, Bremen, and Lars Larsen from Unisense, Aarhus. Furthermore we have to thank Andreas Brand and Mathias Kirf from EAWAG, Luzerne.

References

- BRAND, A.; MÜLLER, B.; WÜEST, A.; DINKEL, C.; REVENSBECH, N. P.; NIELSEN, L. P.; PEDERSEN, O.; DAMGAARD, L. R. LARSEN, L. H. & WEHRLI, B. (2007): Microsensor for in-situ flow measurements in benthic boundary layers at sub-millimeter resolution with extremely low flow. *L&O Methods* 5
- GOHARZADEH, A.; KHALILI, A. & JORGENSEN, B. B. (2005): Transition layer thickness at a fluid-porous interface. *Phys. Fluids*. 17.057102-1 -10.
- KIßNER, T.; RISS, H. W.; STIEF, P. & MEYER, E. I. (2004): Bioturbations- und Bauverhalten von *Chironomus plumosus* (Diptera: Chironomidae) unter verschiedenen Sauerstoffbedingungen. Deutsche Gesellschaft für Limnologie. *Tagungsbericht 2003*. Berlin (2004): 486-489
- LEUCHS, H. (1986): The ventilation activity of *Chironomus* larvae (Diptera) from shallow and deep lakes and the resulting water circulation in correlation to temperature and oxygen conditions. *Arch. Hydrobiol.* 108: 281-292

- LEWANDOWSKI, J. & HUPFER, M. (2005a): Effect of macrozoobenthos on two-dimensional small-scale heterogeneity of pore water phosphorus concentrations in lake sediments: A laboratory study. *Limnol. Oceanogr.* 50: 1106-1118
- LEWANDOWSKI, J. & HUPFER, M. (2005b): Effect of *Chironomus plumosus* on spatial distribution of pore-water phosphate concentration in lake sediments: a laboratory experiment. *Verh. Internat. Verein. theoret. angew. Limnol.* 29: 937-940
- POLERECKY, L.; VOKENBORN, N. & STIEF, P. (2006): High temporal resolution oxygen imaging in bioirrigated sediments. *Environ. Sci. Technol.* 40: 5762-5769
- REVSBECH, N.P. (1989): An oxygen microelectrode with a guard cathode. *Limnol. Oceanogr.* 34: 472-476.
- STOEHR, M. & KHALILI, A. (2006): Dynamic regimes of buoyancy-affected two-phase flow in unconsolidated porous media. *Phys. Rev. E.* 73: 036301-1-8

LILOVER, M.-J.¹²

A cyanobacterial biomass prediction model for the Gulf of Finland based on a reduced number of input parameters

¹ *Tallinn University of Technology, Marine Systems Institute, Akadeemia tee 21, 12618 Tallinn, Estonia*
(madis.lilover@jrc.it)

² *European Commission – DG Joint Research Centre, Institute for Environment and Sustainability, Global Environment Monitoring Unit, Via E. Fermi 1 (TP 272), I-21020 Ispra (VA), Italy*

Abstract

A fuzzy logic model based on a reduced number of forcing parameters was applied to predict the maximum biomass of the two most common cyanobacterial species in the Gulf of Finland. The forecast is given considering the wintertime DIN, DIP and springtime wind data. Three different phosphate sources and underwater light conditions are derived from these data. The surface layer water temperature is regarded as the biomass control parameter and in the forecast simulations it varied from 14 to 23°C providing this way the possible summer scenarios. The model simulations showed that the predicted *Nodularia spumigena* biomass varies strongly from year to year and depends explicitly on the phosphate conditions while being at the same time also a function of the surface layer water temperature.

Introduction

The growth of phytoplankton biomass in the euphotic zone depends on light conditions, on the availability of inorganic nutrients and on physical parameters of environment. For the summer blooming nitrogen-fixing cyanobacteria the following sources of phosphorus are argued: phosphorus excess left after the spring bloom, phosphorus transport from the deeper nutrient rich water by upwelling, phosphorus transport from the deeper nutrient rich water

by vertical turbulent mixing and regeneration of organic phosphorus. Making an effort to account for the availability of light, marine environment physical parameters and all nutrient resources leads modellers to prefer the coupled physical-biogeochemical models. For example that type of ERGOM model is successfully used to study the inter-annual variability in cyanobacteria blooms in the Baltic Sea. This type of model can not be used directly to give a forecast of cyanobacterial bloom intensity and spatial extension because of the lack of long term weather forecasts. Instead pre-defined different weather scenarios are implemented to calculate the potential for bloom formation (Kiiriki et al. 2001). However the coupled 3D ecosystem model is not a simple tool – in the ecosystem part about 10 state variables have to be calculated (considering right initial and boundary values). Both in situ and satellite remote sensing monitoring are scarce and only state the situation. Here we propose a fuzzy logic (Zadeh 1965) model based on a reduced number of forcing parameters to predict the maximum biomass of common cyanobacterial species in the Gulf of Finland. The forcing parameters number is reduced by judgment of the bloom limiting factors and their parameterization through routinely measured parameters. As a result the model considers the phosphate conditions (3 resources, computed basing on the wintertime DIN, DIP and springtime wind data) and the physical conditions (underwater light climate determined by turbulent mixing and water temperature). In this study for the model calibration and validation the wintertime (January) nutrient data (DIN and DIP) sampled in the upper layer at the Gulf of Finland monitoring station F3 were used. The data were collected in the framework of the HELCOM monitoring programme COMBINE. The wind data used (from May to July) were measured at the Kalbådgrund weather station at 3-hour intervals. The used weekly cyanobacteria biomass and surface water temperature data along the transect Helsinki - Tallinn were kindly provided by the Alg@line project community in the frame of EC project HABES (contract EVK2-CT-2000-00092).

Finally on base only the wintertime DIN, DIP and springtime wind data the model calculates the expected biomass as a function of the surface layer water temperature.

Results

Here the model based on the fuzzy logic technique is developed to predict the maximum biomass value in the central part of the Gulf of Finland. According to the conceptual scheme (Fig. 1) the model takes into account the main factors (affecting aspects) that could limit the cyanobacteria biomass (affected aspect). Furthermore the

model build-up includes three steps, common to any fuzzy model approach: 1) fuzzification in which the input data are translated to memberships of sets in qualitative terms, 2) fuzzy inference in which a set of knowledge rules between classes of aspects are defined and 3) defuzzification where the qualitative output of the model is translated into quantitative value.

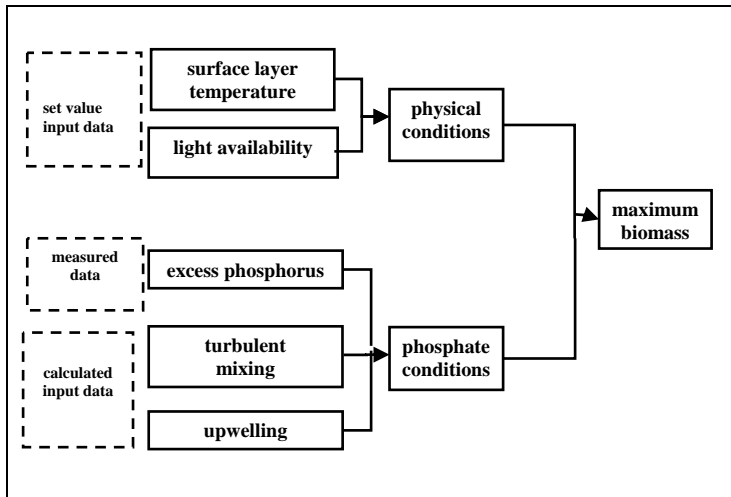


Figure 1 Schematic representation of the fuzzy logic model for early forecast of maximum cyanobacteria biomass.

In addition the model has to pass the calibration, the sensitivity analysis and the validation. The model output, the maximum biomass (maxB), is supposed to give the expected cyanobacteria biomass in the upper mixed layer (UML) of the open sea. In the proposed model the expected maximum biomass depends on physical (surface layer temperature (T_w) and mean light conditions expressed by wind mixing (τ) and phosphate (excess phosphorus (eP), transports by mixing (tP) and by upwelling ($upwP$)) conditions (Fig. 1). The physical conditions form the controlling factors for the cyanobacteria growth. For example the intensive bloom does not develop if the surface layer temperature is lower than 16 °C (in case of *N. spumigena*). The phosphate conditions integrate the phosphate left over from the spring bloom and the subsequent inputs of phosphate into the UML caused by turbulent mixing and coastal upwelling events. The corresponding aspects are calculated using the method given in Lilover&Laanemets (2006).

The two most common cyanobacteria species *Nodularia spumigena* and *Aphanizomenon flos-aquae* in the Gulf of Finland act differently in respect of phosphorus ability and water temperature. Hereafter at first we consider in our model *N. spumigena*. The

observational data revealed that the annual maximum *N. spumigena* biomass is highly dependent on the surface layer temperature ($r^2=0.73$, $p<0.001$, $n=11$, 1992-2003) and on the excess phosphate left over after the spring bloom ($r^2=0.61$, $p<0.05$, $n=8$; 1992-2003) (Laanemets et al. 2006) being in this way a good study object for fuzzy logic model.

The capability of the fuzzy model to forecast early the summer maximum biomass of *N. spumigena* (about a month before the regular bloom occurrence) was tested for the years 1997-2004. The results of the bloom biomass early prediction (biomass potential) based on the phosphate conditions on 15 June (phosphate potential) are presented in Fig. 2 by open circles (note that the wind speed 5.5 m s^{-1} and T_w $23 \text{ }^\circ\text{C}$ is used for all years). The predicted summer maximum biomasses differ strongly and show that the phosphate conditions really differ from year to year. The realization of the phosphate potential by *N. spumigena* depends on the actual surface layer water temperature (lines in Fig. 2). Both, the maximum values of the measured biomasses and the corresponding water temperatures, vary in a wide range (symbols in Fig. 2). In cold summers the water temperature restricts the blooming (e.g. year 2000, where the high bloom potential is not realized due to the low water temperature). In warm summers the biomasses vary because of different phosphate conditions (e.g. year 2001 vs years 1999 and 2002). In 2001 and 2002 the observed biomasses were higher than forecasted pointing to the importance of phosphate input by physical processes after the 15 June. The measured biomasses in years 2003 and 2004 do not fit well into the proposed scheme. Following the previous week wind data it became clear that in these cases there was too weak wind mixing before the sampling of the *N. spumigena* i.e. the actual peak concentration remained in the layer above the sampling depth. Consequently the measured values could not reflect the actual *N. spumigena* biomasses and point in this way to the weakness of the sampling strategy at 5 meters depth. Summing up we conclude that despite relying only on a few widely accessible input data (wintertime DIN and DIP, wind) the model allows for the early prediction (about a month before the usual time of the bloom occurrence) of the annual maximum *N. spumigena* biomass with respect to different surface layer temperatures (weather scenarios).

The fuzzy logic model presented here was calibrated and validated using *N. spumigena* weekly biomass data from years 1997 to 2003. In this way the tuned model is not directly useable to forecast *Aphanizomenon flos-aquae* biomass as there exists some important peculiarities in case of *Aphanizomenon flos-aquae* bloom. In the Gulf of Finland *Aphanizomenon* reaches its maximum biomass in

general about 2 weeks earlier than *N. spumigena*. In this way the maximum biomass was observed at lower water temperatures and wasn't in correlation with the latter. Therefore the water temperature can not be regarded as a parameter controlling the development of biomass (though in cold years for *N. spumigena* blooms *Aphanizomenon flos-aquae* also had slightly lower biomasses). Still the regression between the excess phosphate remaining after the spring bloom and maximum *Aphanizomenon* biomass in the upper mixed layer was good ($r^2=0.62$, $n=7$ and in warm summers $r^2=0.81$, $n=5$) allowing the model to be based on the phosphate conditions to give a forecast.

We would like to point out here that in the case of *Aphanizomenon flos-aquae* the observed maximum biomass (g/m^2) has lower correlation with biomass concentration (g/m^3) than in the *N. spumigena* case. This reflects a fact that maximum biomass was measured after the windy period. Correspondingly at the maximum biomass time the previous week gain of water temperature was small ($\Delta T_w = 1$ deg C) and gain of phosphate by turbulent transport remarkable ($\Delta tP = 0.05$). It could be that to predict the maximum biomass of *Aphanizomenon flos-aquae* new aspects have to be taken into account in the model.

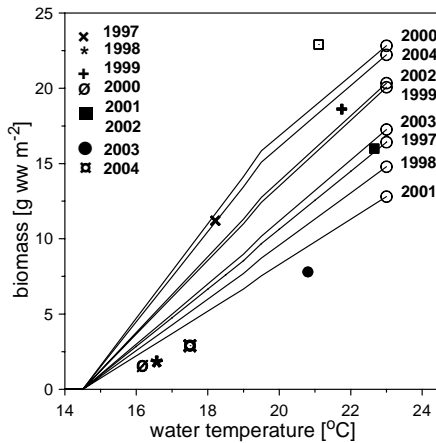


Figure 2 Early prediction of maximum *N. spumigena* biomass on the basis of 1997-2004 data. Open circles on the right mark the bloom potential taking into account the phosphate conditions by 15 June in the respective years. Lines represent the predicted maximum biomass as a function of the surface layer temperature. Symbols indicate the maximum measured biomass and the respective water temperature in summers 1997-2004.

Acknowledgements

The cyanobacteria biomass concentration and temperature data on the transect Helsinki-Tallinn were kindly provided by Alg@line project (Finnish Institute of Marine Research, Uusimaa Regional Environment Centre, City of Helsinki Environment Centre, Estonian Marine Institute). The Finnish Institute of Marine Research kindly provided the nutrient data and Finnish Meteorological Institute the wind data. Research of M.-J. Lilover was supported by a grant received through the Enlargement Action of EU Commission 6th Framework Programme.

References

- KIIRIKKI M, INKALA A, KUOSA H, PITKÄNEN H, KUUSISTO M, SARKKULA J. 2001. Evaluating the effects of nutrient load reductions on the biomass of toxic nitrogen-fixing cyanobacteria in the Gulf of Finland, Baltic Sea. *Boreal Env. Res.* 6: 131-146.
- LAANEMETS J, LILOVER M-J, RAUDSEPP U, AUTIO R, VAHTERA E, LIPS I, LIPS U. 2006. A fuzzy logic model to describe the cyanobacteria *Nodularia spumigena* bloom in the Gulf of Finland, Baltic Sea. *Hydrobiologia* 554: 31-45.
- LILOVER M-J, LAANEMETS J. 2006. A simple tool for the early prediction of the cyanobacteria *Nodularia spumigena* bloom biomass in the Gulf of Finland. *Oceanologia* 48 (S): 213-229.
- ZADEH L. 1965. Fuzzy sets. *Inf. Control* 8: 338-353.

KUZNETSOV, I.S.¹ & YAKUSHEV,
E.V.^{1,2}, & PODYMOV, O.I.²

Modeling of influence of intrusions on biogeochemical structure of the seas with anoxic layers

¹ *Baltic Sea Research Institute, Warnemuende, Seestrasse 15, 18119 Rostock, Germany. E-mail: ivan.kuznetsov@io-warnemuende.de*

² *Shirshov Institute of Oceanology RAS, Southern Branch, Gelendzhik-7, Krasnodarskii Kray, 353467, E-mail: e_yakushev@yahoo.com*

Abstract

In this study we used coupled 1D hydrophysical-biogeochemical model based on the General Ocean Turbulent Model (Burchard et al., 1999) and the RedOx Layer Model, (Yakushev et al., 2006). The model allowed to simulate basic features of biogeochemical structure changes in case of transformation of oxic conditions into anoxic and from anoxic into oxic.

Introduction

Anoxic conditions in water column are a natural feature of many areas in seas. They arise from imbalance in the transport rates of organic matter (OM) and oxygen into deeper layers, when oxygen is depleted and an excess of organic material is yet to be decomposed. Permanent anoxic conditions are observed in numerous lakes, fjords, and some regions of the World Ocean (Black Sea, Baltic Sea Deeps, Cariaco Basin).

We studied influence of oxygenated intrusions on vertical biogeochemical structure in the Black Sea and the Baltic Sea.

Model

This 1D, hydrophysical-biogeochemical model was developed to study cycling of the main elements (O-N-S-P-Mn-Fe) in the pelagic

redox layer in the seas with anoxic conditions. Formation and decay of organic matter; reduction and oxidation of nitrogen, sulfur, manganese, and iron compounds, and transformation of phosphorus compounds were parameterized in the biogeochemical block of the model.

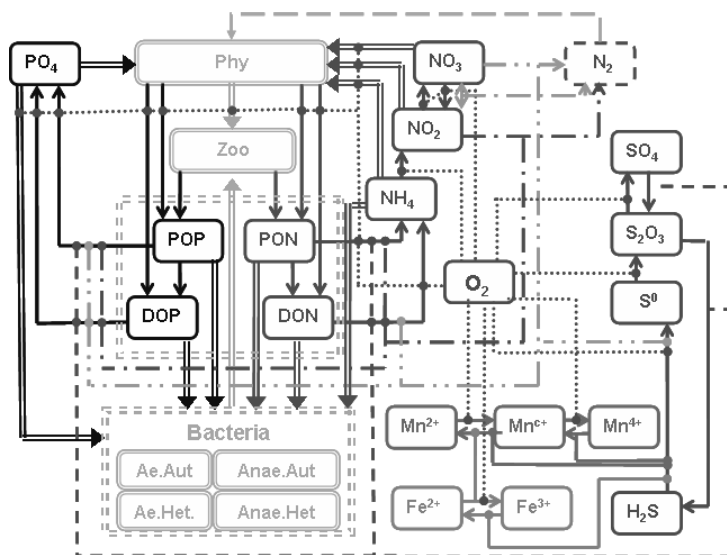


Figure 1 Flow-chart of biogeochemical processes represented in the model.

The following biogeochemical parameters (C_i) were considered (Fig. 1.): dissolved oxygen (O_2), hydrogen sulfide (H_2S), total elemental sulfur (S^0), thiosulfate (S_2O_3), sulfate (SO_4), ammonia (NH_4), nitrite (NO_2), nitrate (NO_3), particulate organic nitrogen (PON), dissolved organic nitrogen (DON), phosphate (PO_4), particulate organic phosphorus (POP), dissolved organic phosphorus (DOP), bivalent manganese ($Mn(II)$), trivalent manganese ($Mn(III)$), quadrivalent manganese ($Mn(IV)$), bivalent iron ($Fe(II)$), trivalent iron ($Fe(III)$), phytoplankton (Phy), zooplankton (Zoo), aerobic heterotrophic bacteria (Bhe), aerobic autotrophic bacteria (Bae), anaerobic heterotrophic bacteria (Bha), and anaerobic autotrophic bacteria (Baa). The detailed description of this model block is given in (Yakushev et al., 2006).

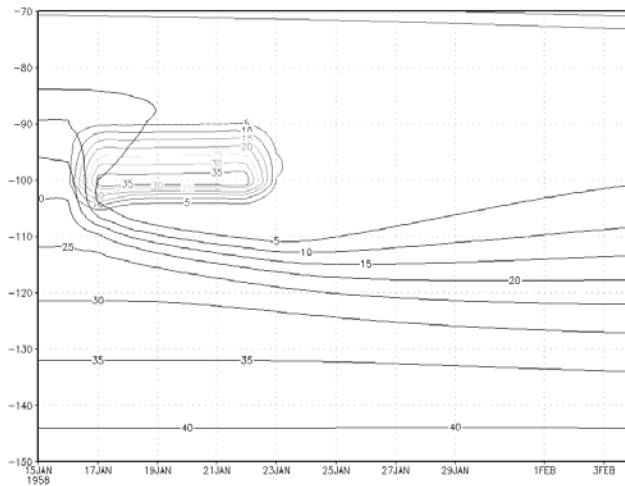
Temporal and spatial developments of the model's variables were described by a system with equations of horizontally integrated vertical diffusion for non-conservative substances. The calculated

spatial and temporal distributions of the above-mentioned parameters were in good agreement with observed vertical distribution patterns of these processes.

The physical scenarios of the model were calculated with the GOTM (Burchard et al., 1999). For the Black Sea we used the climatic-averaged data on the formation and transformation of the Cold Intermediate Layer (Belokopytov, 2004) and the estimates of the Bosphorus parameters (Ozsoy et al., 2001). For the Baltic Sea we used the results of hydrophysical observations at a IOW Gotland Basin monitoring station 273 in 1992-1993.

Results

We carried out the calculations to study consequences of intrusion of oxygenated water in the depth of the Bosphorus Plume in the Black Sea (Fig. 2).



GRAB: COLA/ISES

2007-03-11-12:09

Figure 2 Temporal variability of hydrogen sulfide (black lines) as a reaction to the supply of oxygen (grey lines) from Bosphorus.

These calculations demonstrated that sulfidic boundary deepened in the Bosphorus region returns to its previous position in about 2-3 months. At that time this water can be transported to about 200-300 km.

The model simulations demonstrated that during the inflow events in the Baltic Sea (Fig. 3) an accelerated formation of the particulate forms of Mn and Fe occurs, and these elements will be quickly removed from the water column into sediments.

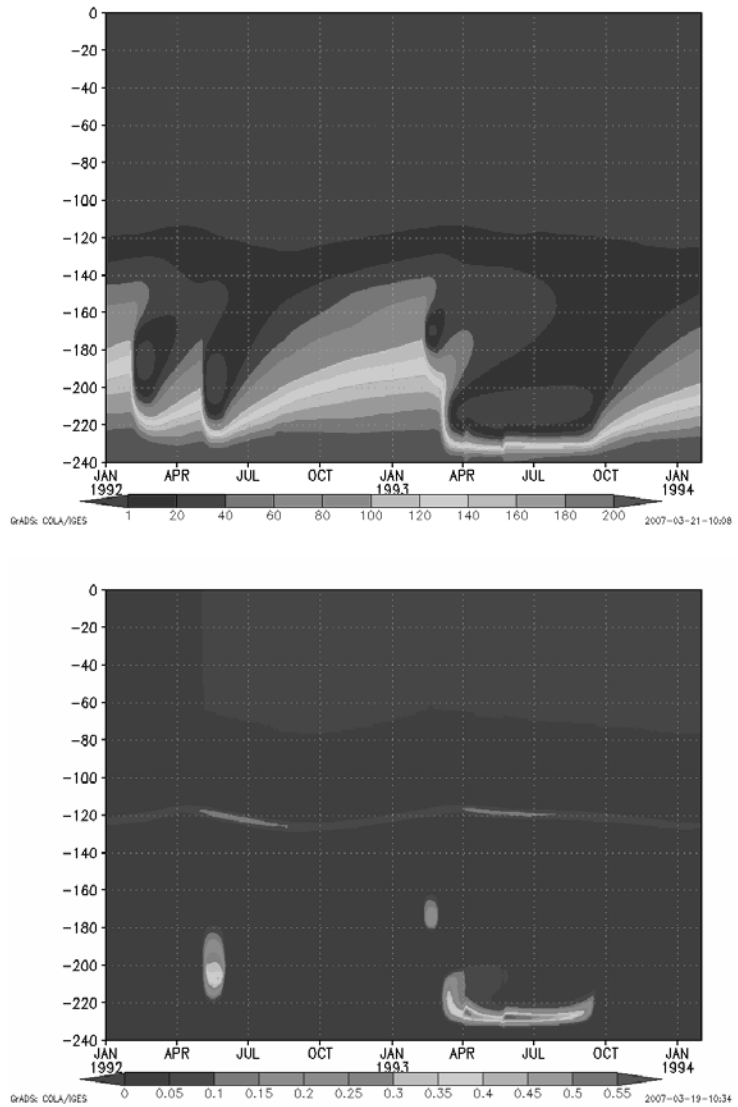


Figure 3 Temporal variability of hydrogen sulfide (top) and particulate Mn (bottom) during the inflows events in the Gotland Deep of the Baltic Sea in 1992-1993.

Conclusions

- Influence of the Marmara Sea water influx through the Bosphorus can be traced only in the south-western region of the Black Sea (about 200-300 km from the Bosphorus).

Vertical structure of other regions of the Black Sea is formed mainly by vertical exchange processes and biogeochemical transformation.

- Variability of the redox interface depth in the Gotland Deep of the Baltic Sea is determined by frequency and intensity of intrusions of the North Sea water.
- Intensification of the redox reactions and growth of bacteria during development of the intrusions leads to increase of particulate matter content and acceleration of sedimentation.

Acknowledgements

This research was supported by Shirshov Institute of Oceanology, RAS, Russian Foundation for Basic Researches grants 05-05-65092, 06-05-96676-Yug, 07-05-0124, CRDF grant RUG1-2828-KS06.

References

- BELOKOPYTOV VN (2004) Hydrophysical structure of the Black Sea. Ph.D. thesis. Marine Hydrophysical Institute, Sevastopol (In Russian).
- BURCHARD H, BOLDING D, VILLAREAL MR. 1999. GOTM, a general ocean turbulence model. Theory, applications and test cases. *European Commission report* EUR 18745 EN, 103
- OZSOY E, DI IORIO D, GREGG MC, BACKHAUS JD. 2001. Mixing in the Bosphorus Strait and the Black Sea continental shelf: observation and a model of the dense water outflow. *J. of Marine Systems* 31: 99-135
- YAKUSHEV EV, POLLEHNE F, JOST G, KUZNETSOV I, SCHNEIDER B, UMLAUF L. 2006. Redox-Layer Model (ROLM): a tool for analysis of the water column oxic/anoxic interface processes. *Meereswissenschaftliche Berichte, Marine Science Report*. 68: 1-54.

Author Index

- Amores, V., 171
Arneborg, L., 19, 79
Baeuerle, E., 29
Basanta, A., 171, 173
Berg, P., 71
Bilaletdin, Ä., 117
Boehrer, B., 53
Bolding, K., 99
Bonhomme, C., 89
Bouffard, D., 81
Bryant, L. D., 33
Budnev, N., 137
Burchard, H., 109
Chubarenko, I., 111
MacCready, P., 123
Crimea Partners, 45
Cruz-Pizarro, L., 171
Cuypers, Y., 89
Demchenko, N., 111
Engelhardt, C., 97, 157
Escot, C., 171, 173
Feistel, R., 143
Filatov, N., 117
Frisk, T., 117
Gale, E., 129
Garcia-Gorriz, E., 99
McGinnis, D. F., 39, 45, 71
Golosov, S., 97, 147, 157
Granin, N., 137
Heise, E., 101
Hoyer, A., 171, 173
Hume, A., 71
Hupfer, M., 179
Ilmberger, J., 53, 55, 61
Kirillin, G., 97, 157
Kourzeneva, E., 101
Kuznetsov, I. S., 193
Lass, H. U., 77
Lemmin, U., 81
Lewandowski, J., 179
Lilover, M.-J., 187
Little, J. C., 33, 39
Lorke, A., 45
Lorrai, C., 71
Mironov, D., 97, 101
Mitrokhov, A., 147
Mohrholz, V., 77, 79
Moreno-Ostos, E., 171, 173
Munroe, J. R., 3
Nützmann, G., 179
Paananen, A., 117
Palshin, N., 147
Pattiaratchi, C., 129
Peters, D., 17
Podsechin, V., 117
Podymov, O. I., 193
Potakhin, M., 147
Poulin, M., 89
Prandke, H., 77
Rigosi, A., 171
Ritter, B., 101
von Rohden, C., 53, 55, 61
Roskosch, A., 179
Rueda, F. J., 171, 173

Schmid, M., 137
Schneider, N., 101
Schultze, M., 53
Schurter, M., 137
Singleton, V. L., 39
Stashchuk, N., 11, 23
Stips, A., 99
Sturm, M., 137
Sutherland, B. R., 3
Tassin, B., 89
Terzhevik, A., 117, 147, 157
Umlauf, L., 79, 109
De-Vicente, I., 171
Vidal, J., 171, 173
Vlasenko, V., 11, 23
Wüest, A., 45, 71, 137
Yakushev, E. V., 193
Yu, A., 157
Zdorovenov, R., 147
Zdorovenova, G., 147
Zilitinkevitch, S., 69
Zuelicke, C., 17, 87
Zverev, I., 157